Theses and Dissertations

December 2015

The Great Lakes' Regional Climate Regimes

Noriyuki Sugiyama
University of Wisconsin-Milwaukee

THE GREAT LAKES' REGIONAL CLIMATE REGIMES

by

Noriyuki Sugiyama

A Dissertation Submitted in

Partial Fulfillment of the

Requirements for the Degree of

Doctor of Philosophy

in Mathematics

The University of Wisconsin at Milwaukee

December 2015

<div align="center">

ABSTRACT

THE GREAT LAKES' REGIONAL CLIMATE REGIMES

by

Noriyuki Sugiyama

The University of Wisconsin at Milwaukee, 2015
Under the Supervision of Professor Sergey V. Kravtsov and Professor Paul
J. Roebber

</div>

For the last couple of decades, the Great Lakes have undergone rapid surface warming. In particular, the magnitude of the summer surface-warming trends of the Great Lakes have been much greater than those of surrounding land (Austin and Colman, 2007). Among the Great Lakes, the deepest Lake Superior exhibited the strongest warming trend in its annual, as well as summer surface water temperature. We find that many aspects of this behavior can be explained in terms of the tendency of deep lakes to exhibit multiple regimes characterized, under the same seasonally varying forcing, by the warmer and colder seasonal cycles exhibiting different amounts of wintertime lake-ice cover and corresponding changes in the summertime lake-surface temperatures. In this thesis, we address the problem of the Great Lakes' warming using one-dimensional lake modeling to interpret diverse observations of the recent lake behavior.

For a one-dimensional model to be able to faithfully simulate the dynamics of the Great Lakes' rapid warming and multiple climate regimes, it needs to accurately represent the lake's climatological seasonal cycle. However, these models (e.g., Hostetler and Bartlein 1990) have been known to simulate seasonal temperature cycles of deep lakes ($> 200m$) poorly. A number of attempts have aimed to improve the Hostetler and Bartlein (1990) model by parameterizing unresolved physical processes in the form of the so-called "enhanced minimum diffusion." In this thesis, we developed an ad hoc modification to the parametrization of the enhanced minimum diffusion, which led to

the 1-D simulations of the lakes' seasonal cycle comparable in quality to those obtained by recent 3-D lake models.

To address the problem of Great Lakes climate dynamics, we considered multi-column generalizations of the improved one-dimensional lake model, which were also coupled to an idealized two-layer atmosphere. The variable temperature of the upper atmospheric layer in this model was a proxy for the large-scale atmospheric forcing, and consisted, in the most general case, of a linear trend mimicking the global warming, and random noise representing atmospheric intrinsic variability, both on top of the prescribed seasonal cycle of the upper-atmosphere temperature. The lower atmospheric layer of the coupled model is able to respond actively to the variability in the lake's surface temperature simulated by the multi-column lake component, and exchanges heat laterally between the lower-atmospheric columns via a diffusive heat transport.

The single-column models were shown to exhibit two possible steady seasonal cycles – with and without lake-ice occurrence in winter and with corresponding cold and warm temperatures in the following summer, respectively, all under an identical external seasonally varying forcing. The basins of attraction of the warm and cold seasonal cycles depend on the annual-mean upper-atmosphere temperature, with warmer temperature leading to the preference of the warm regime and vice versa. The quantitative characteristics of the simulated lake regimes also depend on the depth of the lake column considered: in particular, the distinction in summertime heat content between warm (wintertime ice free) and cold (wintertime ice-covered) regimes is the largest for the deepest lakes. This property ultimately has to do with a shorter dynamical memory of the shallow lakes, which are climatologically characterized by longer duration of the summertime mixed layer; hence, the surface temperature (heat content) anomalies arising due to varying degrees of wintertime ice cover are being lost to the atmosphere over a longer period of time than for deeper lake columns.

A short dynamical memory of shallow lakes and a longer memory of deep lakes also explain the different character of regime transitions under the action of stochastic

forcing associated with intrinsic atmospheric variability. Namely, shallow lakes may exhibit frequent and non-persistent year-to-year transitions from one regime to the other and back due to stochastic agitation. On the other hand, longer-memory deeper lakes tend to exhibit more persistent behavior with inter-annual preference of one regime over the other, with jump-like transitions in between.

Experiments with multi-column coupled models demonstrate analogous regime behavior. The regime structure of the multi-column models of non-uniform depth is more complex and involves an intermediate, partially ice-covered regime. However, in the presence of the efficient lateral heat exchange between the lower atmospheric columns, the transitions between the regimes characterizing different lake columns (shallower and deeper lake regions) synchronize. Under the forcing associated with global warming and superimposed atmospheric intrinsic variability, the multi-column lakes exhibit progressively more frequent (for shallow lakes) or persistent (for deep lakes) transitions to the warmest regime, and eventually switch to the warmest regime for good. Upon the final transition, the largest changes in the summertime maximum temperature occur over the deeper portions of the lake, and the deep lakes warm more than shallower lakes.

We used these modeling results to interpret observations of the recent warming of the Great Lakes. We find that the reason Lake Superior exhibits the strongest warming trend among the Great Lakes is that the eastern part of the lake clearly exhibits distinct regional-climate regimes. As global warming drives Lake Superior's local climate away from the basin of attraction of its colder seasonal regime toward its warmer regime, the surface water temperature of the lake undergoes a more drastic change than the surface temperature of surrounding land. The regime transition takes the form of a discontinuous jump in the Lake Superior surface water temperature, evident, for example, in the August-mean surface water temperature time series at buoy stations in Lake Superior around the years 1997-98. Moreover, we find that the surface water temperature of Lake Superior warms faster than those of the other, shallower Great Lakes, which exhibit less clear indications of the existence of multiple regimes in their

summertime temperatures, consistent with the behavior of one-dimensional lake models.

The apparent correlation between local lake depth and lake-surface temperature warming rates occurs not only between the different lakes, but also within the individual Great Lakes. Our modeling results provide clues to causes of this intriguing property of the Great Lakes warming. Simulations show that due to larger dynamical memory, deeper lakes experience a larger summertime temperature jump when they transition from the colder to the warmer regime than the shallower lakes. Likewise, it is easier for shallow lakes to transition back and forth between its multiple regimes. The more frequently the lake transitions between the warmer and colder climate regimes under the slow global warming, the smaller its associated summer warming trend becomes. In other words, in the presence of global warming, deeper lake regions generally exhibit larger warming trends than shallower lake regions.

Finally, the much discussed observed correlation between summertime surface water temperatures and the amount of wintertime ice cover of the Great Lakes is to be naturally expected within the multiple regimes framework, as these two quantities characterize the main distinctions between the warm and cold simulated climate regimes. We hypothesize that the existence of multiple seasonal-cycle regimes in our lake model and, by inference, in observations is largely due to nonlinearity associated with the ice-albedo feedback. In future work, we plan to map out the detailed dynamics of these nonlinear effects and demonstrate the robustness of the ensuing regime behavior with respect to the model's horizontal resolution.

TABLE OF CONTENTS

LIST OF FIGURES

x

LIST OF TABLES

ACKNOWLEDGEMENTS

have given me support and encouragement.

Chapter 1

Introduction

1.1 Motivation

For the last couple of decades, it has been noted in a number of climate model simulations that land and ocean respond to global warming differently (e.g. Manabe *et al.*, 1991; Sutton *et al.*, 2007; Joshi *et al.*, 2008; Joshi and Gregory, 2008; Byrne and O'Gorman, 2012). Models generally predict more warming over land than over ocean at mid or lower latitudes. Typical land/ocean contrasts of the rates of increase in surface air temperature at mid or lower latitudes, $\Delta T_L/\Delta T_O$, depending on the models, range from 1.36 to 1.84, where ΔT_L and ΔT_O are surface air temperature over land and that over ocean (Sutton *et al.*, 2012). However, when it comes to lakes at mid-latitudes, we hear a different story. In particular, more rapid rates of increase in summer surface water temperature have been observed in most of the Great Lakes than their surrounding regional air temperatures (Austin and Colman, 2007; Hanrahan *et al.*, 2010). For example, the land/lake contrast of the warming trends in summer surface temperature of/around Lake Superior is about 0.5 during the years 1979-2005 (e.g., Austin and Colman, 2007). Similar surface warming has been observed in a number of lakes at mid-latitude globally (Schneider *et al.*, 2010). We ask: Why do a number of lakes at mid-latitudes in summer warm faster than surrounding land, while land in general warms faster than ocean?

1.2 Background

1.2.1 Seasonal Cycles of the Great Lakes

The Laurentian Great Lakes consist of five freshwater lakes, whose sizes range from $2 \times 10^4 km^2$ to $8 \times 10^4 km^2$, and are located in the eastern part of North America (Figure 1). They are dimictic lakes, meaning that their water temperatures become vertically homogeneous twice every year. The reason is as follows. Freshwater is densest at $3.98°C$. The temperatures at the bottoms of the Great Lakes are generally close to this value, especially of the deeper lakes. When the surface water temperature of a lake is warmer or colder than $3.98°C$, water near the surface is less dense than that near the bottom, and

Map data ©2015 Google   100 mi

Figure 1: *The location of the Laurentian Great Lakes and Sparkling Lake. The tip of the red mark is where Sparkling Lake is located.*

this vertical density profile of water discourages vertical mixing. All of the Great Lakes become warmer than $3.98°C$ at some point in summer and colder than $3.98°C$ at some point in winter. Therefore, there are two occasions for each of the Great Lakes every year when its surface temperature becomes $3.98°C$. When this happens, water temperature becomes homogeneous from the top to the bottom and the vertically homogeneous profile of water encourages vertical mixing this time. The time when cold lake water from a winter warms and reaches $3.98°C$ is called "spring overturn." Exactly when their temperatures become vertically homogeneous varies from lake to lake, and even from location to location within a lake. As an example, Figure 2 shows a simulation of water temperature at depth changing from January to December of the year 1996 below buoy station 45002 in northern Lake Michigan.

During winters, ice covers a certain fraction of the Great Lakes. Figures 3 contains the annual time series of maximum ice cover over each of the Great Lakes observed by the satellites for the Great Lakes Surface Environmental Analysis (GLSEA) and documented by NOAA's Great Lakes Environmental Research Laboratory (GLERL). During this period, the amount of ice cover over the Great Lakes exhibited a decreasing trend (Wang *et al.*, 2012).

When ice appears on the surface of a lake, ice reflects a good amount of down-
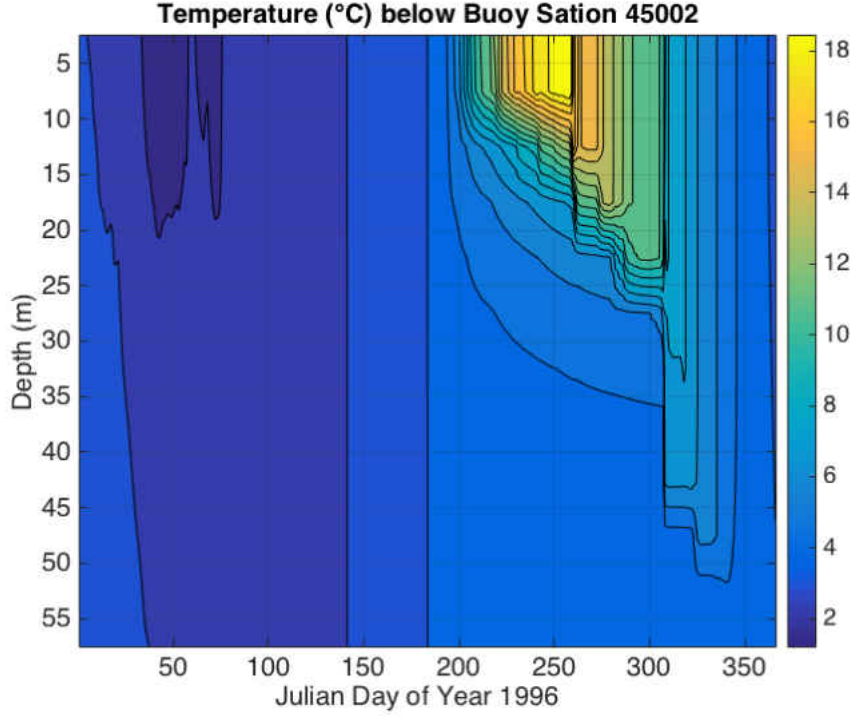
Figure 2: *A simulation the temperature profile at depth below buoy station 45002, in northern Lake Michigan, for the year 1996, with the 5m vertical grid spacing. The abscissa is Julian day, and the ordinate is temperature in °C.*

ward shortwave radiation, resulting in less amount of radiation energy absorbed by the lake. If global warming warms the lake further, the amount of ice cover in winter will decrease, and consequently, the amount of incoming shortwave radiation will increase and the lake will acquire more heat content. This is called *the ice-albedo feedback*. In addition, the amount of sensible and latent heat fluxes at the lake surface also change with the appearance of ice. In the previous subsection, we asked the question: Why do a number of lakes at mid-latitudes in summer warm faster than surrounding land? Although we want to answer this overarching question, first, we need to address a number of smaller questions so that we have deeper understanding of the problem. One of the most important such questions we should ask is: *Are the ice-albedo feedback and other ice-related feedback effects enough to give rise to the strong surface-water warming trends observed in some of the Great Lakes?* This is our *Question 1*.
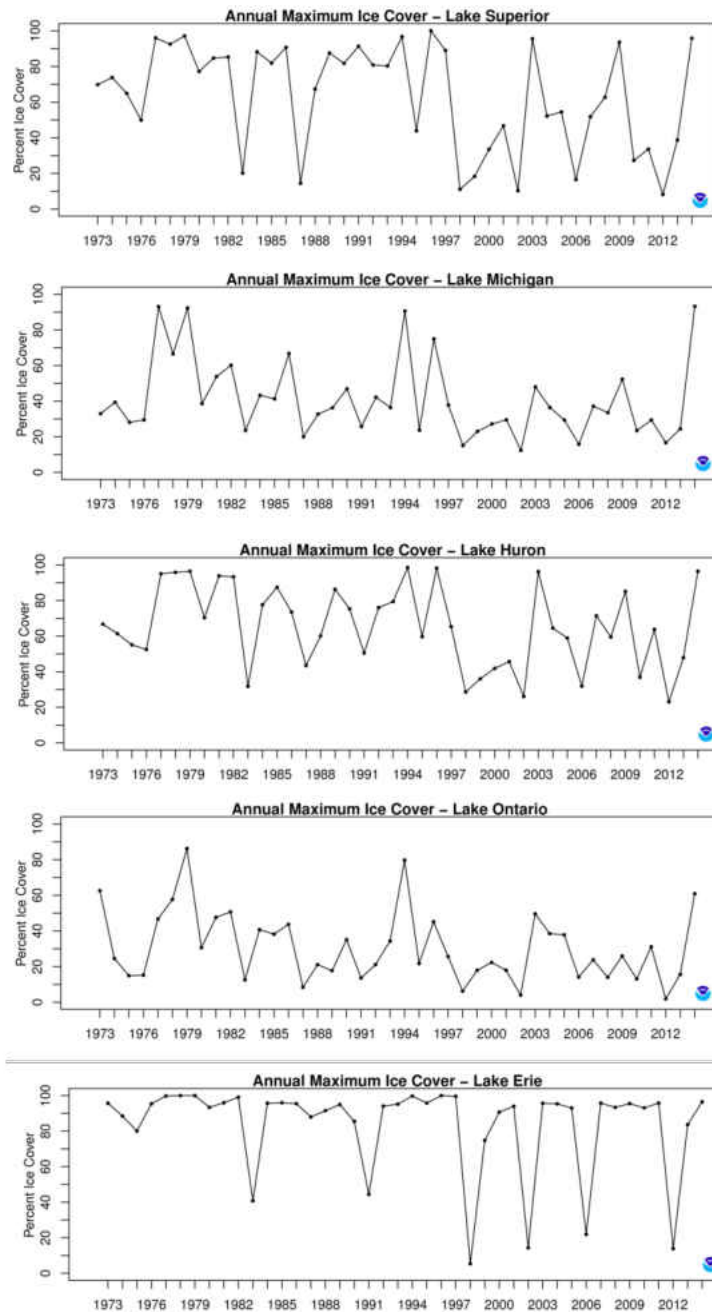
Figure 3: *The annual time series of maximum ice cover over each of the Great Lakes observed by the satellites for the Great Lakes Surface Environmental Analysis (GLSEA) and documented by NOAA's Great Lakes Environmental Research Laboratory (GLERL) for the years 1973-2014. The lakes shown are, from the top to the bottom, Superior, Michigan, Huron, Ontario, and Erie. This figure is adapted from NOAA's GLERL site (http://www.glerl.noaa.gov/data/ice/).*

1.2.2 The Great Lakes' Accelerated Surface-Water and Surface-Air Warming Trends

Table 1: *The warming trends in monthly surface water temperature of each of the Great Lakes based on the GLSEA satellite data for the years 1995-2012 and estimated by linear regression. The units are in °C/year.*

Monthly Warming Trend (°C/year)					
	Superior	Michigan	Huron	Erie	Ontario
January	$0.03_{\pm 0.03}$	$0.03_{\pm 0.04}$	$-0.01_{\pm 0.04}$	$-0.02_{\pm 0.07}$	$0.04_{\pm 0.04}$
February	$0.03_{\pm 0.03}$	$0.05_{\pm 0.03}$	$0.03_{\pm 0.02}$	$-0.03_{\pm 0.06}$	$0.05_{\pm 0.03}$
March	$0.07_{\pm 0.03}$	$0.11_{\pm 0.04}$	$0.08_{\pm 0.03}$	$0.10_{\pm 0.04}$	$0.11_{\pm 0.04}$
April	$0.12_{\pm 0.03}$	$0.14_{\pm 0.04}$	$0.14_{\pm 0.04}$	$0.15_{\pm 0.06}$	$0.14_{\pm 0.04}$
May	$0.16_{\pm 0.04}$	$0.16_{\pm 0.08}$	$0.18_{\pm 0.08}$	$0.18_{\pm 0.08}$	$0.19_{\pm 0.10}$
June	$0.16_{\pm 0.08}$	$0.13_{\pm 0.11}$	$015_{\pm 0.10}$	$0.11_{\pm 0.06}$	$0.19_{\pm 0.10}$
July	$0.27_{\pm 0.15}$	$0.16_{\pm 0.08}$	$0.15_{\pm 0.09}$	$0.11_{\pm 0.06}$	$0.15_{\pm 0.08}$
August	$0.12_{\pm 0.10}$	$0.05_{\pm 0.07}$	$0.06_{\pm 0.05}$	$0.05_{\pm 0.05}$	$0.06_{\pm 0.05}$
September	$0.07_{\pm 0.07}$	$0.04_{\pm 0.05}$	$0.05_{\pm 0.05}$	$0.03_{\pm 0.04}$	$0.06_{\pm 0.04}$
October	$0.11_{\pm 0.05}$	$0.05_{\pm 0.06}$	$0.07_{\pm 0.05}$	$0.01_{\pm 0.06}$	$0.05_{\pm 0.05}$
November	$0.06_{\pm 0.05}$	$0.04_{\pm 0.06}$	$0.04_{\pm 0.05}$	$-0.01_{\pm 0.06}$	$0.08_{\pm 0.05}$
December	$0.00_{\pm 0.02}$	$0.02_{\pm 0.05}$	$-0.03_{\pm 0.04}$	$0.01_{\pm 0.06}$	$0.03_{\pm 0.04}$

Table 1 shows the warming trends in monthly-mean surface water temperature of each of the Great Lakes for the years 1995-2012. The July-mean surface-water warming trend of Lake Superior for the years 1995-2012 is, strikingly, $0.27 \pm 0.15 °C/year$. Can the extra energy Lake Superior receives due to the decrease in ice cover in winter give rise to such a strong summer warming trend?

Figure 4 is a map of linear warming trends in annual-mean air temperature at the 1000mb pressure level for the years 1995-2012. The figure shows that annual-mean air temperatures at the 1000mb pressure level above regions of the Great Lakes increase faster than those above surrounding land as well. In the figure, among the Great Lakes, we find that air at the 1000mb level above Lake Superior warms fastest and that air at that level above Lake Erie warms slowest. It turns out that their surface water temperatures also exhibit this tendency.

1000mb-Level Air Temperature Annual Trend 1995-2012 in ℃/year
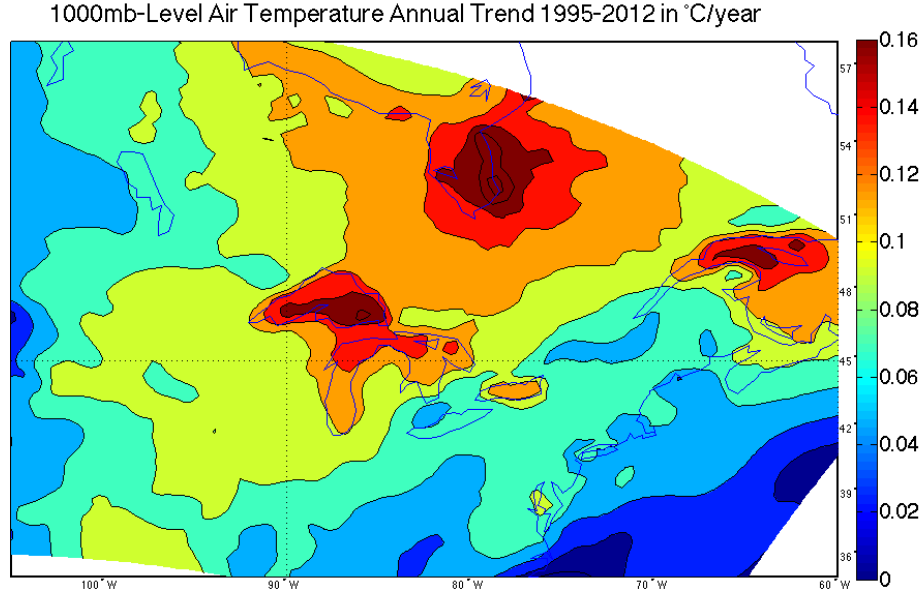
Figure 4: *A map of linear warming trends in annual-mean air temperature at the 1000mb pressure level, based on the NARR reanalysis data between the years 1995 and 2012. The unit is in ° C/year.*

Table 2: *The warming trends in annual surface water temperature of each of the Great Lakes based on the GLSEA satellite data for the years 1995-2012 and estimated by linear regression, shown in the 2nd column. The units are in °C/year. Shown in the 3rd column is the mean depth of each of the Great Lakes in meters.*

	Annual Warming Trend ($°C/year$)	Mean Depth (m)
Lake Superior	0.10 ± 0.04	147
Lake Michigan	0.082 ± 0.04	86
Lake Huron	0.076 ± 0.03	59
Lake Erie	0.057 ± 0.03	19
Lake Ontario	0.096 ± 0.03	85

1.2.3 The Great Lakes' Accelerated Warming Trends as a Function of Water Depth

Table 2 shows the warming trend in annual-mean surface water temperature for the years 1995-2012, as well as the average water depth, of each of the Great Lakes, based on the GLSEA satellite data. By comparing its first column, annual-mean surface-water

7

warming trends, with its second column, average water depths, we again note the following tendency among the Great Lakes: the deeper a lake is, the stronger its surface-warming trend is.
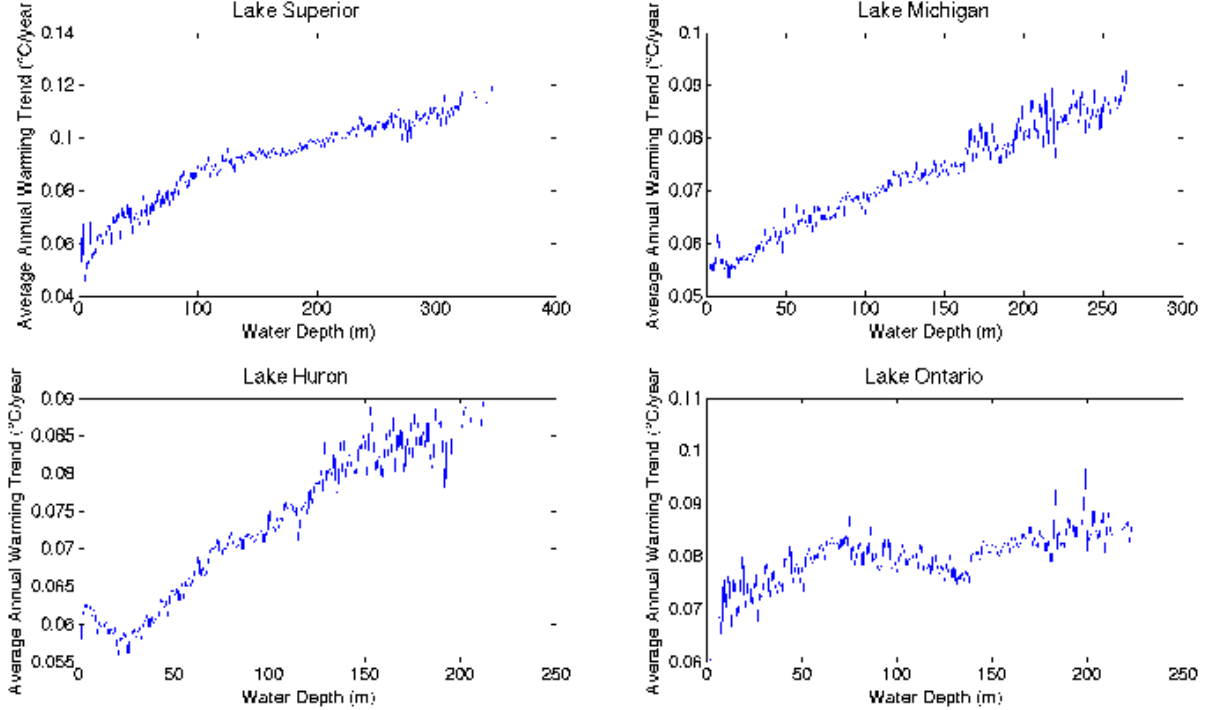
Figure 5: *The average warming trend in annual-mean surface water temperature versus water depth. The horizontal axis is water depth, and the vertical axis is the warming trend in annual-mean surface water temperature for the years 1995-2012, spatially averaged over the surface area whose water depth underneath equals the value on the horizontal axis. (top-left) Lakes Superior, (top-right) Michigan, (bottom-left) Huron, and (bottom-right) Ontario.*

This tendency holds within a single lake as well. The larger water depth is underneath a surface lake point, the stronger the surface-warming trend is at that lake point. Figure 5 shows such a correlation. In Lakes Superior, Michigan, Huron, and Ontario, we clearly see the correlation between water depth and surface-water warming trends (much of Lake Erie is less than 30m deep and hence is not shown).

Figure 6 is a map of warming trends in annual-mean surface water temperature over the Great Lakes, based on the GLSEA satellite data. Figure 7 is the bathymetry of the Great Lakes. The correlation between warming trends in annual-mean surface water temperature and water depth is again apparent. *We want to understand the reason behind*
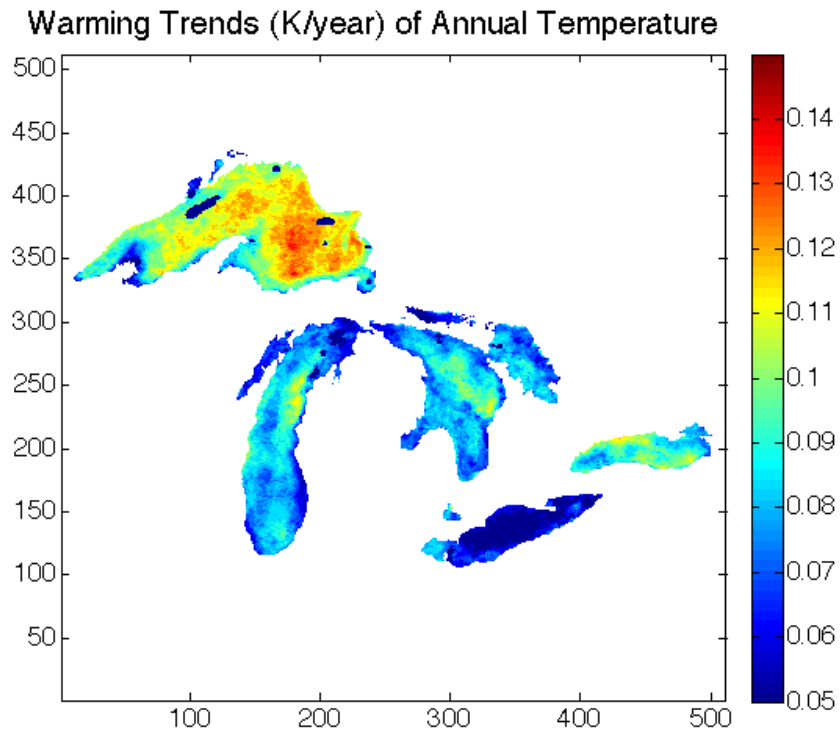
Figure 6: *a map of warming trends in annual-mean surface water temperature over the Great Lakes, based on the GLSEA satellite data, for the years 1995-2012.*
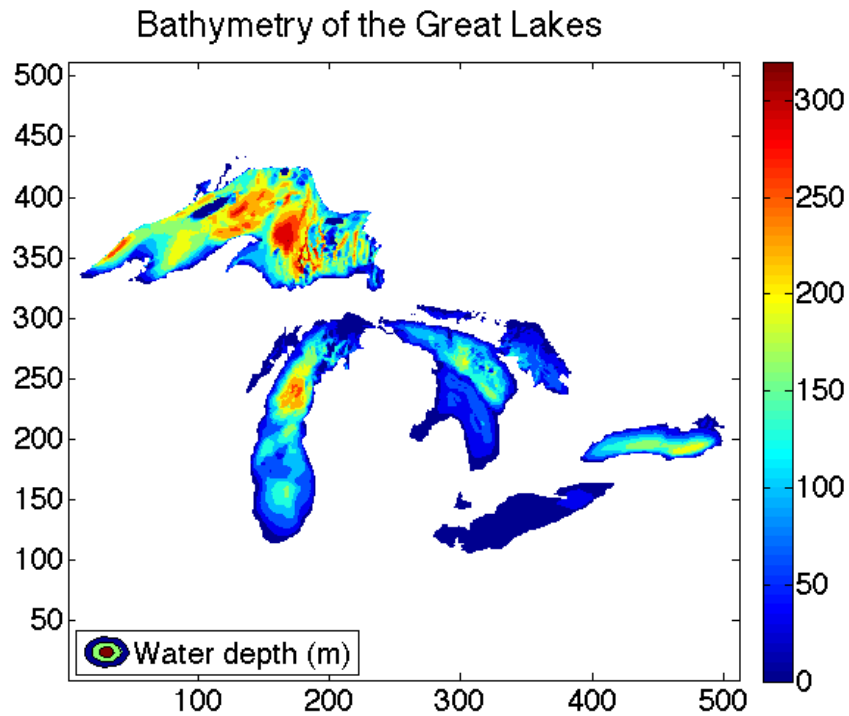
Figure 7: *The bathymetry of the Great Lakes.*

9

1.2.4   Discontinuous Behavior of Deep Lakes
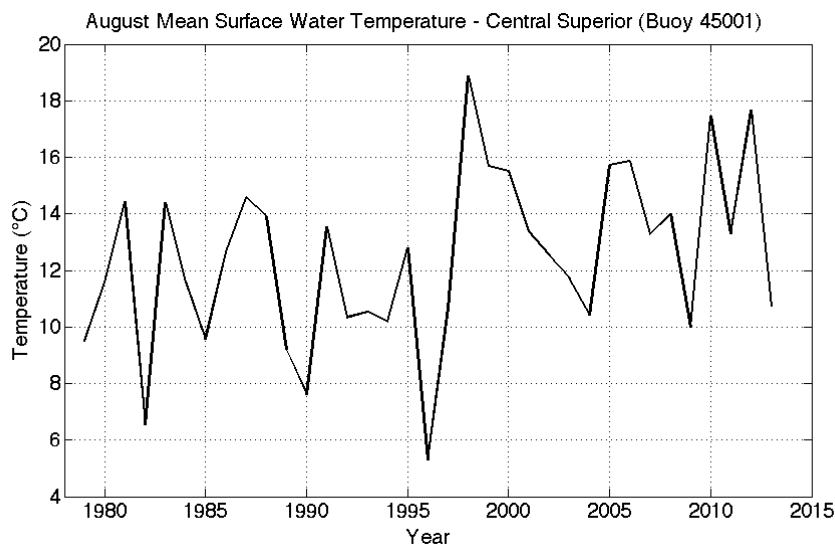
Figure 8: *The August-mean surface water temperature time series of buoy station 45001 in central Lake Superior based on the GLSEA satellite data for the years 1979-2013.*
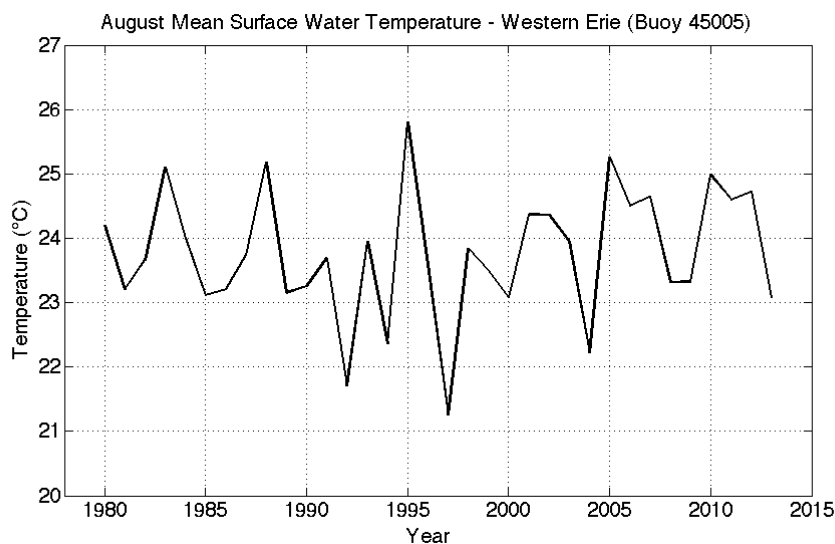
Figure 9: *The August-mean surface water temperature time series of buoy station 45005 in western Lake Erie based on the GLSEA satellite data for the years 1979-2013.*

Not only linear trends in surface water temperature are quantitatively different among lakes of different depth, but also, there exists the following qualitative difference in surface

water temperature time series. Figures 8 and 9 are a comparison of the August-mean surface water temperature time series of buoy station 45001 in central Lake Superior and that of buoy station 45005 in western Lake Erie for the years 1979-2013. What strikes us about the surface water temperature time series of buoy station 45001 in central Lake Superior, is an apparently discontinuous behavior before and after the years 1997-1998. In particular, its August-mean surface water temperature averaged between 1979 and 1997 is $11.0°C$, and that averaged between 1998 and 2013 is $14.1°C$. Between 1979 and 1997, its linear trend is $-0.10°C/year$, and between 1998 and 2013, its linear trend is $-0.12°C/year$. Here, one notices a small negative trend prior to the years 1997-1998, followed by a large jump in the time series at around the years 1997-1998, then followed by another small negative trend after the years 1997-1998. The August-mean surface water temperature time series of Lake Erie, however, lacks such a sudden change. If there exists a physical mechanism behind this qualitative difference between these two time series, then what is it? Lake Superior is a deep lake and Lake Erie is a shallow lake. The water depth below buoy station 45001 is $256m$, and the water depth below buoy station 45005 is $12m$. Does the qualitative difference between their surface water temperature time series have anything to do with lake depth?

Let us take a look at the corresponding August-mean surface water time series of Sparkling Lake, which is located just south of Lake Superior (Figure 1). Figure 10 is the time series. Sparkling Lake is a shallow lake, whose surface area is 64 hectare and maximum depth is $18m$. Just like Lake Erie, it is difficult to find a clearly discontinuous behavior in the time series, despite a general upward trend, whose magnitude is comparable to that of Lake Superior (Lenters 2015, private communication). Lake Erie and Sparkling Lake's temperature time series share common inter-annual characteristics; for example, the August-mean surface water temperatures were significantly higher than their respective longterm mean in 1995 and they were significantly lower in 2004. By contrast, Lake Superior's temperature time series exhibits water temperature only slightly warmer than its longterm mean in 1995 and slightly colder in 2004. Sparkling Lake and Lake Erie are both shallow lakes and do not contain discontinuous behaviors in their
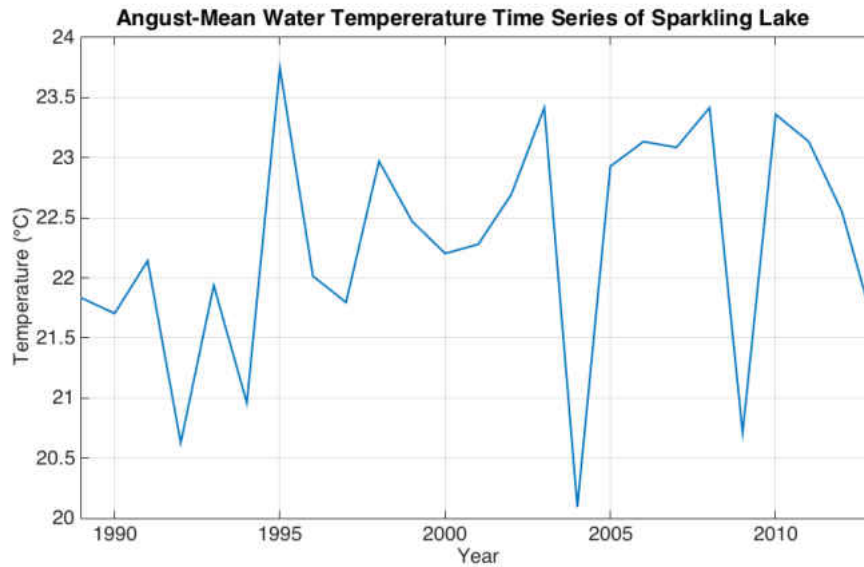
Figure 10: *The August-mean surface water temperature time series of Sparkling Lake, Wisconsin, based on the North Temperate Lakes Long Term Ecological Research program data (https://lter.limnology.wisc.edu/) for the years 1989-2013. The temperature is measured at 1m below the lake surface.*

surface water temperature time series. *What is the source of the qualitative difference between the surface water temperature time series of deep lakes and those of shallow lakes?* If only deep lakes exhibit discontinuous behaviors in their water temperature time series, then why is it so? This is our **Question 3**.

1.2.5 Great Lakes versus Other Lakes in North America

Our Question 3 arises when we compare the summer surface-water warming trend of Lake Erie with that of Sparking Lake. When discussing Question 1 above, we noted the apparent correlation between water depth and surface-water warming trend. Both Lake Erie and Sparkling Lake are shallow lakes. However, the magnitude of the surface-water warming trend of Sparkling Lake is relatively large, comparable to that of Lake Superior, while the magnitude of the surface-water warming trend of Lake Erie is relatively small (Figure 9); in fact, a number of small lakes in California also exhibit strong summer surface-water warming trends (Schneider *et al.*, 2010), comparable to that of Lake Superior. The apparent correlation between water depth and surface-water warming trends

seems to only hold among regions of the Great Lakes. Why does this apparent correlation between water depth and surface-water warming trends seems to hold only among regions of the Great Lakes, but not for Sparkling Lake or lakes in California? *Are different physical mechanisms at work for amplifying surface warming trends of the Great Lakes versus those of smaller lakes? If so, what are they?* This is our **Question 4**.

1.2.6 Correlation between Water Depth and Surface Warming Trends

Another interesting aspect of the annual time series of maximum ice cover over Lake Superior in Figure 3 is the qualitative difference in behavior before and after the years 1997-1998. Just as in the August-mean surface water temperature time series of buoy station 45001 in central Lake Superior we saw in Figure 8, the years 1997-1998 signify a qualitative change in the time series. On the one hand, between the years 1973 and 1997, there were only four winters out of 25 during which the maximum ice cover over Lake Superior was less than 60%. On the other hand, between the years 1998 and 2014, there were only four winters out of 17 during which the maximum ice cover over Lake Superior was more than 60%. *Why are there qualitative similarities between summer surface water temperature time series and winter maximum ice cover time series?* Apparently, the summer surface water temperature of Lake Superior and its winter maximum ice cover are correlated. This correlation is also apparent in Lake Michigan (see, for example, Hanrahan *et al.*, 2010). If the ice-albedo feedback is the only culprit of the amplification of the warming trends of the Great Lakes, then the correlation is a natural consequence of this ice effect. If it is not, then we would want to know the reason for the correlation. This is our **Question 5**.

1.2.7 The Great Lakes Ice Cover Regimes

The discontinuous behaviors both in the August-mean surface water temperature time series at buoy stations in Lake Superior and in the maximum ice cover time series of the
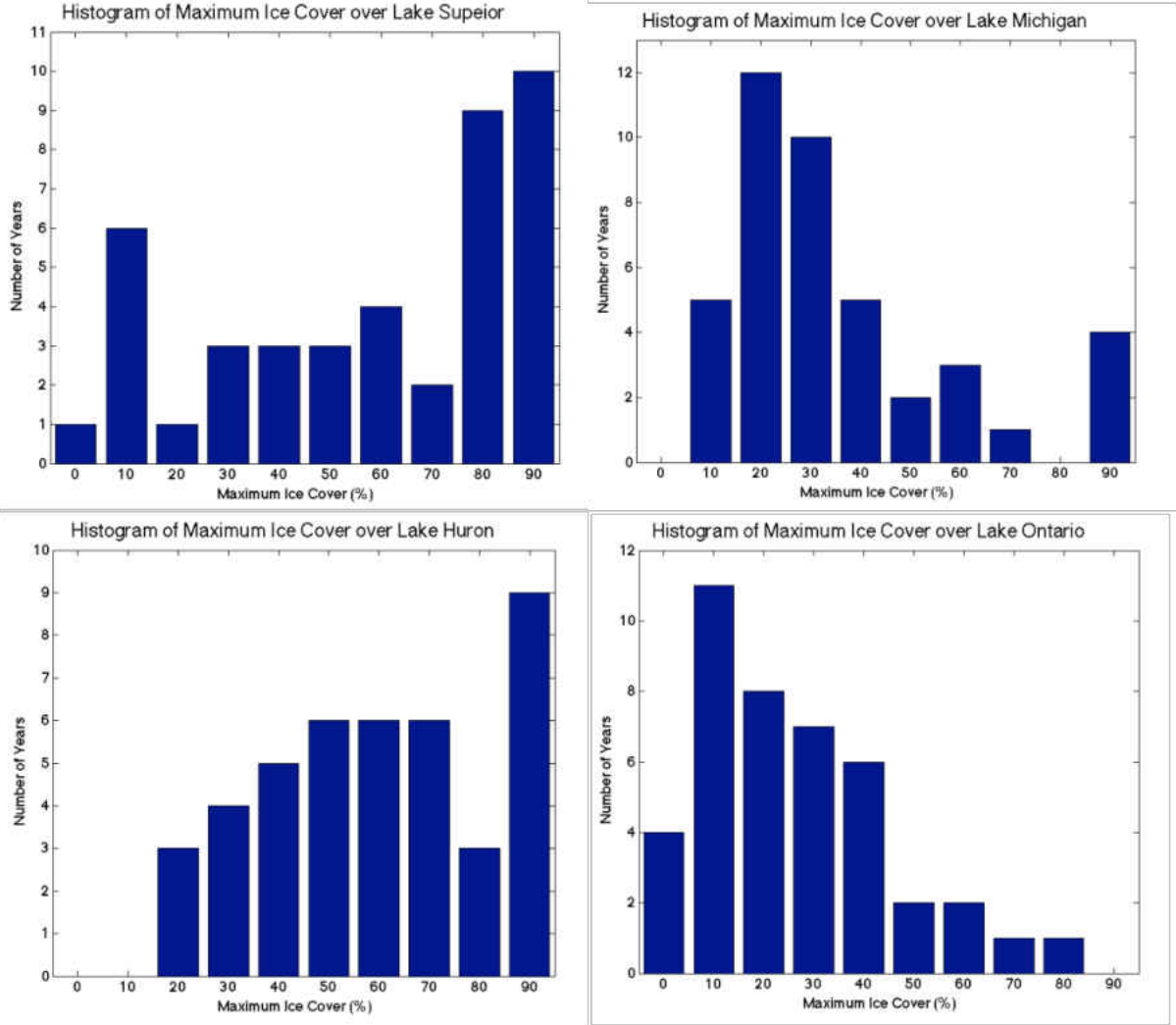
Figure 11: *The histogram of maximum ice cover of Lakes Superior (top-left), Michigan (top-right), Huron (bottom-left), and Ontario (bottom-right) for the years 1973-2014. The vertical axis is the number of winters.*

lake, before and after the years 1997-1998, encourage us to consider the possibility of multiple climate regimes over the lake. Recently, there have been discussions of ice cover regimes of the Great Lakes (for example, see Assel *et al.*, 2003). Figure 11 contains the histograms of maximum ice cover of four of the Great Lakes between the years 1973 and 2014. Multi-modality appears in the histogram for Lakes Superior, the top-left panel of

Figure 11; we note two large peaks of maximum ice cover, one in the 10%-20% slot and the other straddling between the 80%-90% and 90%-100% slots. Our last question to be introduced in this section is: *Is there more than one local-climate regime over Lake Superior? Is there more than one local-climate regime over the Great Lakes?* This is our Question 6.

1.3 Six Questions

Here we list the six questions addressed in the previous section.

(1) Are the ice-albedo feedback and other ice-related feedback effects enough to give rise to the strong surface-water warming trends observed in some of the Great Lakes?

(2) Why are water depth and surface-water warming trends over regions of the Great Lakes correlated?

(3) What is the origin of the qualitative difference between the surface water temperature time series of deep lakes and those of shallow lakes?

(4) Are different physical mechanisms at work for amplifying surface warming trends of the Great Lakes versus those of smaller lakes near Lake Superior and in California? If so, what are they?

(5) Why are the summer surface water temperature of the Great Lakes and their winter maximum ice cover correlated?

(6) Is there more than one local-climate regime over Lake Superior? Is there more than one local-climate regime over the Great Lakes?

We answer these questions in detail later.

1.4   Methodology

We focus our attention to eddy-diffusion-based one-dimensional lake models, namely, modified versions of Hostetler and Bartlein (1990). It is known that many existing one-dimensional models poorly simulate seasonal temperature cycles of deep lakes ($> 200m$). A number of attempts exist to improve versions of Hostetler and Bartlein (1990) by parameterizing unresolved physical processes in the form of "enhanced minimum diffusion" (e.g., Fang and Stephan, 1998; Bennington *et al,*, 2014). We suggest an ad hoc modification to the parametrization of enhanced minimum diffusion. This modification helps identify the start date of summertime thermal stratification of a deep lake better. The importance of the correct identification is as follows. Until summertime thermal stratification starts, the surface water temperature of a deep lake changes only slowly, and once summertime thermal stratification starts, the surface water temperature increases dramatically (for example, see Figure 2). Therefore, correctly estimating the start date of summertime thermal stratification is crucial in estimating the seasonal cycle of a deep lake.

After we develop the necessary tool and present the improvement, we apply the tool to explore the aforementioned questions. We construct a lake-atmosphere-land coupled model. We consider a lake that has a finite number n of lake columns of uniform depth, where n is either 1 or 3. The lake is surrounded by land and overlaid by two layers of atmosphere. Figure 12 is an illustration of the cross-sectional view. For each lake column, we use the aforementioned 1-D lake model to simulate its temperature. Lake columns do not directly interact horizontally. The lake does not directly interact with land. However, the lake exchanges heat with the lower atmosphere at the surface. For an atmospheric model, we consider two layers of atmosphere, the upper and lower, where the upper atmosphere has a uniform temperature and acts as forcing. The lower atmosphere is divided into parts whose boundaries coincide with those of lake columns and land. This
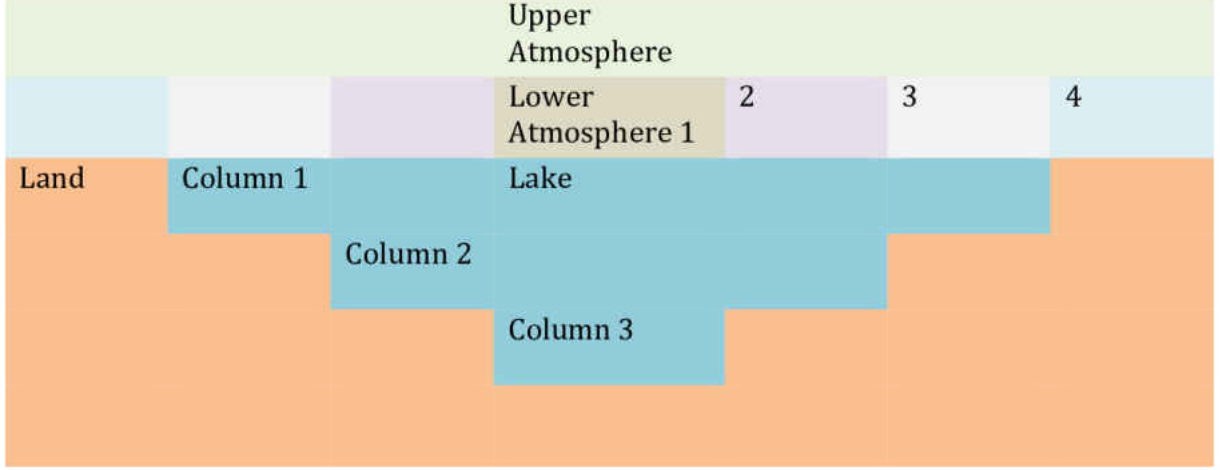
Figure 12: *The illustration of the three-column lake model.*

means that the lower atmosphere is divided into $n + 1$ parts, and we associate each such part with a distinct temperature.

We use this lake-atmosphere-land coupled model to examine the equilibrium states of seasonal cycles of various toy lakes when periodic forcing, which does not contain inter-annual variability, is applied to them. We consider a number of toy lakes whose water depths are comparable to those of the Great Lakes. We consider a range of periodic forcing, from the colder to the warmer, and examine how the temperatures of the equilibrium states of the lakes change as the forcing changes.

We explore the responses of the toy lakes to global warming, by adding the positive $0.04°C/year$ trend to the temperature of the upper atmosphere.

We also consider atmospheric forcing that contains inter-annual variability in the temperature of the upper atmosphere. The inter-annual variability is either stochastic or periodic. With stochastic inter-annual variability, we examine the scatter plots of

surface water temperature versus upper air temperature of various toy lakes. We compare them with corresponding scatter plots based on the observational data of some of the Great Lakes. We choose the data of buoy station 45004, in eastern Lake Superior, as a representative example of a deep lake, and the data of buoy station 45005, in western Lake Erie, as a representative example of a shallow lake.

We discuss cloud feedback on lake-surface warming, and examine atmospheric data of the Great Lakes region to see some evidence of the feedback.

We discuss alternative mechanisms of lake-surface warming as well, especially of shallow lakes. We consider the case of a large-scale positive trend in downward shortwave radiation, by adding the $1W/m^2 year$ trend to our models. We examine if this trend is enough to result in a comparable magnitude of surface-water warming observed in some shallow lakes in California and regions south of the Great Lakes.

We use the Great Lakes Surface Environmental Analysis (GLSEA) data documented by NOAA's Great Lakes Environmental Research Laboratory (GLERL) for surface-water temperatures of the Great Lakes, and the National Centers for Environmental Prediction (NCEP) North American Regional Reanalysis (NARR) data for air temperatures at various pressure levels over North America.

1.5   Structure of Presentation

After we address six outstanding questions as an introduction to the subject in Chapter 1, we first develop a tool to examine these questions in Chapter 2. We introduce a modification to the existing formulas to parameterize unresolved physical processes in the form of enhanced minimum diffusion, first introduced by Fang and Stephan (1998) and later modified by Bennington *et al.* (2014). We present improved results of simulating surface water temperatures at various buoy stations in the Great Lakes, especially those of the deepest Lake Superior.

After presenting the improvement in one-dimensional lake modeling of deep lakes in Chapter 2, we introduce our lake-atmosphere-land coupled model in Chapter 3. We

present results of simulations in the order discussed in Methodology. We introduce the concept of multiple regional-climate regimes in this chapter. We explain how the existence of multiple climate regimes in the eastern part of Lake Superior contributes to the amplification of the surface-water warming trend there.

After presenting results of simulations in Chapter 3, we compare the results with observational data in Chapter 4. We discuss the validity of the hypotheses presented in Chapter 3 by examining the observational data of the Great Lakes.

When a deep lake such as Lake Superior transitions from the colder local-climate regime to the warmer regime, its surface temperature changes noticeably. This sudden change in surface water temperature affect the atmosphere as well. Therefore, after we establish the validity of the multiple local-climate regime hypothesis of deep lakes, we consider atmospheric feedback on these sudden temperature changes. As an example, we examine the cloud feedback that we suspect occurred as a result of the 1997-98 local-climate regime transition of Lake Superior.

After these discussions of the dynamics of the regional climate of the Great Lakes, especially that of the deepest Lake Superior, we turn our attention to shallow lakes in other regions of North America that exhibit comparably strong surface-water warming, and we explore a mechanism, different from the one at work for the Great Lakes, that gives rise to the amplified warming.

We summarize all these results in Chapter 5.

In the appendices that follow, we turn our attention to how changes in the local climate of the Great Lakes affect the climate beyond their local region. In Appendix A, we examine Lake Superior's influence on the atmosphere above the lake. We examine indications that the lake affects the atmosphere high enough for its warming trend to be carried to its downwind regions. In Appendix B, we examine indications of regions downwind of Lake Superior affected by the lake's surface warming. We also examine how the decrease in ice cover over the Great lakes, over Hudson Bay, and over regions southwest of Greenland together, affects the pattern of the atmospheric circulation above the Great Lakes region.

Chapter 2

One-Dimensional Lake–Ice Model

2.1 Advantages and Caveats of One–Dimensional Lake Modeling

When simulating the climate of a region that contains a large lake numerically, one would hope that the regional climate model incorporates a three-dimensional lake model to properly account for the effect of lake circulation on the local climate. However, a 3D lake model is often computationally expensive and a lot of regional-climate models instead use one-dimensional lake models to simulate lakes within a regional-climate system. Therefore, it is important that 1D lake models simulate various thermal properties of a lake well. Most of the existing 1D lake models simulate shallow lakes well, but simulation of surface water temperatures of deep lakes such as those of the deeper regions of the Great Lakes has turned out to be difficult (e.g. Martynov *et al.*, 2010; Subin *et al.*, 2012). As we see later in the thesis, the regions in Lake Superior of the largest water depths possibly influence the overall climate of the Great Lakes region considerably. In some years the surface water temperatures of such regions start sharply increasing in June, and in other years they still hover around at $4°C$ even in mid August. We find indications that this variation is great enough to affect the atmosphere of the Great Lakes region downwind of Lake Superior. The success of regional-climate modeling that contains a large deep lake such as Lake Superior most likely depends on how well the model simulates the surface water temperatures of the deeper regions of the lake. This chapter is devoted to exploring a way to improve a 1D lake model that is computationally inexpensive and can be easily implemented in a regional-climate system.

2.2 Model Formulation

2.2.1 Lake Model

We follow the formulation of a lake model by Hostetler and Bartlein (1990) with modifications. The parameters used as the forcing are the following four: surface air temperature, the amount of downward shortwave radiation at the surface, surface wind speed, and

relative humidity at the surface. Hostetler and Bartlein (1990) is an eddy-diffusion-based finite difference model. The diffusion equation used for the models is based on the method of Henderson-Sellars (1985) as follows.

$$\frac{\partial T}{\partial t} = \frac{\partial}{\partial z}\left\{(k_m + K(z,t))\frac{\partial T}{\partial t}\right\} + \frac{1}{C_w}\frac{\partial \Phi}{\partial z}, \tag{2.1}$$

where T is water temperature, t is time, z is depth from the surface, k_m is the molecular diffusion of water, $K(z,t)$ is eddy diffusivity, C_w is the volumetric heat capacity of water, and Φ is a heat source term. In eddy-diffusion based models, eddy diffusivity parametrizes the amount of mixing of water by surface winds.

The shortwave radiation that penetrates below the surface of the lake is responsible for the heat source term, which is expressed as follows.

$$\Phi = (1 - \beta)SD\mathrm{e}^{-\eta z}, \tag{2.2}$$

where β is the proportion of shortwave radiation absorbed in the very top 0.6m layer, η is the light extinction coefficient of water, and SD is the net shortwave radiation at the surface. Hostetler and Barntlein (1990) follow the assumption by Dake and Harleman (1969) and Ryan and Harleman (1971) that 40% of the net shortwave radiation striking the lake surface is absorbed within the top 0.6m layer. We follow Hakansen (1995), Subin *et al.* (2012), and Bennington *et al.* (2014), and express the light extinction coefficient of water as follows.

$$\eta = 1.19d^{-0.424}, \tag{2.3}$$

where d is the depth in meters of the column of the lake in which the grid cell under consideration is located. The surface boundary condition is

$$(k_m + K(z,t))\frac{\partial T}{\partial z} = SD + LD - LU + SH + LH, \tag{2.4}$$

and the bottom boundary condition is

22

$$(k_m + K(z,t)) \frac{\partial T}{\partial z} = 0, \qquad (2.5)$$

where LD is net longwave radiation absorbed at the lake surface, LU is long-wave radiation emanating from the lake surface, LH is latent heat flux from the atmosphere to the lake, and SH is sensible heat flux from the atmosphere to the lake. As Hostetler and Bartlein (1990) do, we also follow Henderson-Sellers (1985) to determine the value of the diffusion coefficient.

$$K = \frac{4.8 \times 10^{-4} uze^{-k^*z}}{1 + Ri^2}, \qquad (2.6)$$

where Ri is the gradient Richardson number, the parameter k^* is defined as

$$k^* = 6.6(\sin(\phi))^{1/2} u^{-1.84}, \qquad (2.7)$$

where u is the surface wind speed, and ϕ is the latitude of the lake. Henderson-Sellers (1985) parameterize the gradient Richardson number as

$$Ri = \frac{-1 + \sqrt{1 + 40\left(\frac{Nkz}{0.0012u \exp -k^*z}\right)^2}}{20}, \qquad (2.8)$$

where N is the Brunt-Vaisala frequency defined as

$$N = \sqrt{\frac{g}{\rho}\frac{\partial \rho}{\partial z}}, \qquad (2.9)$$

and we follow Heggen (1983) to approximate the density of fresh water, ρ $(kg\ m^{-3})$, as follows.

$$\rho = \left(1 - 1.9549 + 10^{-5}|T_K - 2.77|^{1.68}\right) \times 10^3. \qquad (2.10)$$

where T_K is the water temperature in degrees Kelvin.

Originally, the value of minimum diffusivity, the amount water temperature diffuses without the effects of wind-driven eddy diffusion, was the same as the value of molecular

diffusivity, $1.39 \times 10^{-7} m^2 s^{-1}$. This amount of minimum diffusivity, however, has proved too small, and Fang and Stephan (1998) introduce a formula for minimum diffusivity that better simulates various diffusion processes in deep lakes as follows.

$$k_m = 1.04 \times 10^{-8} \times \left(N^2\right)^{-0.43}. \tag{2.11}$$

This formula is used in regional climate models that incorporate lake modeling as well. For example, the latest version of the Regional Climate Model system (RegCM4), developed by the National Center for Atmospheric Research (NCAR) and maintained by the Abdus Salam International Centre for Theoretical Physics (ICTP), uses this formula in its default model (Bennington *et al.*, 2014). We have found that, however, the amount of minimal diffusivity according to Equation (2.11) is still too weak in winter and spring. Especially at the time of spring overturn when lake temperature is at uniform $4°C$ from the top to the bottom, the model often does not transport heat from the surface to deeper layers as efficiently as we expect. Bennington *et al.* (2014) enhance minimum diffusivity in the default model of RegCM4 by a factor of 1000 when simulating a lake deeper than $50m$, as follows.

$$k_m = 1000 \times 1.04 \times 10^{-8} \times \left(N^2\right)^{-0.43}. \tag{2.12}$$

In this report, we introduce a parameter A as follows.

$$k_m = A \times 1.04 \times 10^{-8} \times \left(N^2\right)^{-0.43}. \tag{2.13}$$

The value of the parameter A at z, the distance from the lake surface, depends on the surface water temperature directly above it, as well as the water depth of the lake column that contains the location, as follows.

$$A = \begin{cases} 1 + 15 \times d \times \exp\left[-(T_{sur} - 3.98)^2/0.5\right] & \text{if } T_{sur} \geq 3.98 \\ 1 + 15 \times d \times \exp\left[-(T_{sur} - 3.98)^2/5.0\right] & \text{if } T_{sur} < 3.98, \end{cases} \tag{2.14}$$

where d is the depth in meters of the lake column in which the grid cell under consideration

is located, and T_{sur} is the surface water temperature in $°C$ of the column. Note that when the surface temperature is equal to $3.98°C$, which is the temperature of water at the time of spring overturn, the value of A is simply $1 + 15d$, the maximum value of A. The motivation here is that we want to capture the vertical mixing of water that occurs at the time of spring overturn by increasing the diffusion coefficient. The deeper a lake is, the greater the vertical mixing of water is at the time of spring overturn. Hence, the value A depends on d, the water depth of the lake column that contains the grid cell in consideration. Once the lake is past the spring overturn and its surface water temperature becomes warmer than $3.98°C$, the overturning of water of the entire lake column is over, and the value of A quickly becomes small. By contrast, when the surface water temperature of the lake is still a couple of degrees below $4°C$, the above formula assumes that the lake undergoes a lot of vertical mixing although not as much as at the time of spring overturn. This assumption is based on observations; the surface water temperatures at buoy stations 45004 and 45001 of Lake Superior, below which the water depth exceeds $200m$, changes very slowly in spring and summer before it reaches $4°C$.

The difference between before and after spring overturn is as follows. Before spring overturn, the lake is below $4°C$ but surface water temperature keeps increasing, albeit slowly. When water at the surface becomes warmer, it starts to sink because it is denser than the water underneath, and this sinking initiates vertical mixing. At the time of spring overturn, the entire lake column is in the neutral buoyancy condition, and the entire lake column is being mixed. Slightly before spring overturn, a large fraction of the entire lake column is in the neutral buoyancy condition, and much of the column is being mixed. Yet before that, a smaller fraction of the lake column is being mixed. Just as the magnitudes of minimum diffusivity in previous eddy-diffusion-based models are too weak for mixing water at the time of spring overturn, we think that they are too weak for mixing water even before spring overturn in much of the lake column where the buoyancy of water is neutral. By contrast, after spring overturn, surface water temperature keeps increasing but this time water at the surface does not sink because it is less dense than the water underneath. Therefore, we think that the "effective" magnitude of minimum

diffusivity quickly drops after spring overturn.

In order to prevent the value of k_m from becoming too large, we let the maximum possible value of k_m be $200m^2day^{-1}$ or $2.3 \times 10^{-3}m^2s^{-1}$. During spring overturn when lake temperature is at uniform $4°C$, the diffusivity of the lake is at this value without wind effects. Martynov *et al.* (2010) find that one-dimensional lake models they selected poorly simulates the temperature of Lake Superior, worst at the time of spring overturn, and one of them is the Hostetler-Bartlein model. They argue that, in this model the value of minimum diffusivity is too small, and that they begin to see some improvement in simulation when they increase the value of minimum diffusivity by a factor of 10^3 or 10^4. This can be achieved in two ways. One is to make the value of the above free parameter A very large, which we do as discussed above. The other is to allow smaller values of N^2 in the same Equation (2.13), thereby increasing the maximum possible value of k_m, which we do as well. When Martynov *et al.* (2010) increases the value of minimum diffusivity by a factor of 10^4, since the original value of k_m is $1.39 \times 10^{-7}m^2s^{-1}$, they have made the maximum possible value of k_m approximately equal to $10^{-3}m^2s^{-1}$. This value is comparable to the above value of $2.3 \times 10^{-3}m^2s^{-1}$ in our model. In our model, this happens only at the location of neutral buoyancy, such as at the time of spring overturn.

Our convective mixing scheme makes a loop from the surface to the bottom of the lake to mix each unstable layer only with a layer above it, but the loop lets the code go through a fixed number of iterations. This does not guarantee complete erasure of instability because mixing is done only with an adjacent layer at each operation. However, by increasing the number of iterations, the lake becomes arbitrarily close to being stable. The sign of the derivative $\partial\rho/\partial z$ could become negative, and when it does we set it equal to 0 to avoid the Brunt-Vaisala frequency becoming an imaginary number.

2.2.2   Ice Model

We use modified versions of the ice models of Semtner (1976), which were originally developed for modeling sea ice. One modification is that, since lake water is made of fresh water but not salt water, we ignore the treatment of brine pockets in the models.

For simplicity, we also ignore the snow component. Instead, when ice thickness becomes larger than $10cm$, we let the surface albedo of the lake be 0.45, which is higher than the albedo of pure ice, assuming that some amount of snow is always on the ice surface, increasing the amount of surface albedo. Between $0cm$ and $10cm$ of ice thickness, the lake surface albedo changes linearly from 0.05 to 0.45.

Semtner (1976) introduces two groups of computational schemes; what he calls the 0-layer model and n-layer models. In the 0-layer model, the conductive flux of ice is expressed as follows.

$$F_S = \frac{K_I (T_B - T_S)}{h_I},\tag{2.15}$$

where F_s is the conductive flux, K_I is the diffusion coefficient of ice, h_I is the ice thickness, T_B is the temperature at the bottom of ice or equivalently that at the top of water, and T_S is the equilibrium surface temperature of the ice. The equilibrium surface ice temperature at time step m is determined by

$$F_s - F_A = 0,\tag{2.16}$$

where F_A is the net heat flux from the ice to the atmosphere, and the ice thickness in the equation is already computed at time step $m - 1$. The change in thickness of ice between time steps m and $m + 1$ is determined by

$$\Delta h = \Delta t \frac{F_B - F_S}{q_I},\tag{2.17}$$

where F_B is the heat flux under ice, q_I is the heat of fusion of ice, and Δt is the time increment. Due to limitation in our computational speed, we use this 0-layer model when ice thickness is too thin for us to use an n-layer model, when ice thickness is between 0cm and 10cm.

In n-layer models, n equally spaced layers are considered, and diffusion equations for ice are introduced as follows.

$$(\rho c)_I \frac{\partial T_k}{\partial t} = K_I \frac{\partial^2 T_k}{\partial z^2}, \tag{2.18}$$

where T_k is the temperature of the k-th layer of ice, $(\rho c)_I$ is the volumetric heat capacity of ice. The relationship between heat fluxes into the ice surface and the equilibrium ice surface temperature is expressed as follows.

$$SD + LD - LU + SH + LH + \frac{K_I(T_1 - T_s)}{h_I/(2n)} = 0. \tag{2.19}$$

Throughout the thesis, we let $n = 4$ and use the 4-layer model. The change in temperature of the top layer of ice at time step m is determined by

$$\Delta T_1 = \Delta t \frac{F_1 - F_s}{(\rho c)_I h_I/n}, \tag{2.20}$$

where F_1 is the conductive flux between the 1st and 2nd layers of ice at time step $m - 1$, F_s is the conductive flux near the top surface of ice at time step $m - 1$, and the ice thickness h_I at time step $m - 1$ is used to compute ΔT_1. The change in temperature of the k-th layer of ice at time step m is determined by

$$\Delta T_k = \Delta t \frac{F_k - F_{k-1}}{(\rho c)_I h_I/n}, \tag{2.21}$$

where $2 \leq k \leq n$, F_k is the conductive flux between the k-th and $k+1$-th layers of ice at time step $m - 1$. The conductive flux near the top surface of ice, F_s, that between the k-th and $k+1$-th layers of ice, F_k, and that near the bottom of ice, F_n, at time step m are computed by

$$F_s = \frac{K_I(T_1 - T_s)}{h_I/(2n)}, \tag{2.22}$$

$$F_k = \frac{K_I(T_{k+1} - T_k)}{h_I/(n)}, \tag{2.23}$$

$$F_n = \frac{K_I \left(T_B - T_n\right)}{h_I / \left(2n\right)}, \tag{2.24}$$

where $1 \leq k \leq n - 1$, T_B is the freezing temperature, and T_s, T_1 through T_n are values at time step m. The change in thickness of ice between time step m and $m + 1$ at the bottom is determined by

$$\Delta h = \Delta t \frac{F_B - F_n}{q_I}, \tag{2.25}$$

where F_B is the heat flux right under ice at time step m and F_1 also at time step m is used. In addition, if the equilibrium surface temperature of ice computed in Equation (2.19) is above the freezing temperature, it indicates that ice is melting at the top. In such a case, we let the surface temperature T_s of ice be equal to the freezing temperature, and we have

$$F_s - F_A \neq 0, \tag{2.26}$$

where F_s is the conductive flux near and right below the top surface of ice and F_A is the net heat flux from the ice to the atmosphere. This difference in heat flux is the energy flux used to melt the ice at the top.

$$\Delta h = \Delta t \frac{F_A - F_s}{q_I}. \tag{2.27}$$

We assume that no shortwave radiation reaches water when ice appears.

2.2.3 Numerical Setup

We use the explicit Euler method for all the simulations. First, we present results when we let the vertical grid spacing be $1m$ in this chapter. After establishing that the vertical grid spacing be $5m$ also gives us comparably good results, we use the $5m$ vertical grid spacing in later chapters. The number of time steps is 2000 per day when $1m$ vertical grid spacing is used, and 200 per day when $5m$ vertical grid spacing is used.

For the initial condition, we start with a lake with uniform temperature of $4°C$ on Julian day 150 of a year for most of the experiments presented in the thesis.

For simulations of seasonal temperature cycles at various buoy stations of the Great Lakes in Chapter 1, the atmospheric parameters for forcing are the following four: surface air temperature, downward shortwave radiation, surface wind speed, and relative humidity. Downward shortwave radiation, surface wind speed, and relative humidity are all based on the National Centers for Environmental Prediction (NCEP) North American Regional Reanalysis (NARR) data. Surface air temperature is based on NOAA's National Data Buoy Center (NDBC) buoy data in spring, summer, and autumn, when such data is available, and is based on the 2m-above-the-surface air temperature data of the NARR reanalysis when the buoy data is unavailable in winter. When we simulate their seasonal cycles of years later than 1990, we start the simulation from Julian day 150 of the year 1980, with the aforementioned initial condition of the uniform temperature of $4°C$.

For all the experiments presented in Chapter 2 and later, the atmospheric parameters for forcing are the following three: surface air temperature, downward shortwave radiation, and surface wind speed. Unlike Chapter 1, relative humidity is set to 0.8. For equilibrium experiments with periodic forcing without inter-annual variability, we start with the aforementioned initial condition of the uniform temperature of $4°C$ on day 150 of a year and discard at least the first six annual cycles. We did not have to discard more than the first ten annual cycles to see the system more or less reaching an equilibrium state. To make hysteresis plots, we initially start with an equilibrium state computed in this manner, and either add the slightly positive linear trend of $0.04°C/year$ or the slightly negative linear trend of $-0.04°C/year$ to the air-temperature forcing. For global-warming experiments, we add the positive linear trend of $0.04°C/year$ to the air-temperature forcing, start with the aforementioned initial condition of the uniform temperature of $4°C$ on day 150 of a year and discard at least the first six annual cycles. Similarly, for experiments with stochastic forcing, we start with the aforementioned initial condition of the uniform temperature of $4°C$ on day 150 of a year and discard the first several annual

cycles.

2.3 Simulation of the Great Lakes Seasonal Temperature Cycles

2.3.1 Examples Simulations with Traditional and Improved Mixing Schemes

We present results of simulating water temperatures below a number of buoy stations in the Great Lakes. First, we present results of simulations with the vertical grid spacing of $1m$.

Figure 13 demonstrates different outcomes between when Equation (2.11 is used and when Equation (2.13 is used as the formula for enhance minimum diffusion.

This figure is about simulating surface water temperature at buoy station 45004 in eastern Lake Superior for the years 1995 (top panel) and 1996 (bottom panel). The blue curves, which are the model-simulated surface water time series with Equation (2.11), are consistent with the results in Martynov *et al.* (2010). Martynov *et al.* (2010) find that the Hostetler and Bartlein lake model often produces more than five months of ice coverage at buoy station 45001 in central Lake Superior, and once ice melts, the surface water temperature jumps up too high, resulting in too early a start of summertime thermal stratification. These are exactly what we see in the blue curves, qualitatively confirming their results. Equation (2.13) is meant to be an improvement of Equation (2.11), and the black curves demonstrate it. The black curves (model-simulated) and green curves (buoy-observed) are much closer to each other than the blue curves. Especially noteworthy is that the model with Equation (2.13) identifies the start date of summertime thermal stratification well, which occurred a few days before day 200 in 1995 and sometime between day 230 and day 240 in 1996. The model still overestimates the duration of ice coverage, but we see some improvements.
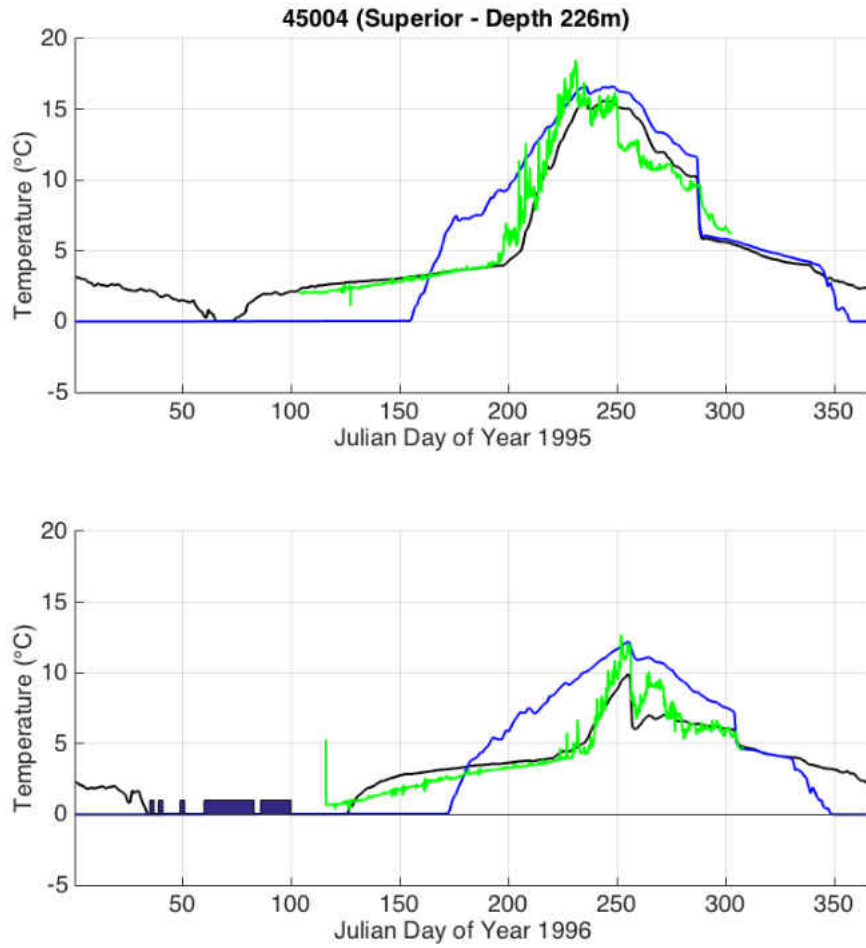
Figure 13: *Results of simulating surface water temperature at buoy station 45004 in eastern Lake Superior for the years 1995 (top panel) and 1996 (bottom panel). Green curves are the buoy-measured surface water temperature time series, black curves are the model-simulated surface water time series with Equation (2.13, blue curves are the model-simulated surface water time series with Equation (2.11, and dark-blue stripes indicate that ice is observed in more than 10% of the vicinity of the buoy station, based on the ice charts on NOAA's GLERL site (http://www.glerl.noaa.gov/data/ice/atlas/). The abscissa is Julian day.*

Simulating the Great Lakes of 1995-1996: Temperatures at Eight Buoy Stations Let us take a look at how this modified version of the Hestetler and Bartlein model simulates surface water temperature at other buoy stations in the Great Lakes. Figure 14 is a result of simulating the surface water temperatures at eight buoy stations in the Great Lakes for the year 1995. Figure 15 is a result of simulating the corresponding surface water temperatures for the year 1996.

One of the most difficult aspects of one-dimensional deep-lake modeling is to estimate

32
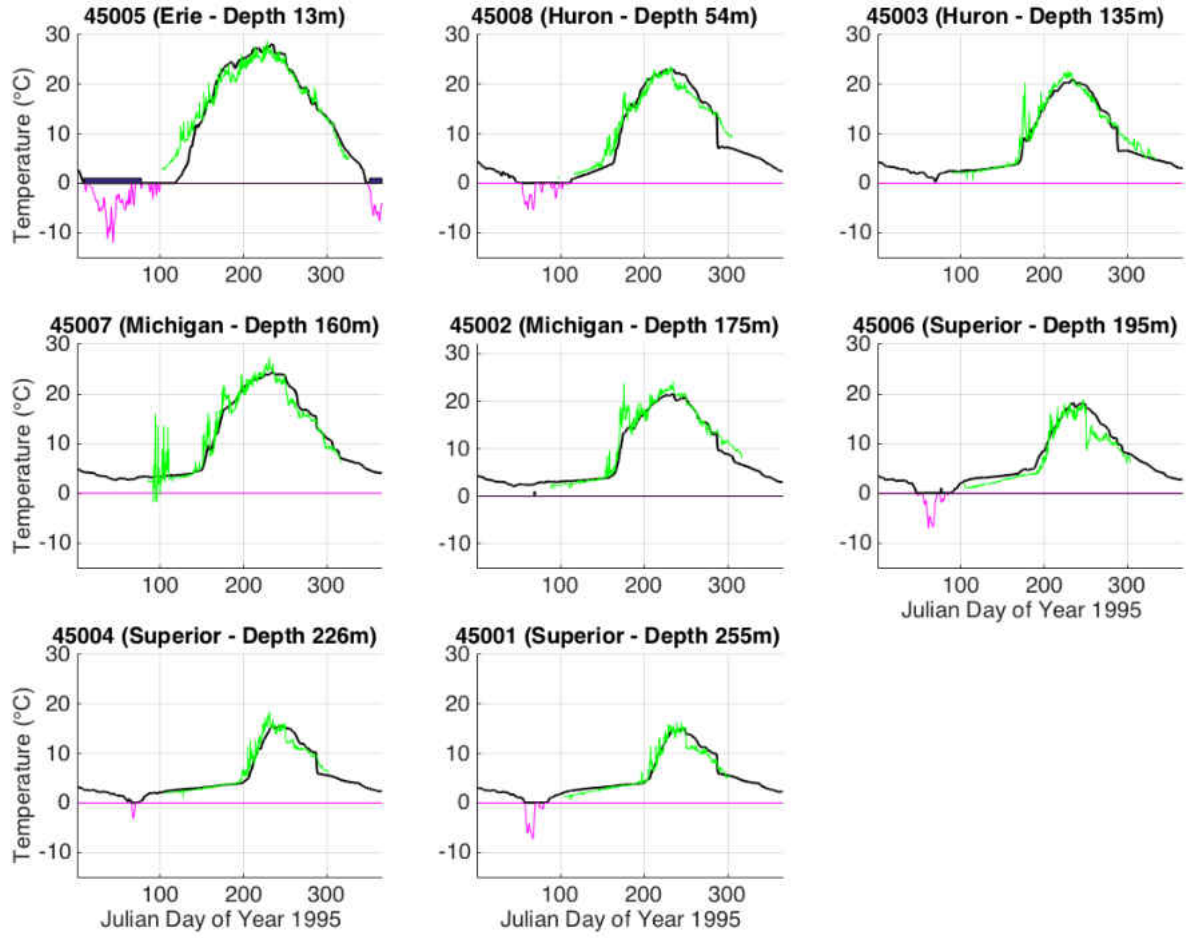
Figure 14: *A result of simulating the surface water temperatures at eight buoy stations in the Great Lakes for the year 1995, with the vertical grid spacing of* $1m$. *Green curves are the buoy-measured surface water temperature time series, black curves are the model-simulated surface water time series with Equation (2.13), and dark-blue stripes indicate that ice is observed in more than 10% of the vicinity of the buoy station, based on the ice charts on NOAA's GLERL site (http://www.glerl.noaa.gov/data/ice/atlas/). The abscissa is Julian day, and the ordinate is surface water temperature in* $°C$.

the start date of summertime thermal stratification (see, for example, Martynov *et al.*, 2010, and Subin *et al.*, 2012). However, until summertime thermal stratification starts, the surface water temperature of a deep lake changes only slowly, and once summertime thermal stratification starts, the surface water temperature increases dramatically. Therefore, correctly estimating the start date of summertime thermal stratification is crucial in estimating the seasonal cycle of a deep lake. As seen in Figures 14 and 15, our model estimates the beginning of summertime thermal stratification relatively well.
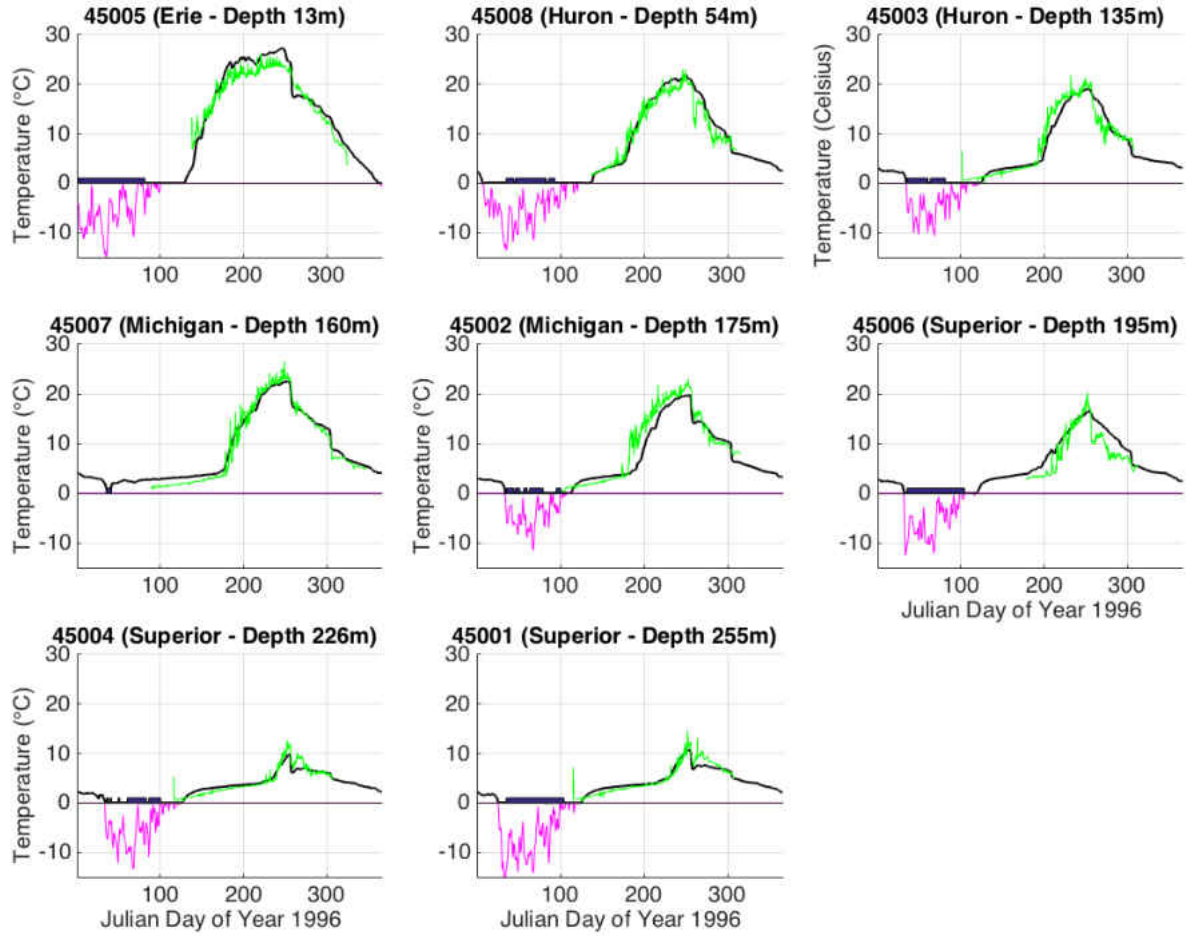
Figure 15: *A result of simulating the surface water temperatures at eight buoy stations in the Great Lakes for the year 1996, with the vertical grid spacing of* 1m. *Green curves are the buoy-measured surface water temperature time series, black curves are the model-simulated surface water time series with Equation (2.13), and dark-blue stripes indicate that ice is observed in more than 10% of the vicinity of the buoy station, based on the ice charts on NOAA's GLERL site (http://www.glerl.noaa.gov/data/ice/atlas/). The abscissa is Julian day, and the ordinate is surface water temperature in* °C.

2.3.2 Comparison with Three-Dimensional Lake Model Simulations

How are these results compared with some results of three-dimensional lake models? A representative example of 3D lake modeling of Lake Superior is in White *et al.* (2012). White *et al.* (2012) contain a figure of surface water temperature time series for the year 2005 at three buoy stations, in eastern, central, and western Lake Superior respectively, both buoy-observed and 3D-simulated. Figure 16 is the corresponding figure by our 1D

model.
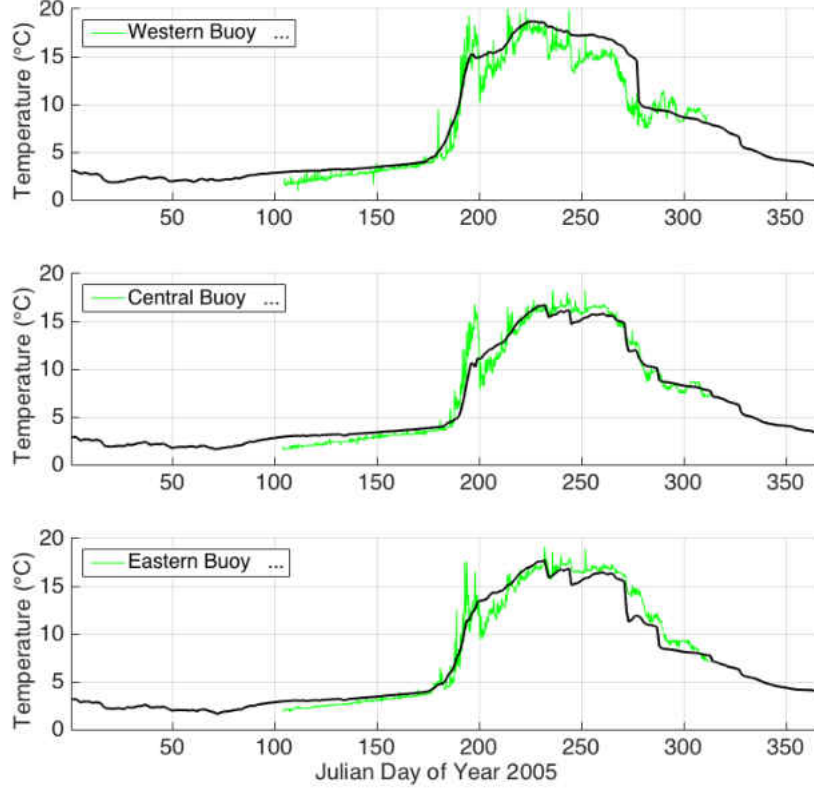
Figure 16: *The surface water temperature time series of the year 2005 at three buoy stations, 45006 in western Lake Superior (top), 45001 in central Lake Superior (center), and 45004 in eastern Lake Superior (bottom), both buoy-observed (green curves) and 1D-simulated (black curves). The abscissa is Julian day, and the ordinate is surface water temperature in °C.*

We note that our results are as good as theirs. This makes us wonder, "Why does our new formula for minimum diffusion 'mimic' the effect of 3D lake circulation well?" More research is necessary to explore the physics behind wintertime mixing of water in a deep lake. Why is the surface water temperature of a deep lake point in Lake Superior colder than $4°C$ sometimes even in early August (for example, see the bottom-left panel of Figure 15)? Results in White *et al.* (2012) indicate that it is due to 3D lake circulation, while our results indicate that we could instead consider an additional amount of wintertime vertical mixing, "effectively" mimicking the role of the physics behind it, that produces rather similar results.

When simulating a deep lake with a one-dimensional lake model, estimating the pe-

35

riod of ice appearance is as vexing as estimating the start date of summertime thermal stratification (see, for example, Martynov *et al.*, 2010). When ice appears, it tends to persist longer than is observed. This problem persists in our lake model as well. Comparing purple curves with dark-blue bands, both Figures 14 and 15 show the model's overestimate of ice duration when ice appears. Results in White *et al.* (2012) indicate that 3D modeling does better jobs. This indicates that 3D circulation might be an important factor for the period of ice appearance of a large lake.

2.3.3   Comparison of 1m versus 5m Vertical Grid Spacing

We find that even when we use $5m$ as the vertical grid spacing, we obtain relatively good results of surface-water-temperature simulation. Figure 17 is a result of simulating the surface water temperatures at eight buoy stations in the Great Lakes for the year 1995, with $5m$ of vertical grid spacing. Figure 18 is a result of simulating the corresponding surface water temperatures for the year 1996.

These two figures demonstrate that grid spacing as large as $5m$ can estimate the surface water temperature of a deep lake relatively well. This is convenient for regional-climate modeling, suggesting that lake models incorporated in a larger regional-climate model do not have to have grid spacing as small as $1m$, which is more computationally expensive. Throughout later chapters, we use $5m$ as the vertical grid spacing for our lake models. A result of simulating the temperature profile at depth below buoy station 45002, in northern Lake Michigan, for the year 1996 in Figure 2 is an example with the $5m$ vertical grid spacing.

2.3.4   Summary

Although a number of three-dimensional lake models are available today, many regional climate models still incorporate 1-D lake models for convenience. It is known that many existing one-dimensional models poorly simulate seasonal temperature cycles of deep lakes ($> 200m$). A number of attempts exist to improve versions of Hostetler and Bartlein (1990) by parameterizing unresolved physical processes in the form of "enhanced mini-
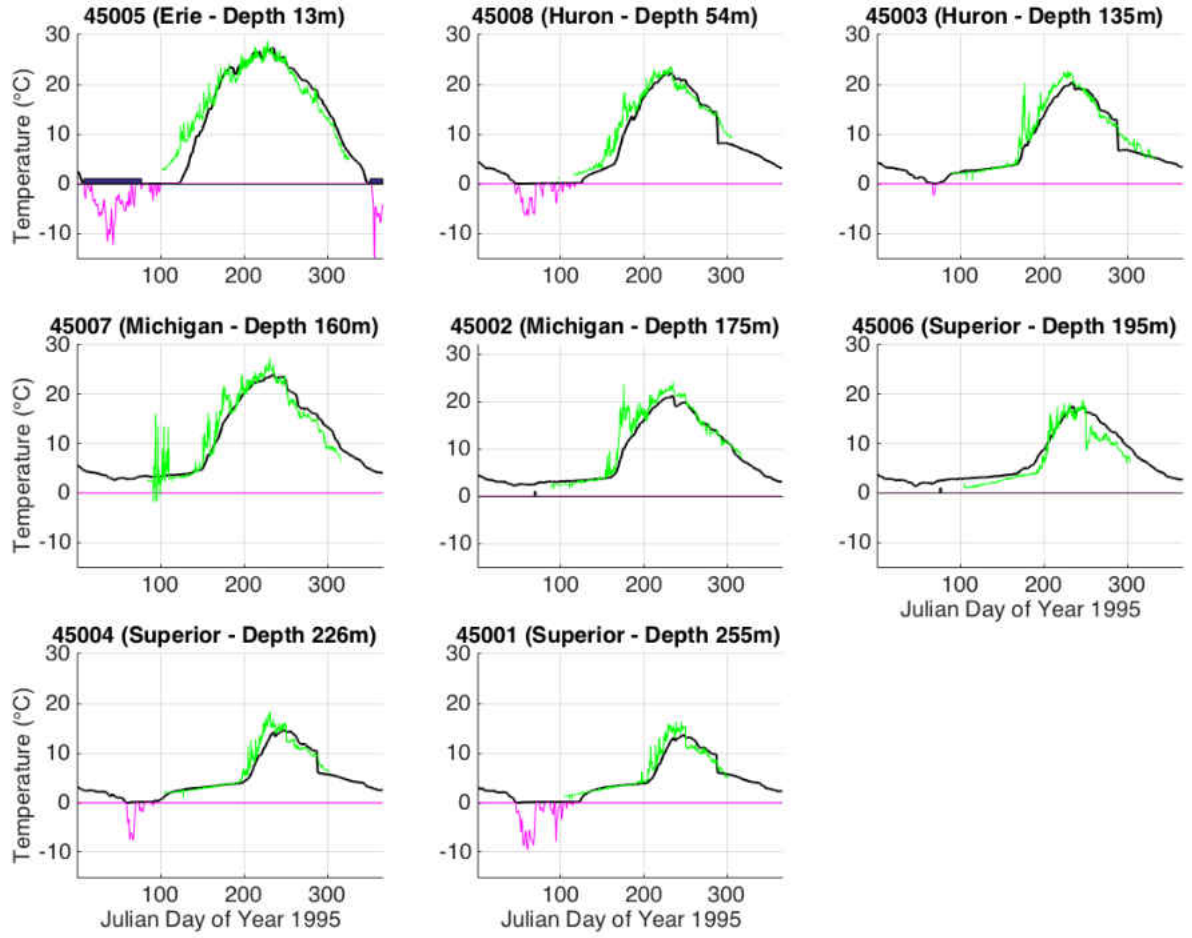
Figure 17: *A result of simulating the surface water temperatures at eight buoy stations in the Great Lakes for the year 1995, with the vertical grid spacing of 5m. Green curves are the buoy-measured surface water temperature time series, black curves are the model-simulated surface water time series with Equation (2.13), and dark-blue stripes indicate that ice is observed in more than 10% of the vicinity of the buoy station, based on the ice charts on NOAA's GLERL site (http://www.glerl.noaa.gov/data/ice/atlas/). The abscissa is Julian day, and the ordinate is surface water temperature in °C.*

mum diffusion" (e.g., Fang and Stephan, 1998; Bennington *et al.*, 2014). We suggested a modification to the parametrization of unresolved physical processes and found improvement in estimating the seasonal cycles at various buoy stations in Lake Superior, the deepest of the Great Lakes. We also found improvement in estimating the start date of summertime thermal stratification below various buoy stations in Lake Superior. Correctly estimating the start date of summertime thermal stratification is crucial in estimating the seasonal cycle of a deep lake because the rate of increase in surface water

37
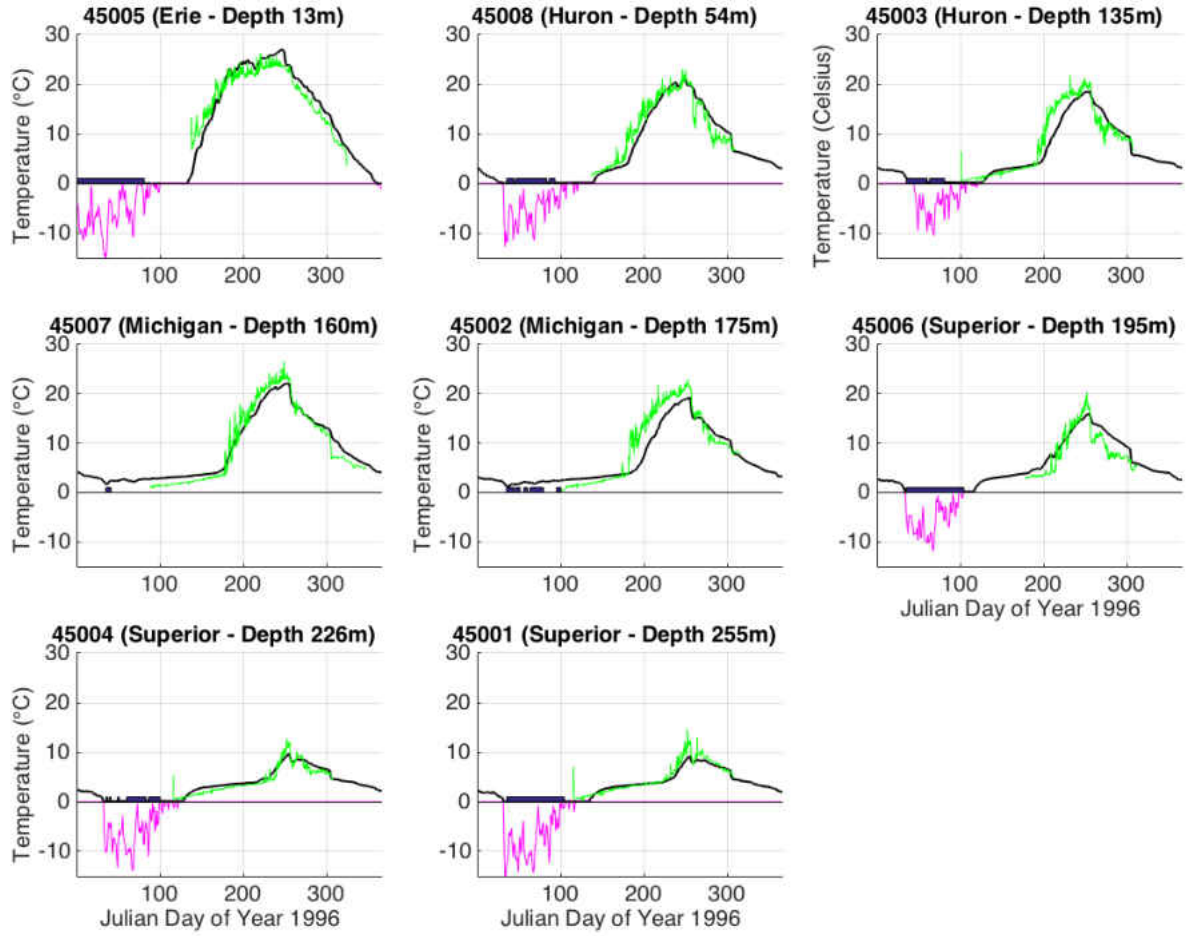
Figure 18: *A result of simulating the surface water temperatures at eight buoy stations in the Great Lakes for the year 1996, with the vertical grid spacing of 5m. Green curves are the buoy-measured surface water temperature time series, black curves are the model-simulated surface water time series with Equation (2.13), and dark-blue stripes indicate that ice is observed in more than 10% of the vicinity of the buoy station, based on the ice charts on NOAA's GLERL site (http://www.glerl.noaa.gov/data/ice/atlas/). The abscissa is Julian day, and the ordinate is surface water temperature in °C.*

temperature changes dramatically before and after spring overturn.

We found that simulations of surface water temperature at various buoy stations in Lake Superior with our one-dimensional lake model was as good as those with three-dimensional lake models in the literature (e.g., White *et al.*, 2012). The reason for this remains to be explored.

We found that the vertical grid spacing of 1*m* and that of 5*m* result in comparable results for simulation of seasonal surface-temperature cycles of deep lakes. This is

convenient for regional-climate modeling that simulates a climate system containing a deep lake, since simulation with the $1m$ vertical grid spacing is more computationally expensive.

Chapter 3

Multiple Climate Regimes and Accelerated Warming Trends in Lake–Atmosphere–Land Coupled Models

3.1 Lake-Atmosphere-Land Coupled Model

3.1.1 Lake-Atmosphere-Land Coupling in Multi–Column Models

Here we introduce a lake-atmosphere-land coupled model. We consider a lake that has a finite number n of lake columns of uniform depth, where n is either 1 or 3. The lake is surrounded by land and overlaid by two layers of atmosphere. Figure 12 is a cross-sectional view of such a system for a three-column lake. The aerial views of a uniform-depth lake and a three-column lake are shown in Figure 19.
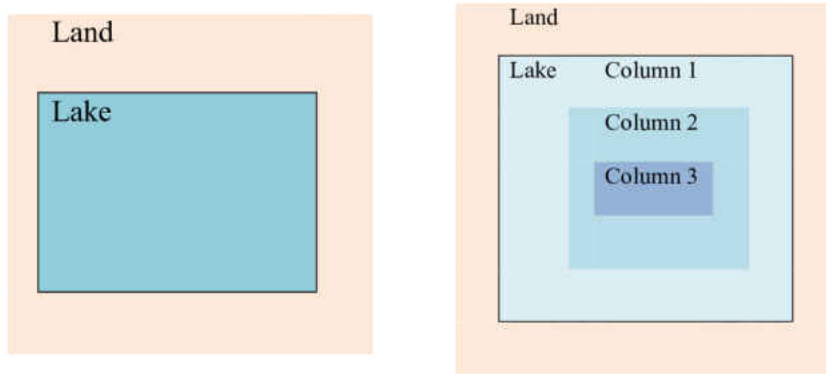
Figure 19: *The boundaries of lake and land regions for the $n = 1$ uniform-depth lake model (left) and the $n = 3$ three-column lake model.*

For each lake column, we use the 1-D lake model described in Part 1. Lake columns do not directly interact horizontally. The lake does not directly interact with land, and the bottom of the lake is closed by the Neumann boundary condition $\partial T/\partial z = 0$. However, the lake exchanges heat with the lower atmosphere at the surface. For an atmospheric model, we consider two layers of atmosphere, the upper and lower, where the upper atmosphere has a uniform temperature and acts as forcing. The lower atmosphere is divided into parts whose boundaries coincide with those of lake columns and land. So, the lower atmosphere is divided into $n + 1$ parts, and we associate each such part with a distinct temperature.

For the simple one-dimensional $n = 1$ (uniform-depth) lake model, the lower atmosphere is coupled to the lake and the land that surrounds the lake by the following energy balance.

$$0 = L_{down} - L_{out} + L_{up,s} - SH_s - LH_s + HT_{ws}/area_s, \qquad (3.1)$$

$$0 = L_{down} - L_{out} + L_{up,w} - SH_w - LH_w - HT_{ws}/area_w, \qquad (3.2)$$

where L_{down} is longwave radiation coming from the upper atmosphere and absorbed by the lower atmosphere, L_{out} is longwave radiation by and emanating from the lower atmosphere, $L_{up,s}$ is longwave radiation coming from the land surface and absorbed by the lower atmosphere, $L_{up,w}$ is that coming from the lake surface and absorbed by the lower atmosphere, SH_s is sensible heat flux from the lower atmosphere to the land, SH_w is sensible heat flux from the lower atmosphere to the lake, LH_s is latent heat flux from the lower atmosphere to the land, LH_w is latent heat flux from the lower atmosphere to the lake, $area_w$ is the area of the lake, HT_{ws} is the transfer of heat between the parts of the lower atmosphere above the lake and above the surrounding land, $area_w$ is the surface area of the lake, and $area_s$ is the surface area of surrounding land. We let the overall surface area of the lake be $8 \times 10^4 km^2$, which is comparable to the surface area of Lake Superior. We let the surface area of the surrounding land be adjustable. The transfer of heat, HT_{ws}, between the two parts of the lower atmosphere, the one above w (water, lake) and the other above s (soil, land), is proportional to the temperature difference between them, and the coefficient for the efficiency of the transfer, $coef_{air}$, is an adjustable parameter:

$$HT_{ws} = coef_{air} \times circ_{ws} \times h_{air} \times (Ta_w - Ta_s), \qquad (3.3)$$

where $coef_{air}$ is the coefficient for the efficiency of atmospheric heat transfer between the adjacent parts of the lower atmosphere, $circ_{ws}$ is the length of the boundary between the two adjacent parts (Figure 19), h_{air} is the height of the lower atmosphere, Ta_w is lower

42

air temperature above the lake, and Ta_s is lower air temperature above the surrounding land. We let $coef_{air} = 500W/m^2\,^\circ C$ and $h_{air} = 2km$ as default values.

The sensible and latent heat fluxes are determined by bulk aerodynamic formulas. To compute these fluxes, we assume for simplicity that wind speed over lake varies sinusoidally from $5m/s$ in summer to $10m/s$ in winter and wind speed over land is even more simply a constant 5m/s. Prinsenberg and Peterson (2002) note that the value of 2.8×10^{-3} is used for the surface drag coefficient over ice by many ice-ocean modelers to forecast ice drift along the Canadian east coast and that the atmospheric model used in the Canadian Meteorological Centre (CMC) uses the value of 1.9×10^{-3}. Here we use 2.0×10^{-3} for the surface drag coefficient over ice. We use 1.0×10^{-3} for the surface drag coefficients over land and water. Longwave radiation emitted by a body (atmosphere, lake, and land) is approximated by the Stephan Boltzmann law. The emissivities of the atmosphere, water, ice, and land are 0.85, 0.97, 0.97, and 0.96, respectively.

For the three-column lake model, the lower atmosphere is coupled to the lake and the land that surrounds the lake by the following energy balance.

$$0 = L_{down} - L_{out} + L_{up,s} - SH_s - LH_s + HT_{w1s}/area_s, \qquad (3.4)$$

$$0 = L_{down} - L_{out} + L_{up,w1} - SH_{w1} - LH_{w1} + (HT_{w2w1} - HT_{w1s})/area_{w1}, \qquad (3.5)$$

$$0 = L_{down} - L_{out} + L_{up,w2} - SH_{w2} - LH_{w2} + (HT_{w3w2} - HT_{w1w2})/area_{w2}, \qquad (3.6)$$

$$0 = L_{down} - L_{out} + L_{up,w3} - SH_{w3} - LH_{w3} - HT_{w2w3}/area_{w3}, \qquad (3.7)$$

where the labels $w1$, $w2$, and $w3$ denote the near-shore, intermediate, and offshore columns of the lake, s the surrounding land, and the other symbols are the same as

43

in the previous paragraph. For example, $L_{up,w3}$ is longwave radiation coming from the offshore lake column and absorbed by the lower atmosphere, HT_{w2w3} is the transfer of heat between the parts of the lower atmosphere above the intermediate and off-shore lake columns, etc. The transfer of heat between two parts of the lower atmosphere is proportional to the temperature difference between them, and the coefficient for the efficiency of the transfer is adjustable.

Similar to uniform-depth lakes, the magnitude of atmospheric transfer of heat between two adjacent parts i and j of the lower atmosphere, HT_{ij}, is given by the following expression:

$$HT_{ij} = coef_{air} \times circ_{ij} \times h_{air} \times (Ta_j - Ta_i), \tag{3.8}$$

where $coef_{air}$ is the universal parameter for the efficiency of atmospheric heat transport between any adjacent parts of the lower atmosphere, $circ_{ij}$ is the length of the boundary between the two adjacent parts i and j, h_{air} is the height of the lower atmosphere (Figure 19), Ta_i is the air temperature of the part i of the lower atmosphere, and Ta_j is the air temperature of the part j of the lower atmosphere.

For either $n = 1, 3$ lake model, we assume that all the sensible and latent heat fluxes are absorbed by the lower atmosphere and do not escape to the upper atmosphere by convection or other means. The boundary condition between the lower atmosphere and the land surface is as follows.

$$0 = SD_s + LD_s - LU_s + SH_s + LH_s, \tag{3.9}$$

where SD_s is shortwave radiation absorbed at the land surface, LD_s is downward longwave radiation absorbed at the land surface, LU_s is longwave radiation emitted by the land surface, SH_s is sensible heat flux from the lower atmosphere to the land, and LH_s is latent heat flux from the lower atmosphere to the land. For the three-column lake model, we have three equivalent equations for the boundary conditions for each of the three lake columns. When computing SD_w, shortwave radiation absorbed at a lake sur-

face, we assume the albedo of water to be 0.05. Depending on how much snow or no snow is present over ice, the albedo of a lake can vary. However, since our models do not consider separately ice and snow that might cover the ice, we set the albedo of the ice/snow combination to be a constant; we choose 0.45 as a default value, larger than the albedo of pure ice. Again, the sensible and latent heat fluxes are determined by bulk aerodynamic formulas.

In more realistic situations, as surface lake temperature reacts to a linear trend in the forcing, surface wind speed would react to the reaction of the surface lake temperature as well. However, we mainly focus on the effect of a warming trend of the upper-atmosphere temperature on a lake without further complications, and assume that other atmospheric parameters such as wind speed do not acquire a linear trend as a reaction to a linear trend in the forcing.

3.1.2 Three-Column Lakes

When $n = 3$, the lake has three distinct lake columns. We use this three-column lake to analyze the relationship between surface-water warming trends and water depth within a single lake as well as among lakes of different water depth.

Table 3: *The properties of each column of the toy Lake 1 model.*

Lake 1	Depth (m)	Proportional Area
Column 1	50	0.1
Column 2	150	0.5
Column 3	225	0.3
Land	-	0.1

Table 4: *The properties of each column of the toy Lake 2 model.*

Lake 2	Depth (m)	Proportional Area
Column 1	30	0.2
Column 2	80	0.5
Column 3	140	0.2
Land	-	0.1

Table 5: *The properties of each column of the toy Lake 3 model.*

Lake 3	Depth (m)	Proportional Area
Column 1	30	0.3
Column 2	60	0.3
Column 3	100	0.3
Land	-	0.1

Table 6: *The properties of each column of the toy Lake 4 model.*

Lake 4	Depth (m)	Proportional Area
Column 1	15	0.4
Column 2	20	0.4
Column 3	40	0.1
Land	-	0.1

Tables 3 through 6 show the water depth and proportional surface area of each of toy lake models used to analyze the Great Lakes. By varying the average depths of three-column lakes, they serve as toy models of the Great Lakes.

Water Depths of the Great Lakes and Toy Models   Table 7 shows how the water depth of each toy lake is compared with that of the corresponding lake. For example, the mean depth of Lake 1 is $164m$, which is comparable to the mean depth of Lake Superior, and the mean depth of Lake 4 is $20m$, which is comparable to the mean depth of Lake Erie.

Table 7: *Comparisons of the mean depths of the Great Lakes and those of the corresponding toy lakes.*

Toy Model	Mean Depth (m)	Great Lakes	Mean Depth (m)
Lake 1	164	Lake Superior	147
Lake 2	82	Lake Michigan	86
Lake 3	63	Lake Huron	59
Lake 4	20	Lake Erie	19

Downward Shortwave Radiation on the Great Lakes and Toy Models   Among the variables of atmospheric forcing: temperature of the upper atmosphere, downward shortwave radiation, and wind speed at the surface, we use the same time series of sur-

face wind speed for all the above three-column lakes. The longterm mean of downward shortwave radiation in each of the above toy lakes models is compared with that of the corresponding lake in Table 8.

Table 8: *Comparisons of the longterm means of downward shortwave radiation above various buoy stations in the Great Lakes based on the NARR reanalysis data for the years 1979-2013 and the chosen longterm means for the corresponding toy lakes. The units are in W/m^2.*

Great Lakes	shortwave radiation
Buoy 45001 (Lake Superior)	181
Buoy 45007 (S. Lake Michigan)	201
Buoy 45002 (N. Lake Michigan)	191
Buoy 45003 (Lake Huron)	185
Buoy 45012 (Lake Ontario)	184
Buoy 45005 (Lake Erie)	199
Lake 1	175
Lake 2	190
Lake 3	180
Lake 4	195

3.2   Multiple Climate Regimes

3.2.1   Multiple Stable Equilibrium States of Seasonal Cycles of Uniform-Depth Lakes

Uniform-Depth Models   In this section, we explore the possibility of the existence of multiple local-climate regimes of a lake, based on model results. Before we consider three-column lakes, let us discuss lakes of uniform depth. Uniform-depth lakes are simpler than multi-column lakes, and results of uniform-depth lakes form a basis to understand more complicated multi-column lakes and more realistic lakes. When we discuss multiple local-climate regimes of lakes of uniform depth, we mean the following two regimes: the warmer regime is associated with ice-free winters, and the colder regime is associated with ice-covered winters, given identical atmospheric forcing to both. Let us take a look at model results. In this section, the forcing is all periodic except that the temperature

of the upper atmosphere has a linear trend of $\pm 0.04°C/year$. The following lists all the forcing and the behaviors of the forcing, whether periodic or constant, whether or not there is a non-zero linear trend.

List of Forcing	
Temperature of the upper atmosphere	periodic + linear trend of $\pm 0.04°C/year$
Downward shortwave radiation	periodic
Surface wand speed	periodic
Surface relative humidity	constant

The periodic part of the temperature of the upper atmosphere is given by,

$$T_{au}(t) = \overline{T} + 16\cos(2\pi\frac{t-180}{365}), \qquad (3.10)$$

where time t is expressed in days and $\overline{T}$ denotes its annual-mean in $°C$. The periodic part of downward shortwave radiation is given by

$$SW(t) = \overline{SW} + 125\cos(2\pi\frac{t-172}{365}), \qquad (3.11)$$

where time t is expressed in days and $\overline{SW}$ denotes its annual-mean in W/m^2. For uniform-depth lakes, we set $\overline{SW} = 175$, which is comparable to the amount of downward shortwave radiation in the Great Lakes region (Table 8). The periodic part of surface wind speed is given by

$$u(t) = 7.5 - 2.5\cos(2\pi\frac{t-195}{365}), \qquad (3.12)$$

where the unit is m/s. The phase shift in the formula of downward shortwave radiation is made so that the radiation reaches its maximum value on June 21st, but the phase shifts in the formulas of the other two quantities are somewhat arbitrary, except that surface wind speed reaches its maximum value in winter and that of upper air temperature in summer. In this chapter and afterward, we keep relative humidity as a constant. The relative humidity at the lake and land surfaces is set to 0.8. With this atmospheric

forcing, we construct the hystereses of summer maximum heat content and summer maximum water temperature of lakes of uniform depth. To make such hystereses, the linear trend of $+0.04°C/year$ is added to the periodic seasonal temperature cycle of the upper atmosphere when we want to slowly increase upper air temperature, and the linear trend of $-0.04°C/year$ is added to the periodic temperature of the upper atmosphere when we want to slowly decrease it.

We let the ratio of the surface area of the lake to that of surrounding land be 7:3.
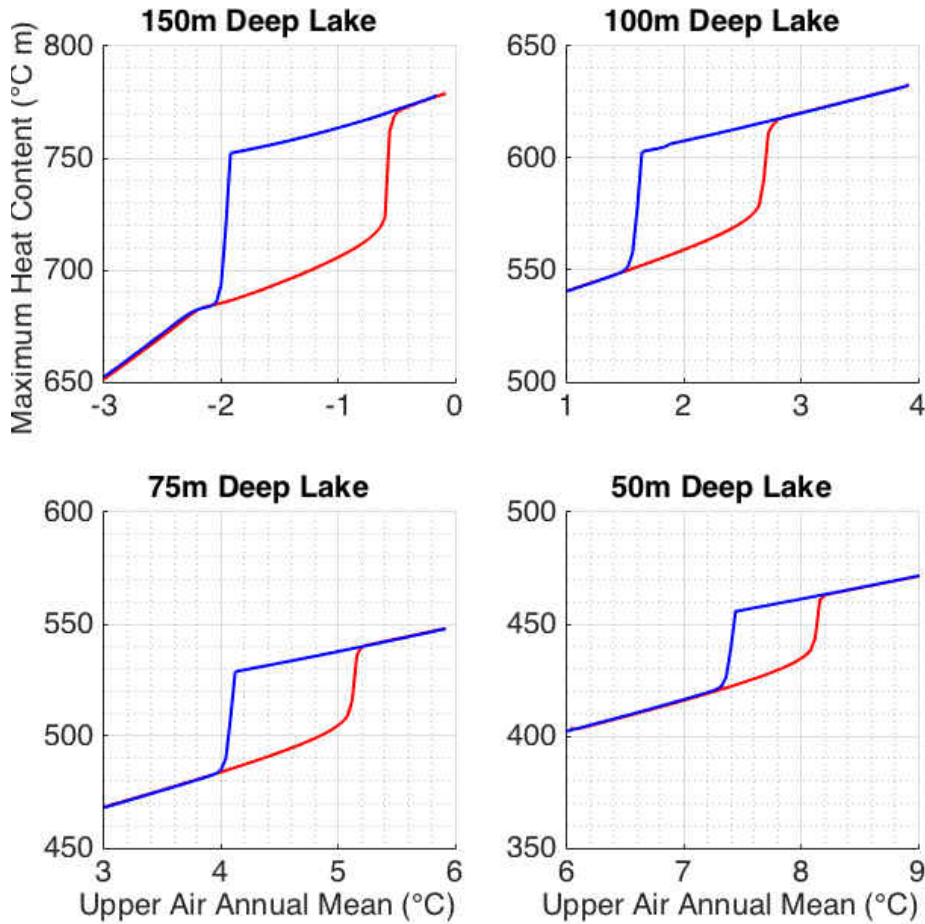
Figure 20: *The hysteresis of summer maximum heat content of the lake of the following depth: 50m, 75m, 100m, and 150m. The abscissa is the annual-mean of periodic upper air temperature, which acts as forcing. The ordinate is summer maximum heat content. The units are in °Cm.*

Hysteresis of Summer Maximum Heat Content of Uniform-Depth Lakes Figure 20 contains the hystereses of summer maximum heat content of the lakes of the follow-

ing depth: $50m$, $75m$, $100m$, and $150m$. Heat content is calculated by integrating water temperature over vertical distance, from the top to the bottom of a lake. We note that, in all the hystereses, there exists a range of upper-atmospheric temperature in which two local-climate regimes exist. What this means is that, given identical atmospheric forcing, there exist two stable "equilibrium" seasonal temperature cycles, or two equilibrium states: one is what we call the "colder regime" and the other is what we call the "warmer regime." In the colder regime, ice covers the surface of the lake during winters. In the warmer regime, ice does not cover the surface of the lake. On the one hand, when ice appears over the surface of a lake, the surface albedo of the lake significantly increases, reducing the amount of incoming shortwave radiation impinging upon the lake. This reduction in incoming shortwave radiation further encourages the formation of ice on the lake surface. On the other hand, when ice does not appear on the surface of a lake, a good amount of incoming shortwave radiation continues to impinge upon the lake. This abundance in incoming energy continues to discourage the formation of ice on the lake surface. Whether ice starts to appear at the surface on the day of the coldest water temperature in winter is the point of bifurcation, giving rise to two stable equilibrium states of the lake.

Depending on whether ice covers the lake during winters, the heat content of the lake changes as well; the two different stable seasonal cycles of the lake have different summer lake temperatures (Figure 21). This is the source of the correlation between the summer surface water temperature of the lake and the amount of its winter ice cover. This answers *Question 5* introduced in Chapter 1: *Why are the summer surface water temperature of the Great Lakes and their winter maximum ice cover correlated?*

Deeper Lakes versus Shallower Lakes   We find two important results.

(Result 1) The difference in summer maximum heat content between the two regimes is larger for deeper lakes.

(Result 2) The range of upper-atmospheric temperature in which the two regimes
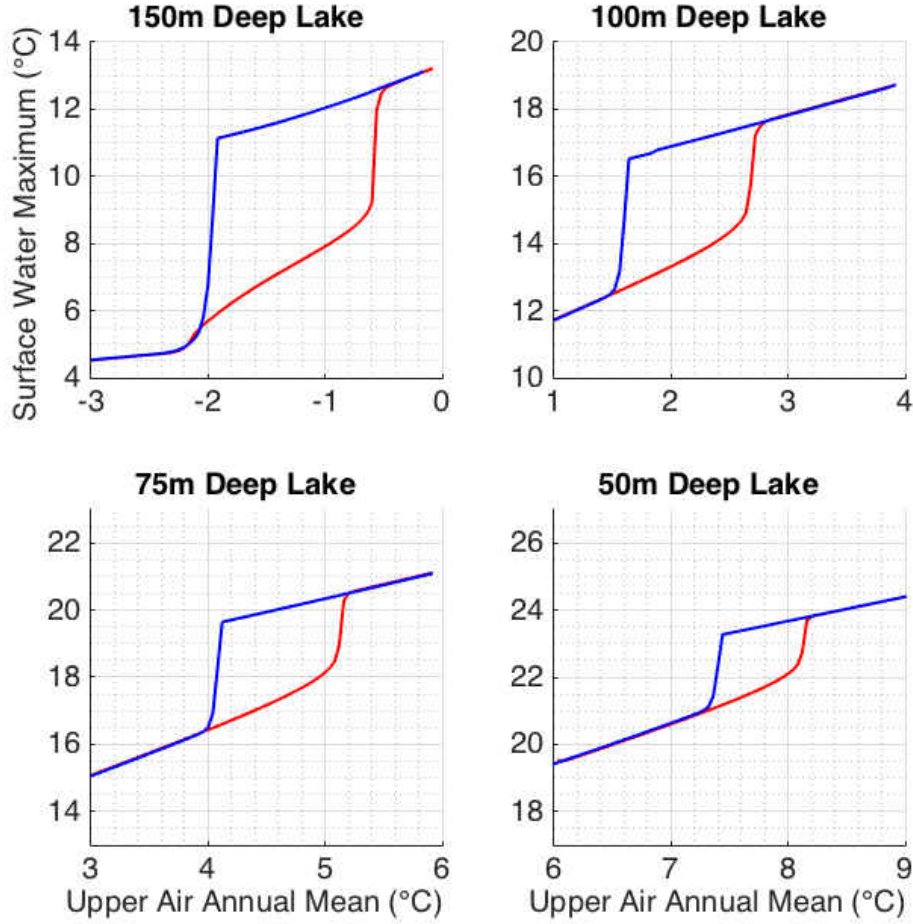
Figure 21: *The hysteresis of summer maximum surface water temperature of the lake of the following depth: 50m, 75m, 100m, and 150m. The abscissa is the annual-mean of periodic upper air temperature, which acts as forcing. The ordinate is summer maximum surface water temperature. The units are in°C*

exist is larger for deeper lakes.

The consequence of these two results is that shallower lakes easily transition from one regime to another, and the more often a lake transitions from one regime to another, the less strong the warming trend of the lake becomes. This partially answers why deeper lakes exhibit stronger surface warming trends than shallower lakes, which is *Question 2* addressed in Chapter 1.

The reason for the above two results is that shallower lakes go through longer duration of summer thermal stratification than deeper lakes and consequently, a longer time to efficiently respond to the summer atmosphere. For simplicity, let us think of a surface

mixed layer having a uniform temperature, from the surface at the top to the location of the thermocline. Then the rate of change in the temperature of the surface mixed layer is approximated by the following equation, which is a modification of Equation (2.1) for a uniform-temperature mixed layer.

$$C_w h \frac{\partial T}{\partial t} = \Delta \Phi \tag{3.13}$$

where h is the depth of the surface mixed layer, C_w is the volume heat capacity of water, and $\Delta \Phi$ is the energy the mixed layer receives from the outside source. We note that the shallower the surface mixed layer is, the faster and more efficient the change in surface water temperature is, given the same $\Delta \Phi$. The typical depth of a summertime surface layer of the Great Lakes is somewhere between $10m$ and $20m$. By contrast, the depth of a wintertime surface layer can be much deeper; it can be deeper than $100m$ below the regions of large water depth (for example, see Assel, 1986). Moreover, when spring overturn arrives, the entire depth from the surface to the bottom of the lake column becomes a mixed layer.
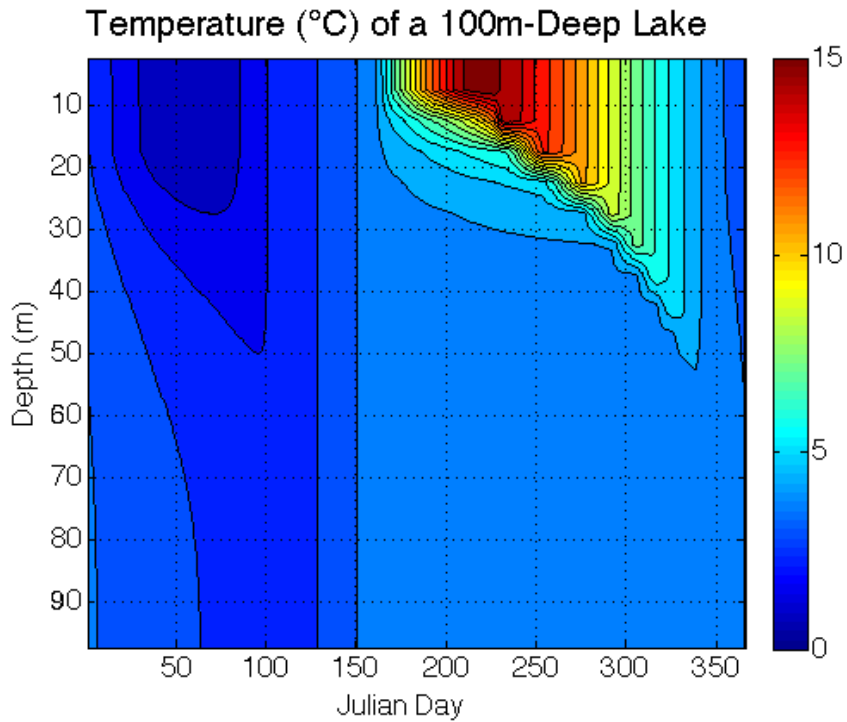
Figure 22: *An example of the vertical water temperature profile of the 100m-deep toy lake. The unit is in°C.*

Figure 22 is a result of simulating the temperature profile of the 100m-deep lake. We note that the thermocline in winter between Julian days 30 and 100 is nowhere as sharp as that in mid summer between Julian days 170 and 250, and between these two periods, the entire lake is mixed. This is the reason that shallower lakes go through longer duration of summer stratification than deeper lakes; for a certain duration of time before spring overturn, water temperature becomes nearly homogeneous from the top to the bottom and the vertically near-homogeneous profile of water encourages vertical mixing of much of the lake column. Deeper lake columns have more water to mix. For this reason, surface water temperature of a deeper lake does not increase much during the period, and the vertical density profile of a deeper lake remains near-homogeneous longer than that of a shallower lake. The end of spring overturn and the appearance of the summertime surface mixed layer arrive later for a deeper lake than a shallower lake; for example, in some years, spring overturn occurs even during August at buoy station 45004 in easter Lake Superior (e.g., Austin and Colman, 2007). For this reason, shallower lakes go through longer duration of summer stratification than deeper lakes.

A shallow lake point such as buoy station 45005 in western Lake Erie starts to stratify on average sometime in May, while a deep lake point such as buoy station 45001 in central Lake Superior starts to stratify on average sometime in July (Austin and Colman, 2007). This is a difference of almost two months. As discussed below, the typical decay time of surface temperature anomalies in summer, when the lake has a summertime surface mixed layer, is a couple of months. So, the difference of two months in summer is relatively large; a summertime shallow lake can lose a good fraction of a surface temperature anomaly it might have had in two months. This is the reason that the difference in summer maximum heat content between two regimes is small in shallow lakes. Consequently, this is also the reason that the range of upper-atmospheric temperature in which two regimes exist is small in shallow lakes.

Three Questions Concerning Regime Transitions   Let us consider a $100m$-deep lake. Let the longterm mean of upper air temperature be somewhere within the range in which two climate regimes exist. With the chosen longterm mean of upper air tempera-

ture, two stable equilibrium states exist, with the associated seasonal temperature cycle for each. Let us make perturbations to these equilibrium states. We might ask three questions about perturbing stable equilibrium states. The first Question A is that, when the temperature of the lake is perturbed from one of the lake's stable seasonal cycles by a relatively small amount, how fast does the system approach back to the equilibrium? The second Question B is that, when the temperature of the lake is perturbed from one of the lake's stable seasonal cycles large enough for the lake to transition to the other seasonal cycle, how fast does the system approach to the new equilibrium? The third Question C is concerned about the preferred direction of regime transitions: Which transition is easier, from the colder regime to the warmer regime, or the other way around?

Typical Decay Timescale of Summertime Surface Temperature Anomalies
The first question is related to the question of the typical lifetime of ocean SST anomalies. Except near the polar regions or at high enough latitudes, oceans in the other regions generally do not freeze. Therefore, there are no multiple local-climate regimes that arise due to an abrupt change in surface albedo over oceans at lower and middle latitudes. When the surface temperature of a region of an ocean at a lower or middle latitude contains an anomaly with respect to its longterm mean, the expected decay time of the anomaly is a good measure of how fast the system approaches back the equilibrium state from a perturbed state. A typical decay time of ocean SST anomalies ranges from three to six months (e.g., Lau and Nath, 1996; Frankignoul and Hasselmann, 1977; Alexander and Penland,1996)).

Figure 23 contains results of perturbing the colder stable equilibrium state of a $100m$-deep lake. Various amounts of heat are added to the top $10m$ of the lake as perturbations to the colder stable equilibrium state on Day 150 of the first year. The black curves are the two stable seasonal cycles associated with the equilibrium states. The red curves are perturbations large enough for the lake to transition to the warmer equilibrium state. The green curves are perturbations small enough for the lake to be attracted back to the old, colder equilibrium state. The blue curves are negative perturbations: heat is taken out of the system, and the system is attracted back to the old, colder equilibrium state. First, let

Figure 23: *Results of perturbing the colder stable equilibrium state of the 100m-deep lake. Various amounts of heat are added to the top 10m of the lake as perturbations to the colder stable equilibrium state on Day 150 of the first year. The black curves are the two stable equilibrium states. The red curves are perturbations large enough for the lake to transition to the warmer equilibrium state. The green curves are perturbations small enough for the lake to be attracted back to the old, colder equilibrium state. The blue curves are negative perturbations: heat is taken out of the system, and the system is attracted back to the old, colder equilibrium state. The unit is in°C.*

us focus on the red curves. Especially, let us pay attention to day 200 of the first year and afterward of the top red curve. The top red curve on day 200 is relatively close to the top black curve, which is the warmer stable seasonal cycle. Therefore, equivalently, we can consider the top red curve on day 200 as a perturbation to the warmer stable equilibrium state on the day, and see how fast the top red curve approaches the warmer equilibrium state as time passes. We note that, three months later, the magnitude of the perturbation, the distance to the warmer stable seasonal cycle, is reduced by approximately one third, from approximately $3°C$ on day 200 to $1°C$ on day 300, suggesting that the typical decay time of these anomalies *in summer* is a couple of months. This is our short answer to Question A. However, let us explore perturbation experiments further. One year later, only a sixth or so of the magnitude of anomaly remains in each of the red curves with respect to the warmer stable seasonal cycle. Let us take a look at the green curves on

day 200 of the first year and how fast they get attracted back to the colder equilibrium state as well. Once again, three months later, the magnitudes of these surface anomalies are reduced by approximately one third, from approximately $4°C$ on day 200 to $1°C$ on day 300, suggesting that the typical decay time of these anomalies in summer, when a summertime surface mixed layer appears in the lake, is a couple of months. When we examine later times, say, one year later, however, the situation becomes different in green and blue curves. In these curves, anomalies are more persistent a year later. A year later, a third or so of the initial anomaly still remains in each green or blue curve. This persistence of anomaly is due to the ice-albedo feedback and other ice-related feedback effects. If heat is added during a summer to create a positive anomaly, most of this extra heat content will be lost by the time ice appears during the winter, but not all will be lost; suppose that $1°C$ of heat is added to the top $10m$ of the lake in the colder climate regime during a summer. Most of this extra heat is lost by the arrival of the winter, but the remaining few percent of the initial anomalous heat delays the formation of surface ice by a day or two, and in these experiments, one full day of extra ice-free time often results in an increase of somewhere between $0.1°C$ and $0.15°C$ in summer maximum surface water temperature. Next summer, this lake would still exhibit $0.3°C$ or so of anomalous heat due to these ice effects, making a contrast against the same lake in the warmer climate regime, in which case the anomaly next year would be only a sixth or so of that of the previous year as Figure 23 demonstrates.

In the figure, we find that, when surface water temperature is below $4°C$, that is, when a summertime surface mixed layer is absent, surface temperature anomalies decrease more slowly. This is expected from the earlier discussion in this section. In addition, we also find that, when surface water temperature increases and rises above $4°C$, the magnitudes of surface temperature anomalies suddenly increase. This is why a deep lake such as Lake Superior exhibits a strikingly large warming trend in mid summer, as seen in Table 1 in Chapter 1.

Timescale of Regime Transitions Questions B and C are related to each other. As we see below, when the temperature of the upper atmosphere is relatively cold, it is

easier for the lake to transition from the warmer regime to the colder regime. When the temperature of the upper atmosphere is relatively warm, then it is the other way around. When the temperature of the upper atmosphere is right in the middle of the range of upper air temperature in which two regimes exists, as in Figure 23, then a transition from the warmer to the colder regime and a transition in the opposite direction are equally likely. However, even if a perturbation makes a lake attracted to a different regime, if the magnitude of the perturbation is relatively small, it might take a couple of years to complete the regime transition. Let us see some examples. Again, let us choose a $100m$-deep lake as an example. Let us choose a relatively cold temperature as the longterm mean of the upper atmosphere, but somewhere in the range of temperatures where two regimes exist. The black dots in Figure 24 describe the temperature chosen for this purpose. Since the chosen temperature is near the cold end of the multiple-regime temperature range, the basin of attraction of the warmer regime is small and a slight negative perturbation to the warmer equilibrium state makes the lake attracted toward the colder regime.
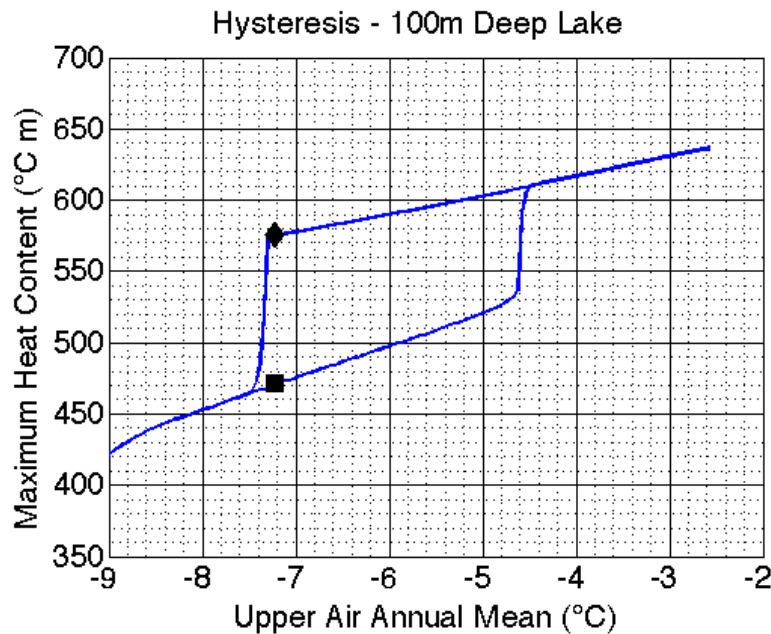
Figure 24: *Identifying equilibrium temperature cycles of colder upper atmosphere. The blue curves are the hystereses of summer maximum heat content of a 100m-deep toy lake. The black dots indicate the annual-mean upper air temperature used as the forcing for the experiments discussed in the main text and the summer maximum heat contents of the corresponding two equilibrium states.*
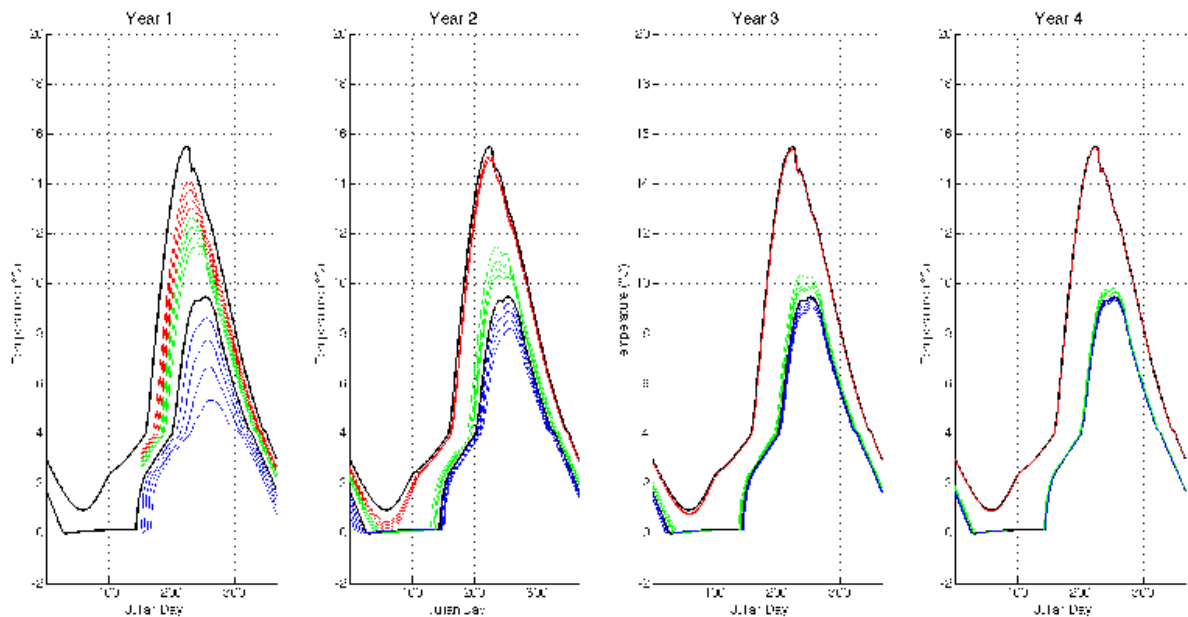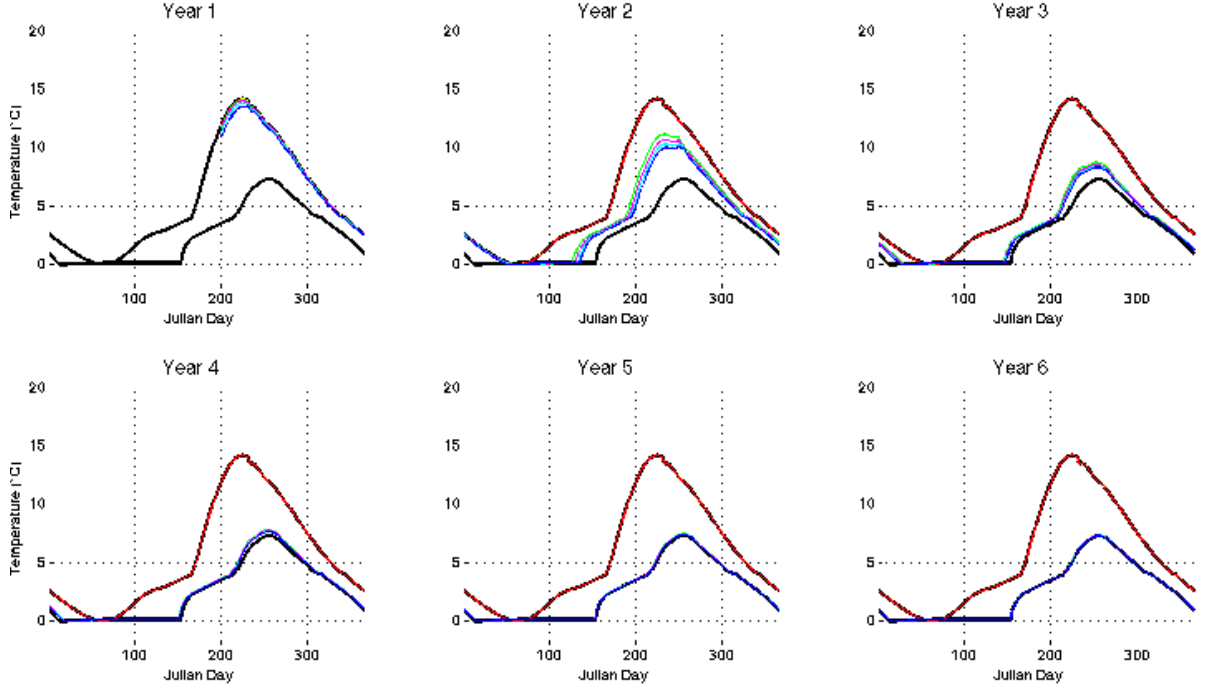
Figure 25: *Results of perturbing the warmer stable equilibrium state of the* 100*m-deep lake. Various amounts of heat are added to the top* 10*m of the lake as perturbations to the warmer stable equilibrium state on Day 200 of the first year. The black curves are the two stable equilibrium states. The red curve corresponds to the case in which* 0.1°*C of heat is subtracted from the top* 10*m of the lake on day 200 of the first year. The red curve corresponds to the case in which* 0.1°*C of heat is subtracted from the top* 10*m of the lake on day 200 of the first year. The green, purple, light blue, and blue curves correspond to the cases in which* 0.2°*C,* 0.3°*C,* 0.4°*C, and* 0.5°*C of heat are subtracted from the top* 10*m of the lake on day 200 of the first year.*

Figure 25 shows the time necessary to complete the transition. We note that only the red curve is attracted back to the original warmer equilibrium state. The other curves are all attracted to the colder equilibrium state, and a couple of years later, transition to the colder regime. As we see in the figure, the initial perturbations of all these curves are relatively small. Therefore, Figures [25 demonstrates that when the temperature of the upper atmosphere is relatively cold, it is easier for the lake to transition from the warmer regime to the colder regime than the other way around.

Next, let us choose a relatively warm temperature as the longterm mean of the upper atmosphere, still somewhere in the range of temperatures where two regimes exist. For example, the black dot in Figure 26 describe such a temperature. This temperature is near the warm end of the multiple-regime temperature range. So, the basin of attraction
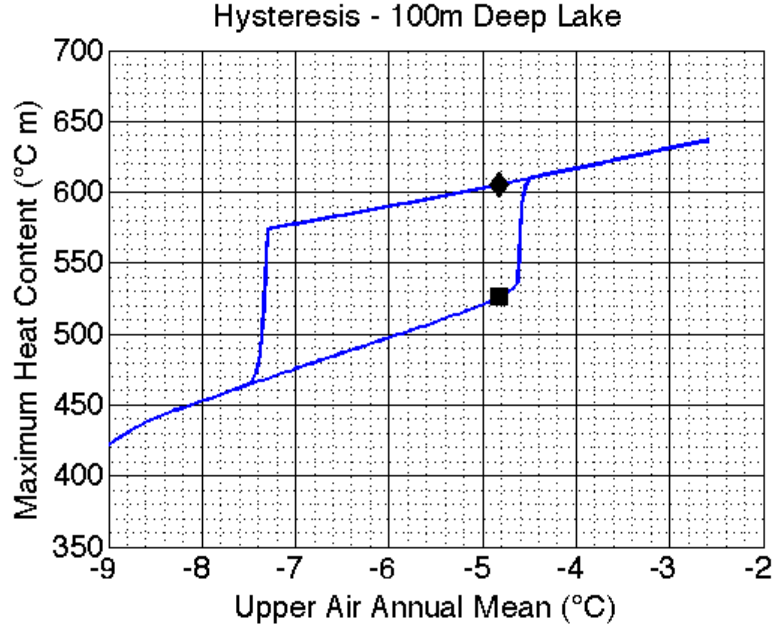
Figure 26: *Identifying equilibrium temperature cycles of warmer upper atmosphere. The blue curves are the hystereses of summer maximum heat content of a 100m-deep toy lake. The black dots indicate the annual-mean upper air temperature used as the forcing for the experiments discussed in the main text and the summer maximum heat contents of the corresponding two equilibrium states.*

of the colder regime is small and a slight positive perturbation to the colder equilibrium state makes the lake attracted to the warmer regime.

Figure 27 shows the time necessary to complete the regime transition. In the blue curve, which corresponds to the case in which $0.1°C$ of heat is added to the top $10m$ of the lake on day 200 of the first year, although initially a slight perturbation to the colder equilibrium state, the lake is attracted to the warmer equilibrium state and several years later, transitions to the warmer regime. In the green curve, however, the lake transitions to the warmer regime in only a couple of years. We note that, the closer the perturbed state is to the equilibrium state it is attracted to, the shorter the time of the transition is. Overall, Figure 27 demonstrates that when the temperature of the upper atmosphere is relatively warm, it is easier for the lake to transition from the colder regime to the warmer regime.
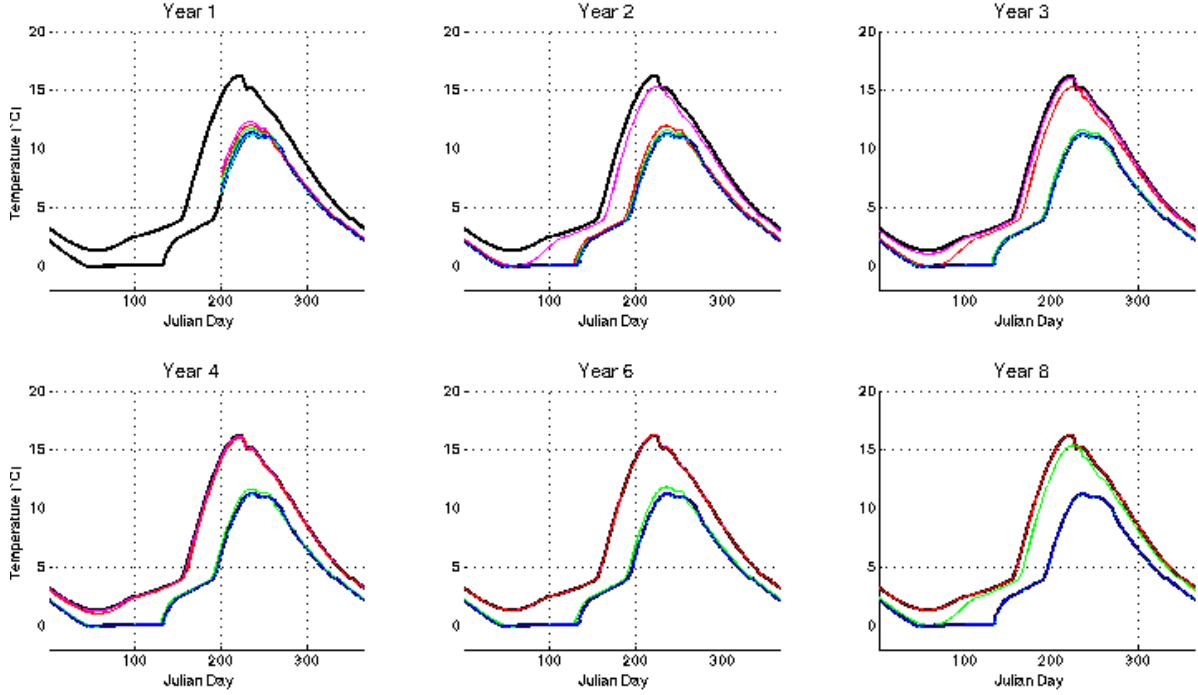
Figure 27: *Results of perturbing the colder stable equilibrium state of the* 100*m-deep lake. Various amounts of heat are added to the top* 10*m of the lake as perturbations to the colder stable equilibrium state on Day 200 of the first year. The black curves are the two stable equilibrium states. The red curve corresponds to the case in which* 0.1°*C of heat is subtracted from the top* 10*m of the lake on day 200 of the first year. The blue curve corresponds to the case in which* 0.1°*C of heat is added to the top* 10*m of the lake on day 200 of the first year. The light blue, green, purple, and red curves correspond to the cases in which* 0.2°*C,* 0.3°*C,* 0.4°*C, and* 0.5°*C of heat are added to the top* 10*m of the lake on day 200 of the first year.*

3.2.2   Application: Discontinuity in Lake Superior's Ice Cover and Summer Temperature Time Series

In Chapter 1, we briefly discussed the August-mean surface water temperature time series of buoy station 45001 in central Lake Superior and that the time series contained a discontinuous behavior before and after the years 1997-98. We also discussed a discontinuous behavior in the maximum ice cover time series of Lake Superior before and after the years 1997-98. Between the years 1973 and 1997, there were only four winters out of 25 during which the maximum ice cover over Lake Superior was less than 60%, and between the years 1998 and 2014, there were only four winters out of 17 during which the maximum ice cover over Lake Superior was more than 60%. A possible interpreta-

60

tion of this behavior is as follows. Global warming has been warming the Great Lakes region; the climate of the Great Lakes after the year 1998 is generally warmer than the climate before the year 1997. We interpret that, before the year 1997, the atmospheric forcing on Lake Superior had been such that the lake was more attracted to its colder local-climate regimes, and after the year 1998, the atmospheric forcing has been such that the lake is more attracted to its warmer local-climate regimes. At around the years 1997-1998, the colder and warmer regimes were more or less equally likely. This interpretation only states the inclination of the lake toward some regimes, and does not state the specific regime of the lake. Therefore, it is possible that the lake undergoes some warmer local-climate regimes, such as the years 1983 and 1987, even when the atmospheric forcing creates an environment favorable toward colder local-climate regimes. Similarly, it is possible that the lake undergoes some colder local-climate regimes, such as the years 2003 and 2009, even when the atmospheric forcing creates an environment favorable toward warmer local-climate regimes. This interpretation is based on the discussion we have had in this section: when the temperature of the upper atmosphere is relatively cold, it is easier for the lake to transition from the warmer regime to the colder regime, but the opposite transition is still possible, and when the temperature of the upper atmosphere is relatively warm, it is easier for the lake to transition from the colder regime to the warmer regime, but again, the opposite transition is still possible.

How do we make sense that Lake Superior exhibits a discontinuous behavior at around the years 1997-1998 most dramatically among the Great Lakes? The reason for this is that Lake Superior is the deepest lake among the Great Lakes, and according to Result 2 earlier in this section, deeper lakes tend to reside more persistently in one regime than shallower lakes do, and according to Result 1 and Figure 21, deeper lakes ($100m <$ average depth $< 200m$) generally experience more dramatic changes in surface water temperature when they change regimes than shallower lakes (average depth $< 100m$).

3.2.3 Multiple Stable Equilibrium States of Seasonal Cycles of Three-Column Lakes

As we saw in the previous section, a lake of uniform depth gives rise to a range of upper-atmospheric temperature in which two climate regimes exist: one regime in which ice covers the entire lake during winters and the other regime in which no ice appears over the lake. This time, we explore lakes with three uniform-depth columns, each of which has distinct water depth, with the shallowest near-shore, the deepest at the center, and the intermediate between them (Figure 12). We use the three-column toy models discussed in §3.1.2. In three-column lakes, more than two climate regimes possibly arise theoretically. For example, in one possible regime, ice might cover the entire lake surface during winters. In another regime, ice might cover only the shallowest and intermediate lake columns during winters. In yet another regime, ice might cover only the shallowest lake column during winters. In the case of the toy Lake 2 model, that is what happens.

Figure 28 is the hysteresis of summer maximum water temperature of Lake 2 toy model. In the figure, we see three hystereses presented with different colors; the black curve corresponds to the hysteresis of the 140m-deep lake column, the cyan curve corresponds to the hysteresis of the 80m-deep lake column, and the red curve corresponds to the hysteresis of the 30m-deep lake column. For each lake column, we find a range of upper air temperature in which three climate regimes coexist, between $-3.9°C$ and $-3.3°C$ of the horizontal axis. Moreover, the range of upper air temperature in which three climate regimes coexist is identical for all the three lake columns. Similarly, the range of upper air temperature in which only two climate regimes coexist is also identical for all the three lake columns. When the deepest lake column is following its warmest stable seasonal temperature cycle, then the shallowest and intermediate lake columns are also following their respective warmest stable seasonal temperature cycles. Similarly, when the deepest lake column is following its intermediate (or coldest) stable seasonal temperature cycle, then the shallowest and intermediate lake columns are also following their respective intermediate (or coldest) stable seasonal temperature cycles. What this implies is that, as far as models with periodic forcing without inter-annual variability are
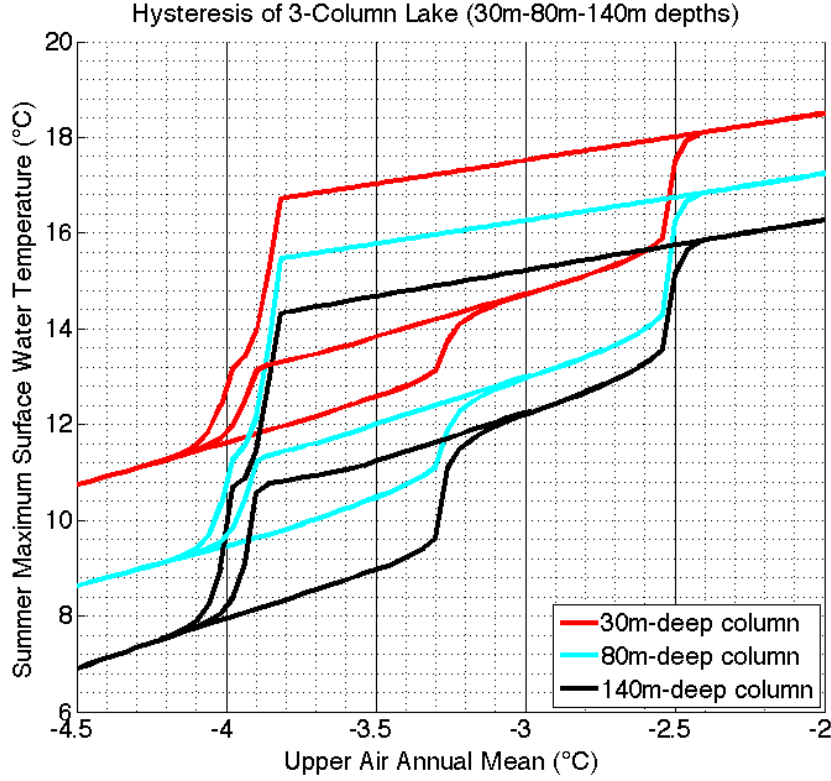
Figure 28: *The hysteresis of Lake 2 model. The abscissa is the annual-mean of periodic upper air temperature, which acts as forcing. The ordinate is summer maximum surface water temperature. The black curve corresponds to the hysteresis of the 140m-deep lake column, the cyan curve corresponds to the hysteresis of the 80m-deep lake column, and the red curve corresponds to the hysteresis of the 30m-deep lake column. The units are in °C.*

concerned, all lake columns share the same climate regime.

In Figure 28, the coldest regime is such that ice covers the entire lake surface during winters. The intermediate regime is such that ice covers only the shallowest and intermediate lake columns during winters. The warmest regime is such that ice covers only the shallowest lake column during winters. One interesting result is that, when the lake transitions from the intermediate regime to the warmest regime, the deepest lake column is ice-free before and after the transition, yet the gap between the intermediate and warmest regimes of the deepest lake column (black curve) is almost as large as that of the intermediate lake column (blue curve). This implies that, even if it is perennially ice free, if neighboring regions transition from being wintertime-ice-covered to being perennially-ice-free, the deepest lake column would exhibit a strong surface warming

trend. This observation is important since the deepest lake points of Lakes Michigan and Ontario have been mostly ice-free for the last couple of decades yet have exhibited stronger surface-water warming trends than the neighboring shallower lake points.

Figure 29: *The hysteresis of Lake 1 model. The abscissa is the annual-mean of periodic upper air temperature, which acts as forcing. The ordinate is summer maximum surface water temperature. The black curve corresponds to the hysteresis of the 225m-deep lake column, the cyan curve corresponds to the hysteresis of the 150m-deep lake column, and the red curve corresponds to the hysteresis of the 50m-deep lake column. The units are in °C.*

Figure 29 is the hysteresis of summer maximum water temperature of Lake 1 toy model. We find a range of upper air temperature in which two climate regimes coexist, between $-4.5°C$ and $-2.5°C$ of the horizontal axis, but not three. The colder regime is such that ice covers the entire lake surface during winters. The warmer regime is such that ice covers only the shallowest lake column during winters. In this toy lake, the deepest and intermediate lake columns transition from being wintertime ice-covered to perennially ice-free almost simultaneously.

Figure 30 is the hysteresis of summer maximum water temperature of the Lake 3 toy

Figure 30: *The hysteresis of Lake 3 model. The abscissa is the annual-mean of periodic upper air temperature, which acts as forcing. The ordinate is summer maximum surface water temperature. The black curve corresponds to the hysteresis of the 100m-deep lake column, the cyan curve corresponds to the hysteresis of the 60m-deep lake column, and the red curve corresponds to the hysteresis of the 30m-deep lake column. The units are in °C.*

model. We find a range of upper air temperature in which two climate regimes coexist, between $-2.9°C$ and $-2.0°C$, between $-1.5°C$ and $-0.8°C$, and between $0.6°C$ and $1.2°C$ of the horizontal axis. However, we do not find a range of upper air temperature in which more than two regimes coexist. When upper air temperature is between $-2.9°C$ and $-2.0°C$, the colder regime is such that ice covers the entire lake surface and the warmer regime is such that ice covers only the shallowest and intermediate lake columns during winters. When upper air temperature is between $-1.5°C$ and $-0.8°C$, the colder regime is such that ice covers only the shallowest and intermediate lake columns and the warmer regime is such that ice covers only the shallowest lake column during winters.

Figure 31 is the hysteresis of summer maximum water temperature of Lake 4 toy model. We find a range of upper air temperature in which two climate regimes coexist,
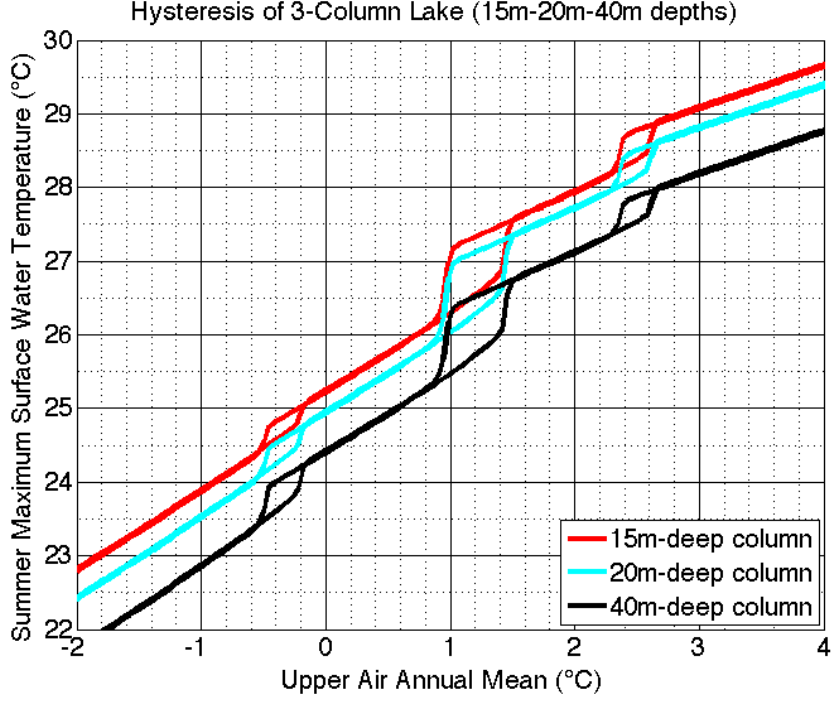
Figure 31: *The hysteresis of Lake 4 model. The abscissa is the annual-mean of periodic upper air temperature, which acts as forcing. The ordinate is summer maximum surface water temperature. The black curve corresponds to the hysteresis of the 40m-deep lake column, the cyan curve corresponds to the hysteresis of the 20m-deep lake column, and the red curve corresponds to the hysteresis of the 15m-deep lake column. The units are in °C.*

between $-0.4°C$ and $-0.2°C$, between $1.0°C$ and $1.4°C$, and between $2.4°C$ and $2.6°C$ of the horizontal axis. As in Lake 3, we do not find a range of upper air temperature in which more than two regimes coexist. When upper air temperature is between $-0.4°C$ and $-0.2°C$, the colder regime is such that ice covers the entire lake surface and the warmer regime is such that ice covers only the shallowest and intermediate lake columns during winters. When upper air temperature is between $1.0°C$ and $1.4°C$, the colder regime is such that ice covers only the shallowest and intermediate lake columns and the warmer regime is such that ice covers only the shallowest lake column during winters. When upper air temperature is between $2.4°C$ and $2.6°C$, the colder regime is such that ice covers only the shallowest and lake column and the warmer regime is perennially ice-free.

One drawback of our lake-atmosphere-land coupled model is that the atmosphere has only two layers and we let surface air temperature equal to the overall temperature of
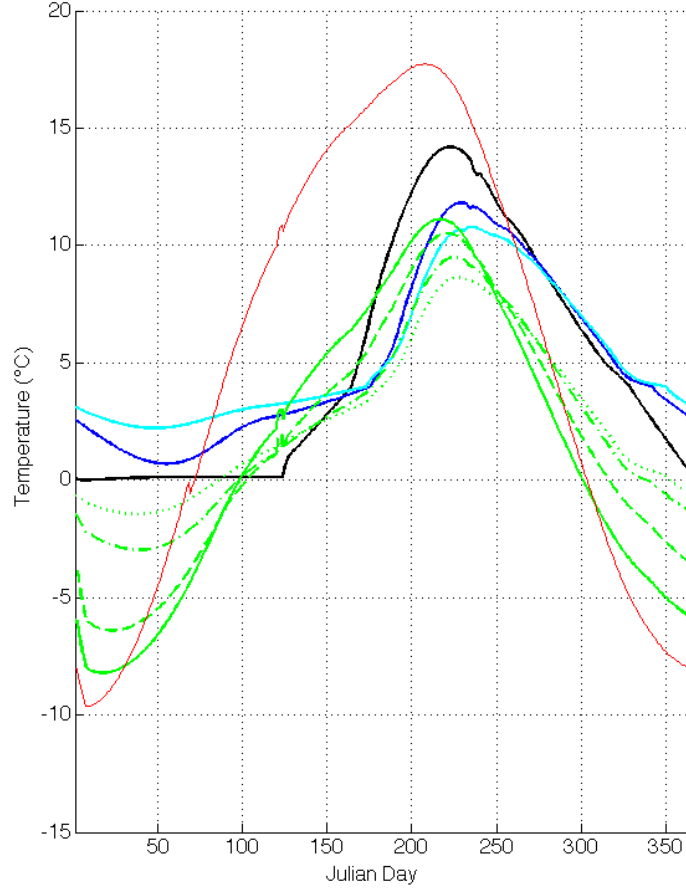
Figure 32: *An example of seasonal temperature cycles of the Lake 1 model. The abscissa is Julian day of a ceartain year. Plotted are the surface water temperatures of the 50m-deep lake column (black curve), 150m-deep lake column (blue curve), and 225m-deep lake column (cyan curve), the surface land temperature of surrounding land (red curve), and the surface air temperatures above the 50m-deep lake column (green dash-dotted curve), 150m-deep lake column (green dashed curve), and 225m-deep lake column (green dotted curve), the surface land temperature of surrounding land (green solid curve) . In this particular example, the 50m-deep lake column is ice-covered in winter and the other two lake columns are ice-free.*

the lower atmosphere; in reality, we expect surface air temperature to be several degrees Celsius warmer. In our lake models, the amounts of sensible and latent heat fluxes are proportional to the difference between surface air temperature and surface water temperature. Therefore, when the difference between the two temperatures is overestimated, the energy escaping from the lake to the atmosphere, in the form of sensible and latent heat fluxes, is also overestimated. Figure 32 shows an example of a seasonal temperature cycles of Lake 1. In the figure, the 225m-deep lake column is ice-free, yet the summer

maximum surface air temperature above it is only approximately $8°C$. This is a little too cold a summer for the climate of some 200m-deep lake in which ice does not appear in winter. We suspect that this is the reason that summer surface water temperatures of deeper lakes in our lake-atmosphere-land model are generally several degrees colder than the actual Great Lakes of comparable depths, despite that the other atmospheric parameters such as the amounts of downward shortwave radiation are comparable. This is especially true of the toy Lake 1, the deepest lake among those introduced in §3.1.2. The summer surface water temperature of Lake 2 is comparable to that of the real Lake Superior. This is why the hystereses of summer maximum water temperatures of Lake 2, those of the warmest and coldest regimes, turn out to be a relatively good fit to the observed data of the colder and warmer regimes of Lake Superior.

Speculation of the $n \to \infty$ Limit of n-Column Lakes A natural question we might think of is, "What would happen if we increase the number of lake columns?" For example, the lake models used in the ICTP RegCM regional climate models are lakes that consist of numerous lake columns, each of which acts as a one-dimensional lake without lateral interactions (Bennington *et al.*, 2014). Would we find hundreds of distinct local-climate regimes associated with a lake of hundreds of columns? A natural extension of this question is, "What would happen to the number of local-climate regimes associated with a lake if we let n, the number of lake columns, approach infinity?" Figure 33 is only an example of thought experiment of what a hysteresis plot might look like if we increase the number of lake columns. If we keep increasing n, what will happen to the range of possibilities of the number of multiple climate regimes and their properties? What we are most interested in is whether multiple climate regimes disappear in the $n \to \infty$ limit under some conditions, and if they do, in what conditions. What we are also interested in is whether the number of climate regimes remain finite or approaches infinity in some conditions, and if it does, in what conditions.

Of course, a yet natural extension of these questions is, "how many local-climate regimes might a *real* lake have?" In the next chapter, we compare these model results with observational data based on the NARR reanalysis in detail. We find indications of
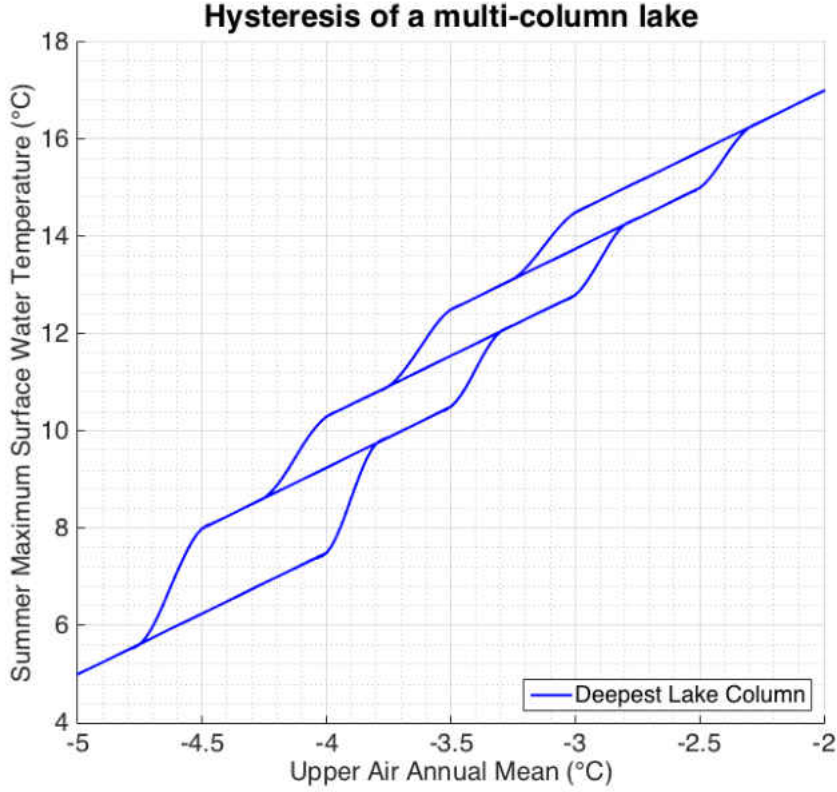
Figure 33: *An example of what a hysteresis plot of a multiple-column lake might look like when n > 3, the number of lake columns is mo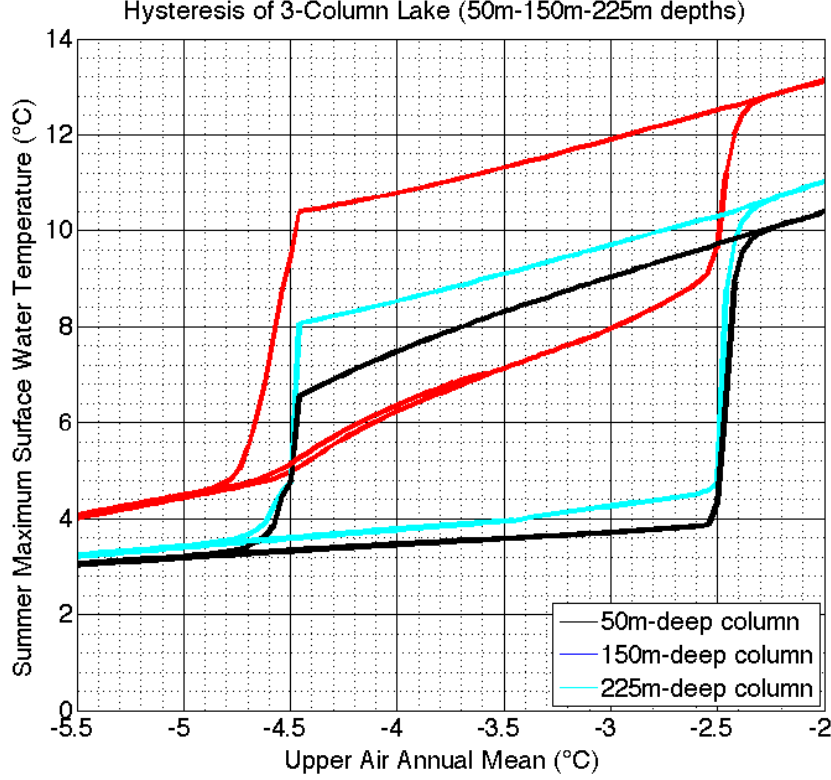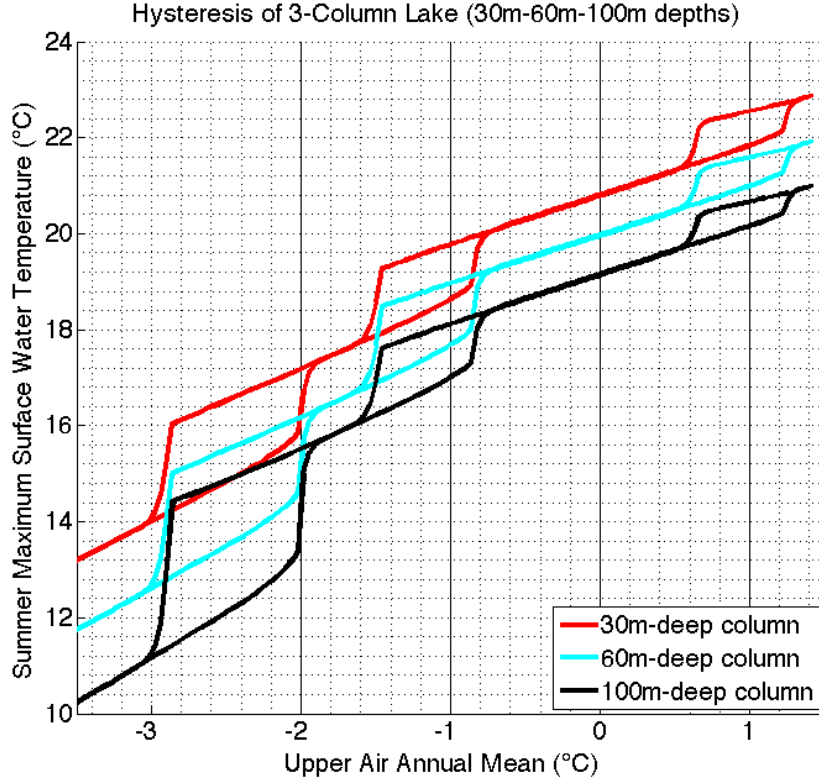re than three. The abscissa is the annual-mean of periodic upper air temperature, which acts as forcing. The ordinate is summer maximum surface water temperature of its deepest lake column. The units are in °C.*

distinct local-climate regimes over the eastern part of Lake Superior, suggesting that, in some real lakes, a finite number of local-climate regimes do arise.

3.2.4 Multiple Climate Regimes of Three-Column Lakes in the Presence of Stochastic Forcing

Stochastic Forcing In this subsection, we introduce Gaussian noises in the temperature of the upper atmosphere and the amount of downward shortwave radiation. We generate seasonal anomalies as follows. We split one year into four seasons and assign an anomaly, a Gaussian noise, to each season. We do this for upper air temperature and for downward shortwave radiation separately. The standard deviation of the Gaussian noise for seasonal temperature anomalies of the upper atmosphere is $2°C$ and that for down-

ward shortwave radiation is $6W/m^2$. The magnitudes of these anomalies are compared with the NARR reanalysis data in Tables 9 and 10.

Table 9: *The standard deviations of seasonal-mean air temperature at various pressure levels above buoy station 45001 in central Lake Superior, based on the NARR reanalysis data for the years 1979-2013. JFM is the January-February-March mean, AMJ is the April-May-June mean, JAS is the July-August-September mean, and OND is the October-November-December mean. The units are in $°C$.*

STD above buoy 45001	JFM	AMJ	JAS	OND
850mb	2.2	1.5	1.1	1.7
700mb	1.8	1.4	1.0	1.4
500mb	1.4	1.2	0.8	1.5

Table 10: *The standard deviations of seasonal-mean downward shortwave radiation at various buoy stations in the Great Lakes, based on the NARR reanalysis data for the years 1979-2013. JFM is the January-February-March mean, AMJ is the April-May-June mean, JAS is the July-August-September mean, and OND is the October-November-December mean. The units are in W/m^2.*

Downward Shortwave STD	JFM	AMJ	JAS	OND
buoy 45001 (Superior)	7.5	11.9	10.9	4.2
buoy 45002 (Michigan)	8.8	13.4	10.8	4.2
buoy 45003 (Huron)	7.5	12.8	9.3	4.6
buoy 45012 (Ontario)	8.6	13.1	9.1	5.3
buoy 45005 (Erie)	6.7	12.3	10.7	5.0

We use a spline method to connect the anomalies of neighboring seasons so that the time series of the anomaly is continuous on a daily timescale. These noises are added to the periodic parts of the atmospheric forcing used in the two previous subsections. In these experiments, the atmospheric forcing has no linear trend. For this experiment, we use the Lake 2 toy model because this toy turns out to produce summer maximum surface water temperatures comparable to those over Lake Superior. We let the longterm mean of upper air temperature be roughly $-3°C$.

Scatter Plots of Summer Water Temperatures Versus Upper Air Temperatures Figure 34 is the scatter plot of three-year mean, from September of year $x - 3$
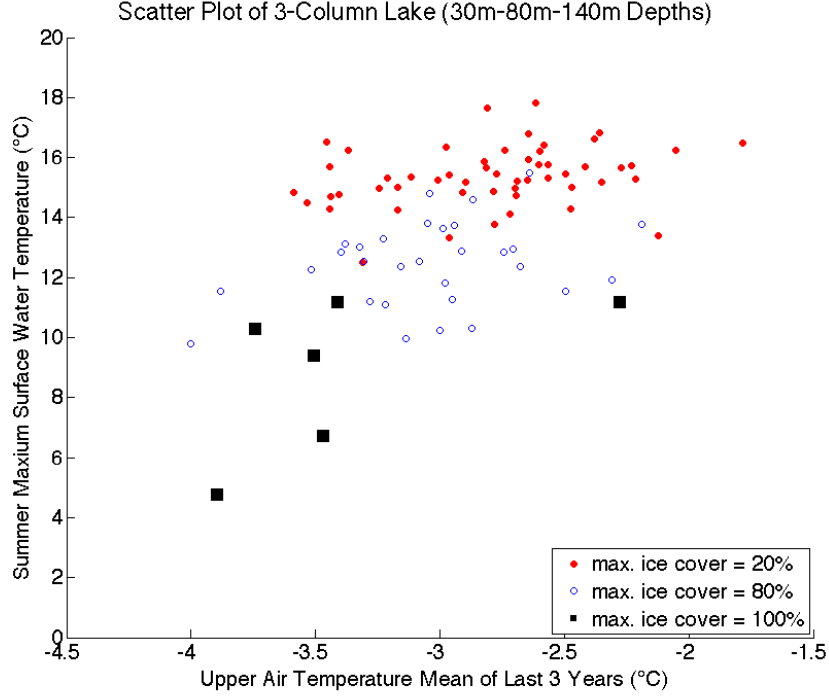
Figure 34: *The scatter plot of three-year mean, from September of year $x-3$ to August of year x, of upper air temperature on the horizontal axis, versus summer maximum surface water temperature of the deepest column of Lake 2 of year x on the vertical axis, after we run more than 50 years of time series. Filled black squares correspond to the cases in which ice covers 100% of the lake during the winter of year x. Blue circles correspond to the cases in which ice covers 80%, only the shallowest and intermediate lake columns, of the lake during the winter of year x. Red circles correspond to the cases in which ice covers 20%, only the shallowest lake column, of the lake during the winter of year x.*

to August of year x, of upper air temperature on the horizontal axis, versus summer maximum surface water temperature of the deepest column of Lake 2 of year x on the vertical axis, after we run more than 50 years of time series. Here, we choose three-year mean of air temperature on the horizontal axis because we saw in §3.2.1 that it sometimes took a few years for a lake to transition to a new climate regime when it was disrupted. We choose three years as a representative timescale of the slowest regime transitions.

Let us compare this model result with some observational data. Figure 35 contains the scatter plots of three-year mean, from September of year $x-3$ to August of year x, of air temperature anomalies at the 800mb pressure level right above buoy station 45004, in eastern Lake Superior, on the horizontal axis, versus August-mean surface water temperature of year x at buoy station 45004 on the vertical axis. We find that,
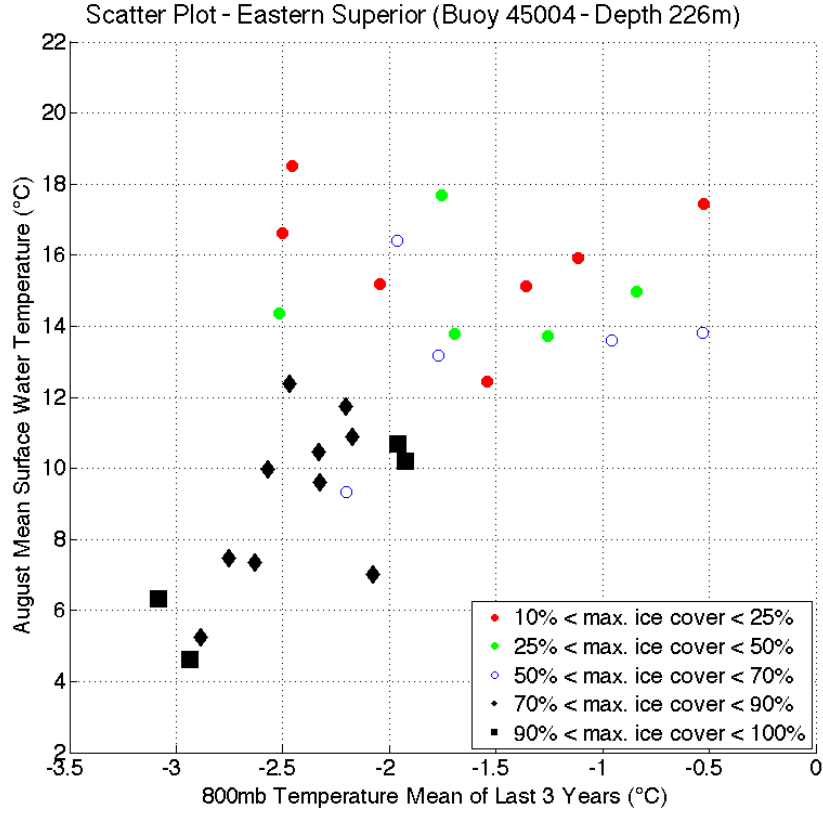
Figure 35: *The scatter plots of three-year mean, from September of year x−3 to August of year x, of air temperature anomalies at the 800mb pressure level right above buoy station 45004, in eastern Lake Superior, on the horizontal axis, versus August-mean surface water temperature of year x at buoy station 45004 on the vertical axis. In the figure, black squares and black diamonds correspond to the cases in which ice covers more than 90% and between 70% and 90% of Lake Superior, respectively, during the winter of year x. Blue circles correspond to the cases in which ice covers between 50% and 70% of the lake during the winter of year x. Green circles and red circles correspond to the cases in which ice covers between 25% and 50% and between 10% and 25% of the lake, respectively, during the winter of year x. The year x runs from 1982 to 2013.*

in both Figure 34 and Figure 35, the black dots, which represent winters of relatively large ice cover, are mostly confined to the lower-left corner. They spread between $4°C$ and $12°C$ of the vertical axis. In addition, in both figures, the blue, green, and red dots, which represent winters of smaller ice cover, spread wide horizontally. The vertical spread of the red dots is roughly between $14°C$ and $18°C$ in both figures. These observations indicate that the toy Lake 2 captures a number of features in the relationship between summer surface water temperature and three-year mean of air temperature anomalies of eastern Lake Superior relatively well.

3.3   Responce to Global Warming

3.3.1   Lake Warming Trends in the Presence of Global Warming

Periodic Forcing with Positive Linear Trend   In this section, we present results of global warming experiments by adding a positive trend to the forcing. We still use three-column lakes introduced in §3.1.2. The forcing is all periodic except that the temperature of the upper atmosphere has a linear trend of $0.04°C/year$ in addition to its periodic component. Other than the linear trend, there is no inter-annual variability in the forcing in this subsection. The following lists all the forcing and the behaviors of the forcing, whether periodic or constant, and whether or not there is a non-zero linear trend.

List of Forcing	
Temperature of the upper atmosphere	periodic + linear trend of $0.04°C/year$
Downward shortwave radiation	periodic
Surface wand speed	periodic
Relative humidity	constant

The periodic parts of the temperature of the upper atmosphere, downward shortwave radiation, and surface wind speed are given by Equations (3.10-3.12). Again, the relative humidity at the lake and land surfaces is set to 0.8. The longterm mean of downward shortwave radiation for each three-column toy model is given in Table 8. We compute 100-year-or-more time series of surface water temperature for each toy model, and compute how their surface-warming trends change as a function of time.

A result for the toy Lake 1 model is in Figure 36, which shows how the 20-year warming trend in annual surface water temperature of Lake 1 changes in time. A warming-trend peak appears at around year 83, with the deepest lake column exhibiting the strongest surface-water warming trend of $0.20°C/year$, the intermediate lake column the trend of $0.19°C/year$, and the shallowest lake column the trend of $0.14°C/year$. This results is consistent with the observed correlation between water depth and surface-water warming trends.
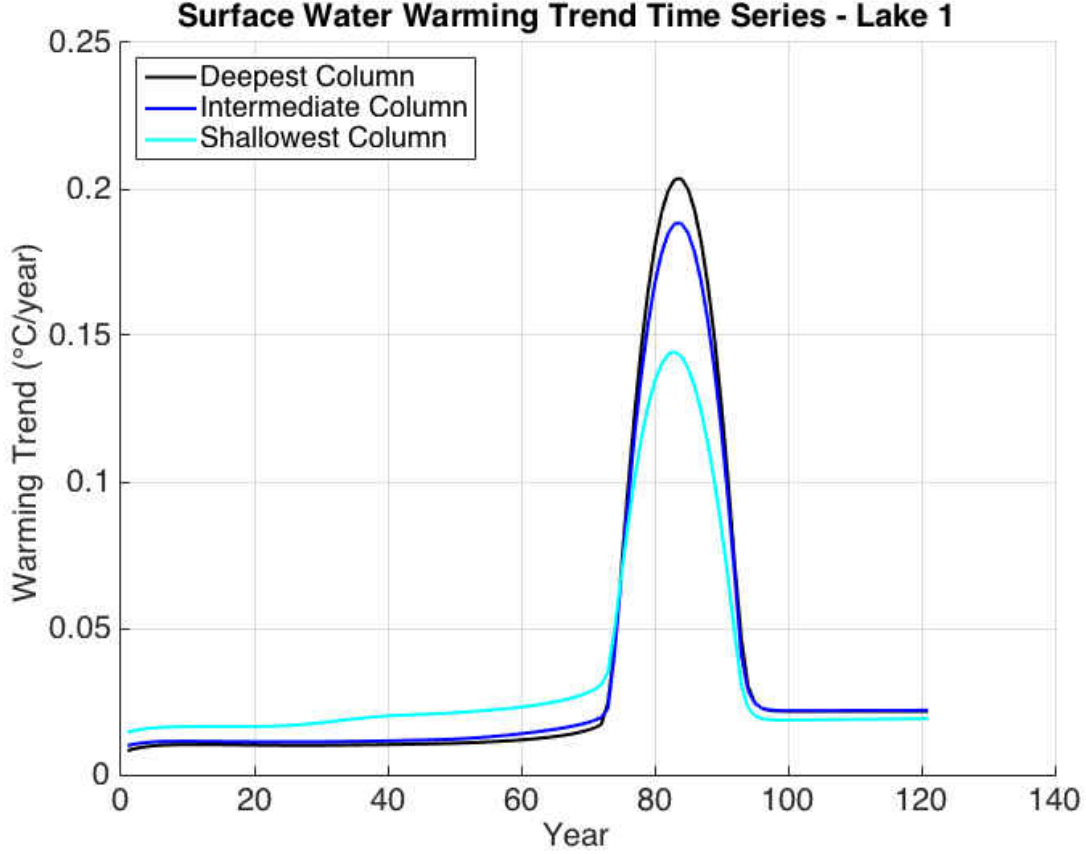
Figure 36: *The time series of the 20-year warming trends in annual-mean surface water temperature of Lake 1 (toy Superior). The black curve is about the 225m-deep column. The blue curve is about the 150m-deep column. The cyan curve is about the 50m-deep column. When computing a warming trend, a moving window of 20 years is applied to a surface water temperature time series and linear regression is used to estimate the warming trend of the portion of the time series inside the 20-year window. The forcing contains the steady warming at 0.04 K/year of the upper-atmosphere.*

Figure 37 is of Lake 2. The first warming-trend peak occurs at around year 63, when the deepest lake column transitions from being wintertime-ice-covered to being perennially ice-free, and the second warming-trend peak occurs at around year 81, when the intermediate lake column transitions from being wintertime-ice-covered to being perennially ice-free. The largest peak is the second peak, with the intermediate lake column exhibiting the strongest surface-water warming trend of $0.16°C/year$, the deepest lake column the trend of $0.11°C/year$, and the shallowest lake column the trend of $0.10°C/year$. We note that this largest warming-trend peak occurs when the intermediate lake column transitions from being wintertime-ice-covered to being perennially ice-free. During the period of this warming-trend peak, the deepest lake column is perennially ice-free.

74
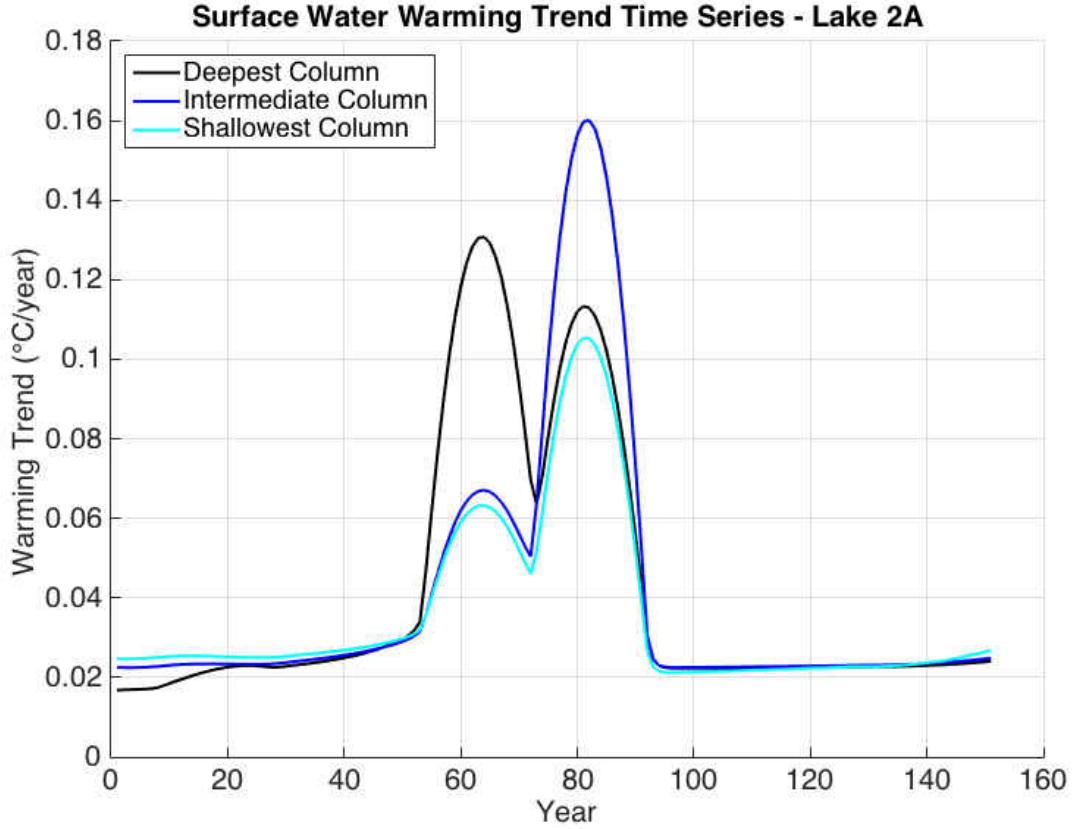
Figure 37: *The time series of the 20-year warming trends in annual-mean surface water temperature of Lake 2 (toy southern Michigan). The black curve is about the 140m-deep column. The blue curve is about the 80m-deep column. The cyan curve is about the 30m-deep column. When computing a warming trend, a moving window of 20 years is applied to a surface water temperature time series and linear regression is used to estimate the warming trend of the portion of the time series inside the 20-year window. The forcing contains the steady warming at 0.04 K/year of the upper-atmosphere.*

Despite this, the warming-trend peak of the deepest lake column within the period is relatively strong, reaching $0.11°C/year$. An important outstanding problem is to understand why the deepest lake points of Lakes Michigan and Ontario still exhibit stronger warming trends than shallower lake points do, despite the fact that they have been mostly ice-free and the direct ice effects are not expected there. This result indicates the possibility that the flow of air over the lake is one factor that amplifies the warming trends of regions of large water depth.

We list the magnitudes of the largest warming-trend peaks of these toy lakes in Table 11.

Table 11: *The 5-year moving averaged peak warming trends in annual-mean surface water temperature of various toy lakes with upper atmospheric forcing with the 0.04°C/year linear trend. The time series of a warming trend is first computed by applying a 20-year moving window to the time series of surface water temperature and by computing the trend by linear regression of each 20-year time period. Then, the 5-year moving window is applied to compute the time series of the 5-year average of the warming trend time series. The second column is about the shallowest lake column. The third column is about the intermediate lake column. The fourth column is about the deepest leks column. The units are in °C/year.*

Warming-Trend Peak	Shallowest col.	Intermediate col.	Deepest col.	Overall
Lake 1	0.141	0.185	0.200	0.185
Lake 2	0.104	0.157	0.112	0.132
Lake 3	0.070	0.084	0.141	0.098
Lake 4	0.080	0.119	0.086	0.098

Forcing with Linear Trend and Inter-Annual Variability   In this subsection, we introduce inter-annual variability, in addition to the positive linear trend, to the upper atmospheric forcing. The purpose of the experiment is as follows. In §3.2.1, we obtained the two important results in the case of bi-modal regimes,

(1) The difference in summer maximum heat content between the two regimes is larger for deeper lakes.

(2) The range of upper-atmospheric temperature in which the two regimes exist is larger for deeper lakes.

As already discussed, these two results are natural consequences of the fact that shallower lakes go through longer duration of summer stratification than deeper lakes and consequently, enjoy a longer time to efficiently respond to the summer atmosphere; deeper lakes have longer memory of ice effects, maintaining the clearer difference between the warmer and colder regimes. What these two results would lead to is that shallower lakes more easily transition between regimes than deeper lakes do because of the less distinction between the regimes. When we introduce inter-annual variability in atmospheric forcing in addition to a linear warming trend, we expect that the surface-warming trend of Lake

Table 12: *The units are in °C/year. The 5-year moving averaged peak warming trends in annual-mean surface water temperature of various toy lakes with upper atmospheric forcing with the 0.04°C/year linear trend plus periodic inter-annual variability. The time series of a warming trend is first computed by applying a 20-year moving window to the time series of surface water temperature and by computing the trend by linear regression of each 20-year time period. Then, the 5-year moving window is applied to compute the time series of the 5-year average of the warming trend time series. The second column is about the shallowest lake column. The third column is about the intermediate lake column. The fourth column is about the deepest leks column.*

Warming-Trend Peak	Shallowest col.	Intermediate col.	Deepest col.	Overall
Lake 1	0.137	0.171	0.183	0.171
Lake 2	0.090	0.119	0.129	0.116
Lake 3	0.071	0.097	0.107	0.092
Lake 4	0.063	0.085	0.092	0.076

4, the shallowest of the toy lakes, drops most.

As in the previous subsection, we compute 100-year or longer time series of surface water temperature for each toy model. However, the inter-annual variability we introduce in this subsection is not stochastic; we simply add the constant $+2°C$ temperature anomaly to the first two years of the time series, the constant $-2°C$ temperature to the next two years, and we keep alternating these addition and subtraction of the $2°C$ temperature anomaly every two years. The standard deviation of seasonal temperature anomalies of this times series is $2°C$, which is comparable to the standard deviation of seasonal air temperature anomalies based on the NARR reanalysis in Table 9. The reason we introduce such simple inter-annual variability in this subsection is to demonstrate that this simple variability is enough to qualitatively reproduce the correlation between water depth and surface-water warming trends of regions of a lake consistent with observational data.

The results are in Table 12. In this table, we list the magnitudes of the largest warming-trend peaks of these toy lakes as we did in Table 11. Comparing Table 12 with Table 11, we find that the inter-annual variability of upper air temperature affects the overall surface-warming trend of the shallowest lake (Lake 4) most. Moreover, with atmospheric inter-annual variability, we recover the expected correlation between water depth

and surface-water warming trends of a lake. This is because the distinctions between the first and second warming-trend peaks of these lakes become blurry by adding inter-annual variability.

What are other implications of this result for large lakes such as the Great Lakes? This indicates that, when inter-annual variability is added to atmospheric forcing, lake points of larger water depth and those of shallower water depth react differently. When periodic forcing with a steady and small linear trend is applied to a three-column lake, the three columns share the same equilibrium state. However, atmospheric noise in a model constantly disrupts the lake from its equilibrium states. By adding atmospheric stochasticity, different lake columns of a single lake begin to acquire individuality, with a deep lake column responding to the atmospheric noise slightly more like a deep lake does, with a shallow lake column responding to the atmospheric noise slightly more like a shallow lake does.

Ice-Free Regions of Lakes Michigan and Ontario and Their Surface Warming Trends This observation gives us a hint for the situation of Lakes Michigan and Ontario. In Figure 5, the top-right panel shows the correlation between water depth and the warming trends of surface lake points of Lake Michigan. The horizontal axis is water depth, and the vertical axis is the warming trend in annual-mean surface water temperature, based on the GLSEA satellite data, spatially averaged over the surface area whose water depth underneath corresponds to the value on the horizontal axis. The bottom-right panel of Figure 5 is the corresponding figure for Lake Ontario. Lake Michigan especially shows a monotonic relationship between water depth and the warming trends of surface lakes points. However, the warming trends in the figure are based on the GLSEA data between the years 1995 and 2012, and during this period, the surface regions of largest water depths of Lake Michigan were mostly ice-free. Therefore, these surface regions did not receive ice-related feedback effects, at least not directly. Instead, we hypothesize that, with atmospheric stochasticity, a deeper lake column responds to atmospheric noise slightly more like a deep lake does, retaining anomalous heat or loss of heat better, and a shallower lake column responds to atmospheric noise slightly more like a shallow lake

does, losing anomalous heat or loss of heat faster. With extra heat or loss of heat being transported by atmospheric transport and lake circulation, even though surface regions of largest water depths do not directly receive the ice-albedo feedback, these regions still exhibit the strongest warming trends. As we noted in §3.2.3 and earlier in this section, the flow of air in the lower atmosphere plays an important role in transporting heat, and Figure 28 demonstrates that a regime transition of a shallower lake column affects the surface water temperatures of the deepest columns considerably. Lake circulation might also plays a comparably important role in transporting heat. Our hypothesis is that, once the regions of large water depths receive heat or loss of heat due to ice-related feedback effects from the neighboring regions, they retain the anomaly longer than their shallower neighbors do due to their longer memory. However, we would need a full 3D lake model to verify this hypothesis.

3.3.2 The Role of Atmospheric Heat Transport in Synchronizing Regime Transitions

A Question of Simultaneity among Regions of the Great Lakes In this latter part of the section on lakes' responses to global warming, we address the following question. It is not one of the six questions introduced in Chapter 1, but here is another important question.

In §3.2.1, we discussed multiple climate regimes of lakes of uniform depth. Figure 38, which we saw in §3.2.1, contains the hystereses of summer maximum heat content of the lakes of various depths. In this figure, we notice that the ranges of upper air temperature in which two climate regimes exists greatly differ among lakes of different depths. For example, of the 100m-deep lake, two climate regimes coexist approximately between $1.5°C$ and $2.5°C$. Of the 150m-deep lake, however, two climate regimes coexist approximately between $-2°C$ and $-0.5°C$. Yet all of the Great Lakes, whose average depths vary from 19m to 147m, seem to be transitioning from higher-level ice cover regimes to lower-level ice cover regimes today almost simultaneously, albeit slowly.

Lake Superior was more than 90% ice-covered in some winters and less than 20%
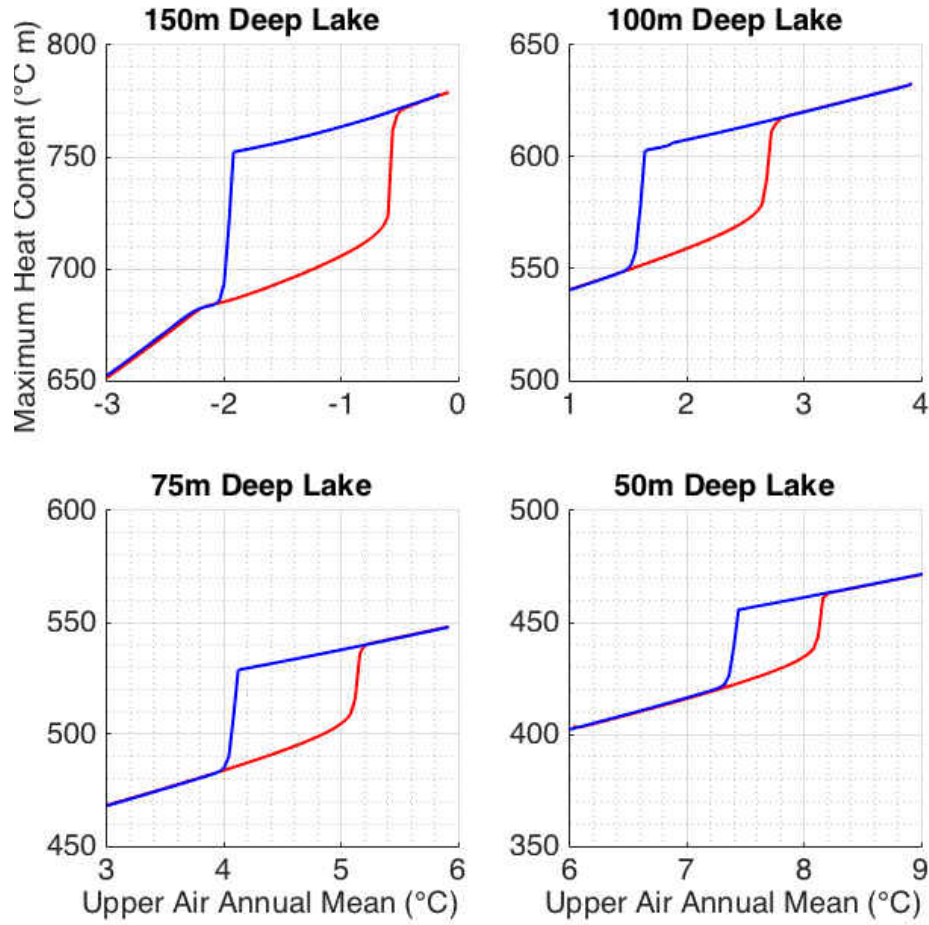
Figure 38: *The hysteresis of summer maximum heat content of the lake of the following depth: 50m, 75m, 100m, and 150m. The abscissa is the annual-mean of periodic upper air temperature, which acts as forcing. The ordinate is summer maximum heat content. The units are in °Cm.*

ice-covered in some other winters. Similarly, Lake Erie was more than 90% ice-covered in some winters and less than 20% ice-covered in some other winters. This means that the inter-annual variability of atmospheric forcing has been large enough to have both Lakes Superior and Erie experience two extremes in recent years: largely ice-free winters and nearly 100% ice-covered winters. The average depth of Lake Superior is $147m$ and its maximum depth is $406m$. The average depth of Lake Erie is $19m$ and its maximum depth is $64m$. As we see in Figure 38, it is much easier to freeze shallow lakes than deep lakes, and it is easier to keep deep lakes ice-free than shallow lakes. Within a single lake, the same can be said of its shallow near-shore regions and deep offshore regions. It is easier to freeze shallow near-shore regions than deep offshore regions, and it is easier to keep

deep offshore regions ice-free than shallow near-shore regions. *Why is the magnitude of inter-annual variability in atmospheric forcing, of which the standard deviations of seasonal-mean temperatures between the 850mb and 500mb pressure levels are somewhere between $1°C$ and $2°C$ and the standard deviation of seasonal-mean downward shortwave radiation at the surface is somewhere between $5W/m^2$ and $10W/m^2$, enough to make Lake Superior exhibit two extremes: an almost ice-free surface in some winters and a nearly 100% ice-covered surface in other winters?* This is the question we would like to address in this subsection.

Atmospheric Heat Transport Experiment There is a parameter that changes the efficiency of heat transport between separate air masses in the lower atmosphere. To remind the reader, in our lake-atmosphere-land model, the lower atmosphere is split into smaller parts, whose boundaries coincide with the boundaries of lake columns and land. In making Figures 36-37, this efficiency of heat transport between parts of the lower atmosphere, $coef_{air}$, is set to $500W/m^2°C$ (Equation (3.8)). What if we change the value of this parameter, without changing anything else in the setup used to make Figures 36-37? Figure 39 is a result of such a change, when we use $coef_{air} = 50W/m^2°C$.

The figure contains the time series of the 20-year warming trends in annual-mean surface water temperature of Lake 1, given two different efficiencies of lower atmospheric heat transport. In the figure, both "1A" represented in blue and "1B" represented in black are the toy Lake 1, but the efficiency of heat exchange between the air masses in the lower atmosphere is greater over 1A. Comparing 1A represented in blue and 1B represented in black, we notice the following. In 1B, we find two peaks in the time series of the 20-year warming trend in annual surface water temperature in each curve. One peak corresponds to when the deepest lake column transitions from being wintertime ice-covered to being perennially ice-free. Another peak corresponds to when the intermediate lake column transitions from being wintertime ice-covered to being perennially ice-free. As discussed in §3.2.3, as far as models with quasi-steady periodic forcing (meaning that the linear trend is small) are concerned, the local-climate regimes of all the three lake columns share the same "mode." That is, when the deepest lake column is in its warmest
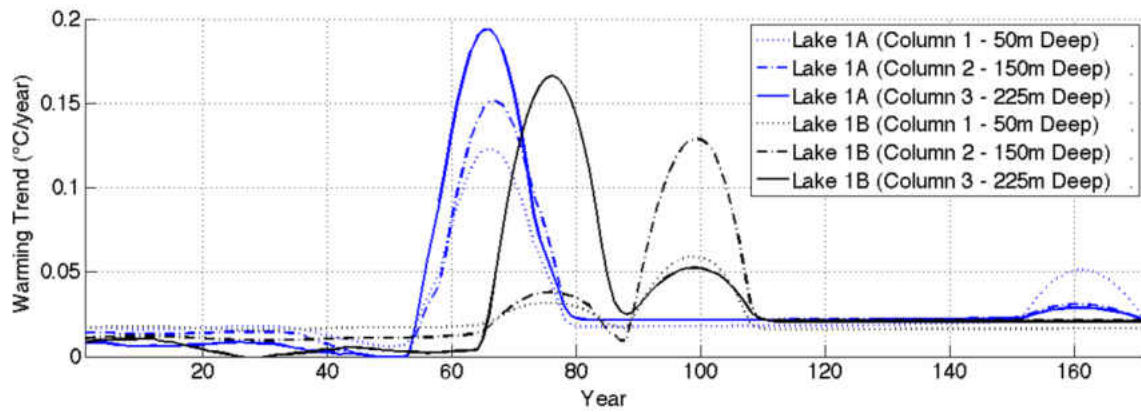
Figure 39: *The time series of 20-year warming trends in annual-mean surface water temperature of Lake 1 (toy Superior) given two different efficiencies of lower atmospheric heat transport. Both "1A" represented in blue and "1B" represented in black are the toy Lake 1, but the efficiency of heat exchange between the air masses in the lower atmosphere is greater over 1A. The solid curves are about the 225m-deep column. The dash dotted curves are about the 150m-deep column. The dotted curves are about the 50m-deep column. When computing a warming trend, a moving window of 20 years is applied to a surface water temperature time series and linear regression is used to estimate the warming trend of the portion of the time series inside the 20-year window. The forcing contains the steady warming at 0.04 K/year of the upper-atmosphere.*

stable equilibrium state, then the shallowest and intermediate lake columns are also in their respective warmest equilibrium states. Similarly, when the deepest lake column is in its intermediate (or coldest) equilibrium states, then the shallowest and intermediate lake columns are also in their respective intermediate (or coldest) equilibrium states. That we find two peaks in the time series of the 20-year warming trend in annual surface water temperature in the black curves means that the lake represented in black transitions from its coldest regime to its intermediate regime at the first peak in the time series of the 20-year warming trends, and it transitions from its intermediate regime to its warmest regime at the second peak in the time series of the 20-year warming trends. Of 1A, the blue curves, with more efficient heat transfer between parts of the lower atmosphere, however, we find only one peak in each curve, meaning that the lake transitions not only from its coldest regime to its intermediate regime but also from the intermediate regime to its warmest regime, the two steps, almost simultaneously. This means that, unlike 1B, effectively no intermediate regime exists in this lake-atmosphere-land coupled system. The implication of these results is that the atmosphere near the surface acts as a medium to transfer heat (or loss of heat) between shallow near-shore regions and deep offshore regions, facilitating the spread of ice formation (or ice disappearance) from one region to other regions. This is why a relatively modest magnitude of inter-annual variability in atmospheric forcing is enough to make Lake Superior almost ice-free in some winters and nearly 100% ice-covered in other winters.

We expect that this assistance of the flow of air in the lower atmosphere in spreading ice formation (or preventing ice formation) plays a role not only within a single lake but also for multiple lakes in proximity to each other. We hypothesize that a local regime transition of Lake Superior assists the other Great Lakes in transitioning to similar local-climate regimes with help of westerly winds, since climatologically, winds roughly flow from the west to the east over the Great Lakes. In Appendix B, we discuss Lake Superior's influence on its downwind regions in more detail.

3.3.3 Jump-like Behavior in Deep Lakes

Here, we present another global-warming experiment, but this time, stochastic noise is added to the atmospheric forcing in addition to the linear trend. With the same stochastic and periodic components of forcing used in §3.2.4 and an additional linear trend of $0.04°C/year$ in upper air temperature, Figure 40 is one realization of more than 100 years of time series of the toy Lake 1 model.
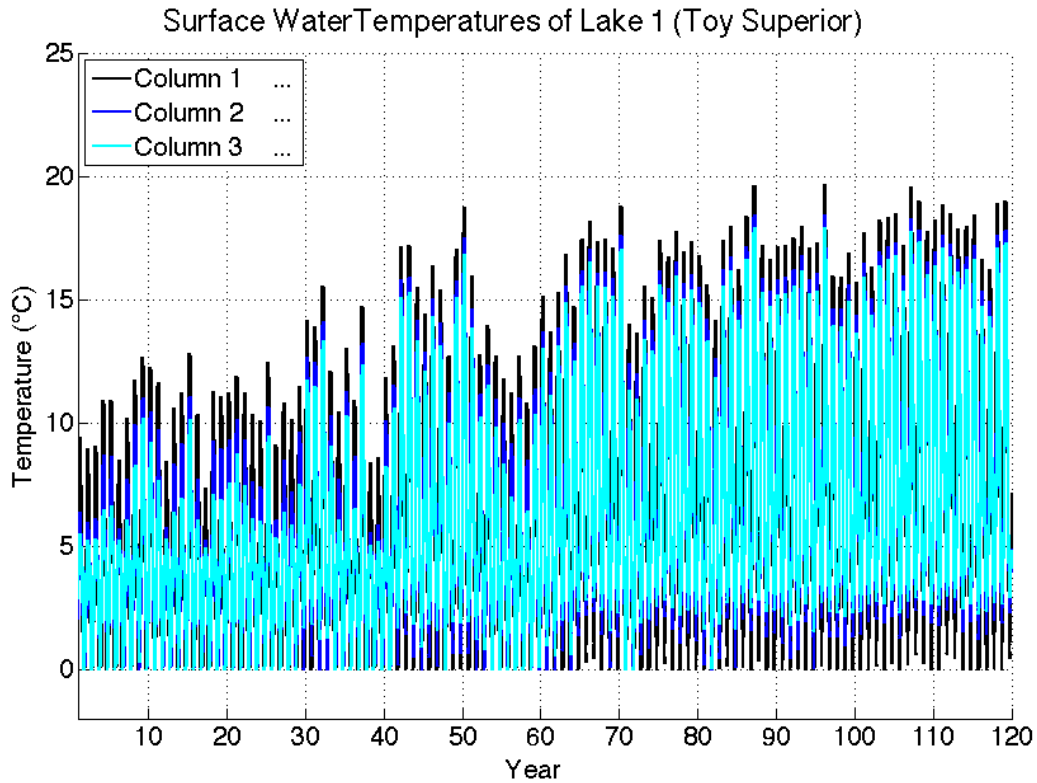
Figure 40: *A realization of more than 100 years of time series of Lake 1. The black curve denotes the surface water temperature of the shallowest lake column, the blue curve denotes the surface water temperature of the intermediate lake column, and the cyan curve denotes the surface water temperature of the deepest lake column.*

This is one example of a realization in which the lake transitions back to its colder regime a couple of times before it permanently moves to the warmer local-climate regime. Lake 1 is a deep lake, whose deepest column has water depth of 225m. By contrast, the time series of surface water temperatures of shallower toy lakes exhibit less clear regime transitions, and it is most difficult to recognize regime transitions in the time series of Lake 4, the shallowest among them (not shown).

Chapter 4

Multiple Climate Regimes of the Great Lakes in Observations

4.1 Multi-Modality in Atmospheric Data – Upwind Temperature as a Measure of Climate Forcing

In this chapter, we compare model outputs with data based on the NARR reanalysis, and examine whether results from our lake-atmosphere-land coupled model are consistent with observations. We especially use the NARR reanalysis data of air temperature at various pressure levels over North America. In §3.2.4, we discussed the scatter plot, whose horizontal axis was three-year mean of upper air temperature, from September of year $x - 3$ to August of year x, and whose vertical axis was summer maximum surface water temperature of the deepest column of the toy Lake 2 of year x, of more than 50 years of time series. We chose three-year mean of air temperature on the horizontal axis because we saw in §3.2.1 that it sometimes took a few years for a lake to transition to a new climate regime when it was disrupted. We chose three years as a representative timescale of the slowest regime transitions. Here, we construct similar scatter plots based on the NARR reanalysis data, but this time, with one-year mean of air temperature on the horizontal axis. The advantage of using one-year mean of air temperature for analysis, instead of three-year mean, is that such a data set is a collection of "independent variables." For example, there is no overlap of information between the one-year mean from September of year $x - 1$ to August of year x and the one-year mean from September of year x to August of year $x + 1$. This is unlike a data set of three-year mean air temperature used in §3.2.4, in which there exists a two-year overlap of information between the three-year mean from September of year $x - 3$ to August of year x and the three-year mean from September of year $x - 2$ to August of year $x + 1$.

In our lake-atmosphere-land coupled model, the temperature of the upper atmosphere is used as the boundary condition. The upper atmosphere is not affected by whatever happens below, and the lower atmosphere is affected both by the upper atmosphere and the surface. This asymmetric direction of influence gives rise to the difference in appearance of two scatter plots, one whose horizontal axis is one-year mean of *upper* air temperature, and the other whose horizontal axis is one-year mean of *lower* air tempera-
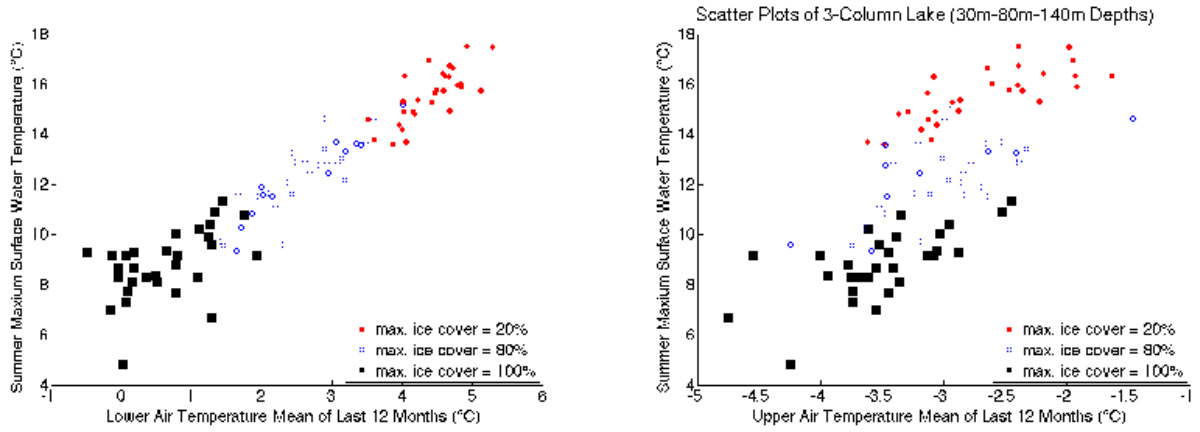
Figure 41: *The scatter plot of one-year mean of upper or lower air temperature versus summer maximum surface water temperature of the deepest column of Lake 2. The right panel is the scatter plot of one-year mean, from September of year $x-1$ to August of year x, of upper air temperature on the horizontal axis, versus summer maximum surface water temperature of the deepest column of the Lake 2 toy model of year x on the vertical axis, after we run more than 50 years of time series. Filled black squares correspond to the cases in which ice covers 100% of the lake during the winter of year x. Blue circles correspond to the cases in which ice covers 80%, only the shallowest and intermediate lake columns, of the lake during the winter of year x. Red circles correspond to the cases in which ice covers 20%, only the shallowest lake column, of the lake during the winter of year x. Similarly, the left panel is the scatter plot of one-year mean, from September of year $x-1$ to August of year x, of lower air temperature on the horizontal axis, versus summer maximum surface water temperature of the deepest column of the Lake 2 toy model of year x on the vertical axis, from the same time series.*

ture. Let us see some example of model results. In Figure 41, the right panel is the scatter plot of one-year mean, from September of year $x-1$ to August of year x, of *upper* air temperature on the horizontal axis, versus summer maximum surface water temperature of the deepest column of the toy Lake 2 of year x on the vertical axis, after we run more than 50 years of time series. Compared to the model-generated scatter plot in §3.2.3, we slightly lower the longterm mean of upper air temperature this time so that the numbers of black, blue, and red dots are comparable to each other, but the standard deviation of noise in the forcing remains the same.

In a real regional climate system, we cannot separate the atmosphere into the part that acts as forcing and the part affected by the forcing. What we expect, above a real lake, of corresponding scatter plots with air temperature at various levels would be something in between the left and right panels of Figure 41. For example, if air temperature near the surface is plotted on the horizontal axis, such a plot would look like the left panel, but

87

if air temperature at a high altitude is plotted on the horizontal axis, such a plot would look like the right panel. If air temperature at an altitude neither too high nor too low is plotted on the horizontal axis, the plot would look neither like the left nor like the right panel of Figure 41, but a mixture of the two figures. A question is, in a real regional climate system containing a large lake such as Lake Superior, how high above does air have to go in order to avoid the effect of the lake completely? Air temperature data at what altitude or pressure level should we use to make a comparison with the model result whose horizontal axis is the forcing: the temperature of the upper atmosphere? We address this question in detail later in Appendix B. For now, to circumvent such a question, what we can do is to look at a region upwind of the Great Lakes.
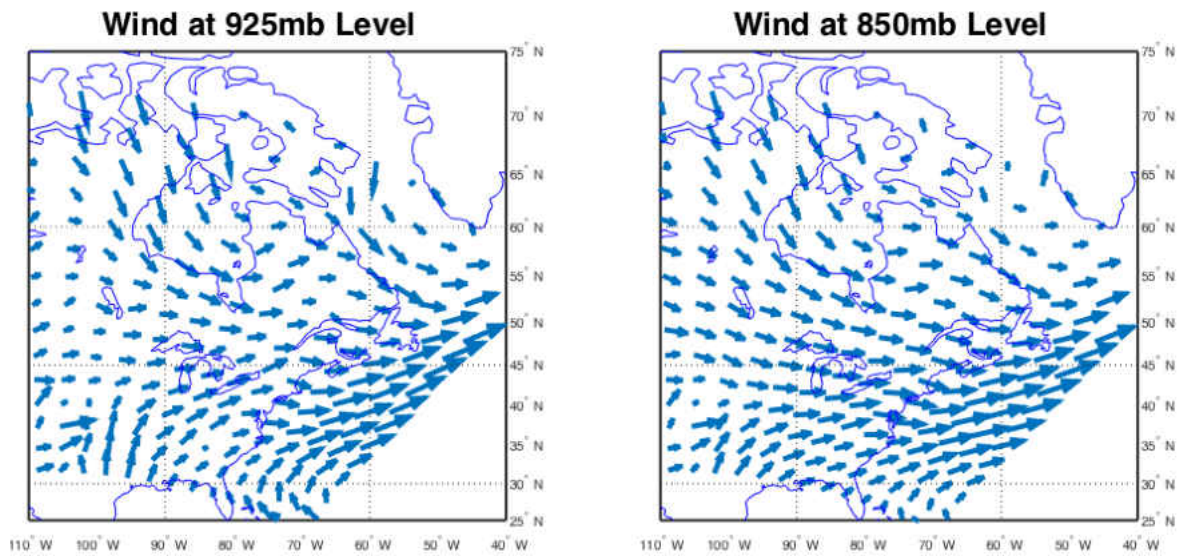
Figure 42: *The longterm-mean wind fields (left) at the 925mb level and (right) at the 850mb level over the eastern part of North America for the years 1979-2013, based on the NARR reanalysis data.*

Figure 42 shows the longterm-mean wind fields at the 925mb and 850mb pressure levels over North America for the years 1979-2013, based on the NARR reanalysis data.

Climatologically, we can roughly think that wind flows from the west to the east over the Great Lakes. Therefore, the atmosphere above a region upwind of the Great Lakes must be less affected by the lakes than the atmosphere directly above the lakes.
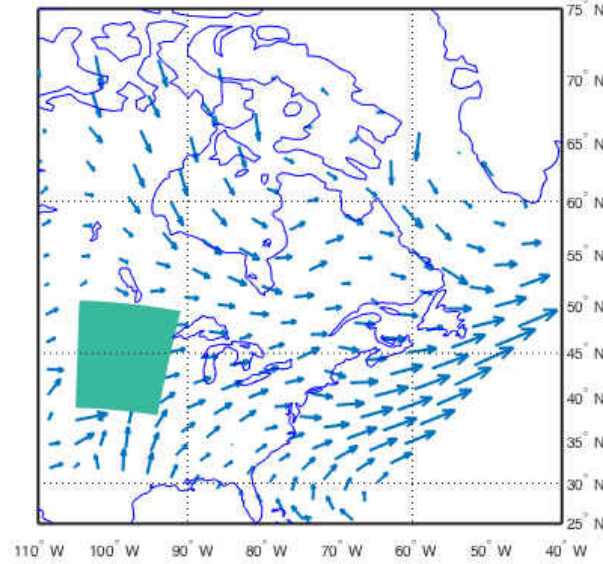
Figure 43: *A rectangular box region for spatial averaging to compute mean air temperature upwind of the Great Lakes. The arrows show a map of longterm-mean wind field at the 925mb pressure level average for the years 1979-2013.*

Based on this idea, let us take a look at the air temperature data at various pressure levels, based on the NARR reanalysis data, upwind of the Great Lakes, spatially averaged over a rectangular box region shown in Figure 43.

To make sure that this region is little affected by the Great Lakes, Table 13 shows the comparison of warming trends between those above the aforementioned box region and those right above buoy station 45004 in eastern Lake Superior. We note that the magnitudes of the warming trends at the 1000mb and 900mb pressure levels above this upstream region are less than a half of those right above buoy station 45004 in eastern Lake Superior. So, let us use this air temperature data as a proxy for the forcing to explore indications of multiple climate regimes of some of the Great Lakes.

Table 13: *The warming trends in annual-mean air temperature at various pressure levels above the rectangular box region of Figure 43 upwind of the Great Lakes (2nd column) and above buoy station 45004 (3rd column), by linear regression based on the NARR reanalysis data for the years 1988-2007. The units are in °C/year.*

Pressure Level	Warming Trend 1 (°C/year)	Warming Trend 2 (°C/year)
1000mb	0.06 ± 0.04	0.14 ± 0.04
900mb	0.06 ± 0.04	0.12 ± 0.04
800mb	0.07 ± 0.03	0.10 ± 0.03
700mb	0.08 ± 0.02	0.10 ± 0.03
600mb	0.07 ± 0.02	0.09 ± 0.03
500mb	0.05 ± 0.02	0.06 ± 0.02
400mb	0.04 ± 0.02	0.05 ± 0.02
300mb	0.03 ± 0.02	0.02 ± 0.02
200mb	-0.02 ± 0.02	-0.01 ± 0.02

4.1.1   A Deep–Lake Example: Manifestations of Multiple Climate Regimes of Lake Superior

Figures 44-45 contain the scatter plots of one-year mean, from September of year $x - 1$ to August of year x, of air temperature anomalies at various pressure levels, spatially averaged over the aforementioned box region, on the horizontal axis, versus August-mean surface water temperature of year x at buoy station 45004, in eastern Lake Superior, on the vertical axis. There are two reasons we are particularly more interested in buoy station 45004, in eastern Lake Superior, than those in central or western Lake Superior: (1) this buoy station is the closest to the region of the strongest warming trends of Lake Superior (Figure 46) and (2) it is also the closest to the region of the largest water depths (Figure 46) of the lake despite that the water depth below the station itself is 226m.

The top-left panel of Figure 44 is the scatter plot with one-year mean of air temperature anomalies at the 900mb level on the horizontal axis. In this panel, we find that dots make a parallelogram between -1.5 °C and 0.5 °C of the horizontal axis and between 5 °C and 15 °C of the vertical axis, reminding us of the hysteresis plots of toy lakes in §3.2.3. We find that dots branch off at the lower-left corner of the parallelogram as air temperature on the horizontal axis increases, again reminding us of the hysteresis plots of toy lakes in §3.2.3. This is another indication that eastern Lake Superior possibly exhibits

Figure 44: *Scatter plots of one-year mean, from September of year $x - 1$ to August of year x, of air temperature anomalies at various pressure levels, spatially averaged over the aforementioned box region (Figure 43), on the horizontal axis, versus August-mean surface water temperature of year x at buoy station 45004, in eastern Lake Superior, on the vertical axis. The figure contains four panels, whose horizontal axes are air temperature anomalies at the 900mb level, 800mb level, 700mb level, and the 600mb level. In these panels, black squares and black diamonds correspond to the cases in which ice covers more than 90% and between 80% and 90% of Lake Superior, respectively, during the winter of year x. Blue diamonds and blue circles correspond to the cases in which ice covers between 70% and 80% and between 50% and 70% of the lake, respectively, during the winter of year x. Green circles and red circles correspond to the cases in which ice covers between 25% and 50% and between 10% and 25% of the lake, respectively, during the winter of year x. The year x runs from 1981 to 2013.*

bi-modality. In the top-right panel, with one-year mean of air temperature anomalies at the 800mb level on the horizontal axis, we find a range of air temperature, between -0.4 °C and 0.7 °C, where black, blue, green, and red dots all coexist but are layered vertically. This range is where multiple local-climate regimes apparently exist. In model results in §3.2.3, we saw that the widths of the ranges of upper atmospheric forcing that admitted
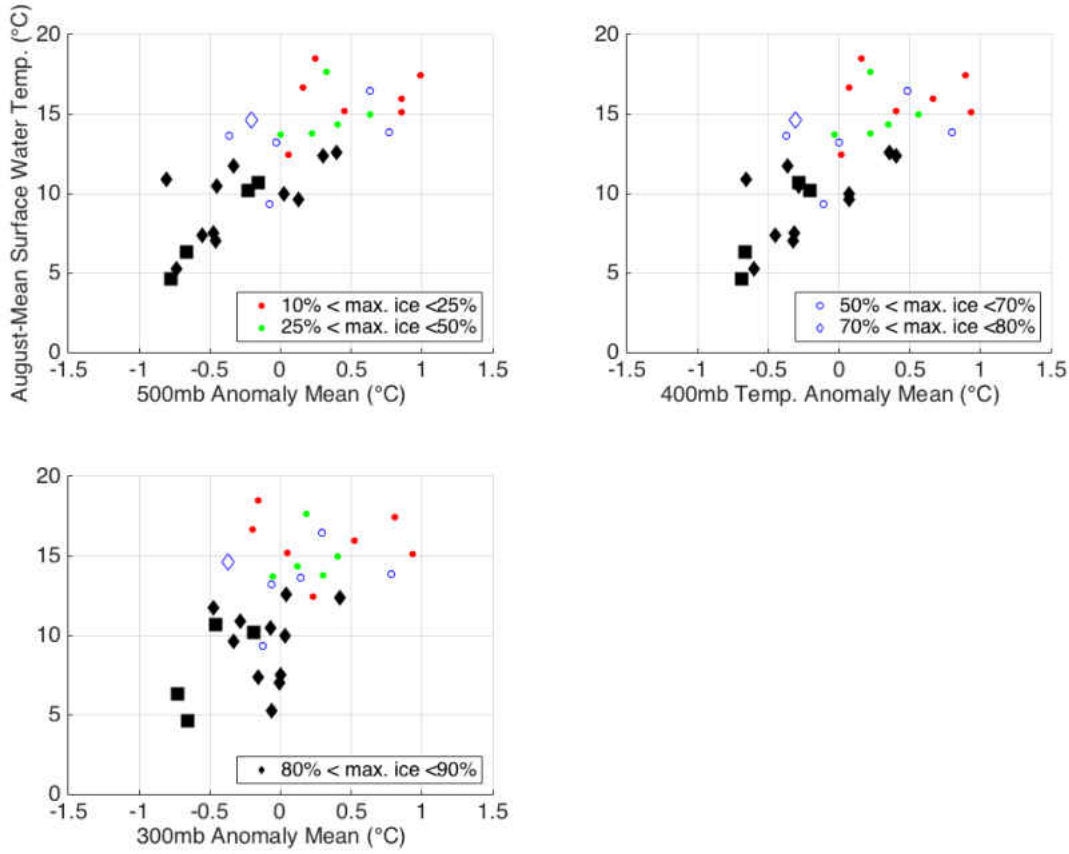
Figure 45: *Scatter plots of one-year mean, from September of year $x - 1$ to August of year x, of air temperature anomalies at various pressure levels, spatially averaged over the aforementioned box region (Figure 43), on the horizontal axis, versus August-mean surface water temperature of year x at buoy station 45004, in eastern Lake Superior, on the vertical axis. The figure contains three panels, whose horizontal axes are air temperature anomalies at the 500mb level, 400mb level, and the 300mb level. In these panels, black squares and black diamonds correspond to the cases in which ice covers more than 90% and between 80% and 90% of Lake Superior, respectively, during the winter of year x. Blue diamonds and blue circles correspond to the cases in which ice covers between 70% and 80% and between 50% and 70% of the lake, respectively, during the winter of year x. Green circles and red circles correspond to the cases in which ice covers between 25% and 50% and between 10% and 25% of the lake, respectively, during the winter of year x. The year x runs from 1981 to 2013.*

multiple climate regimes were often somewhere between 0.5 °C and 2 °C (Figures 28-31).

Therefore, both observational data and model results suggest that numbers between 0.5 °C and 2 °C are typical widths of atmospheric-forcing ranges that admit multiple climate regimes.
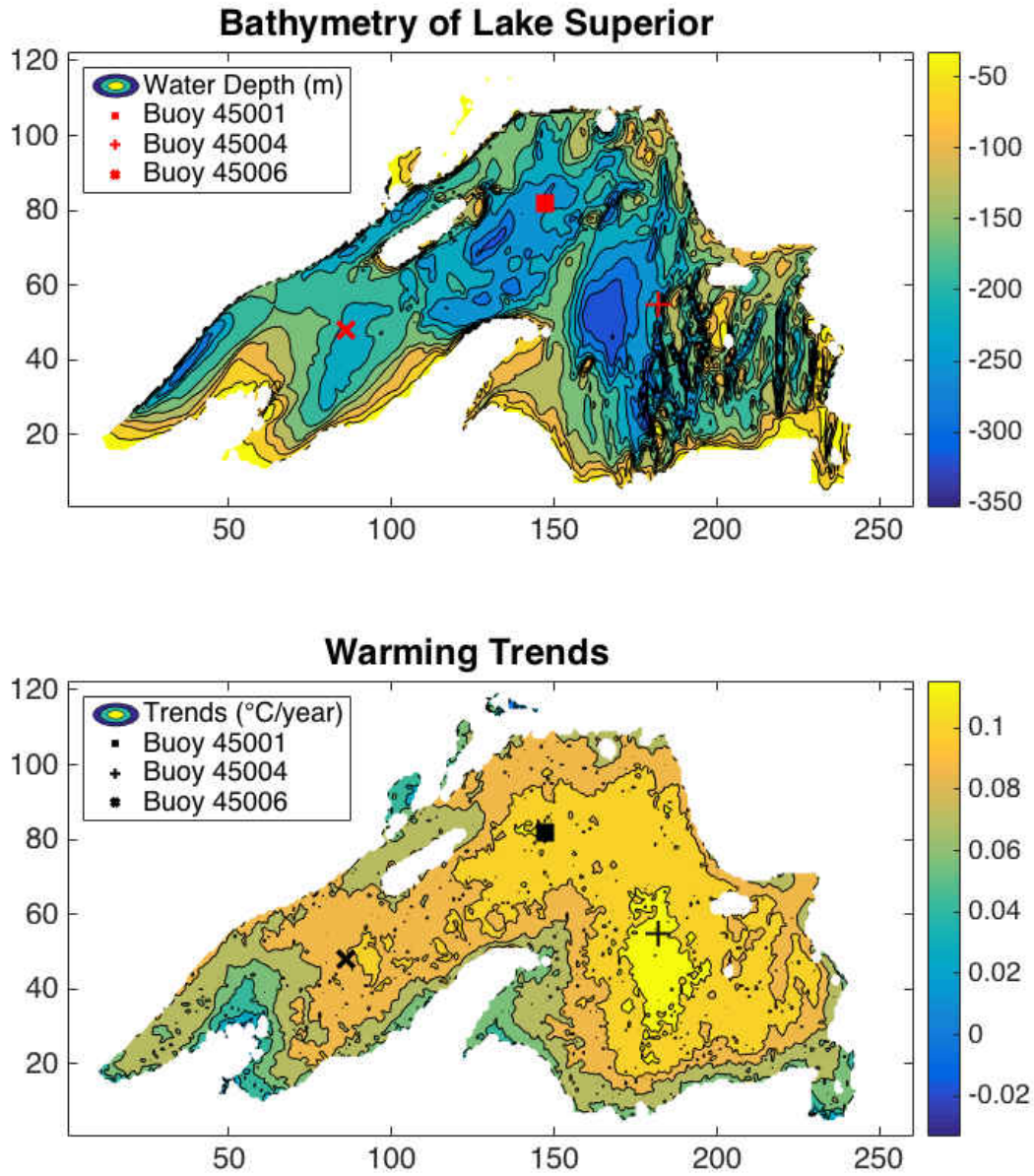
Figure 46: *(Top panel) A map of water depth of Lake Superior in meters. The square dot is the location of buoy station 45001. The "+" dot is the location of buoy station 45004. The "×" dot is the location of buoy station 45006. (Bottom panel) A map of warming trends in annual-mean surface water temperature of Lake Superior based on the GLSEA satellite data for the years 1995-2012, in the unit of °C/year. The square dot is the location of buoy station 45001. The "+" dot is the location of buoy station 45004. The "×" dot is the location of buoy station 45006.*

4.1.2   A Shallow–Lake Example: Climate Regimes of Lake Erie

By contrast, Lake Erie looks quite different. Figure 47 contains the scatter plots of

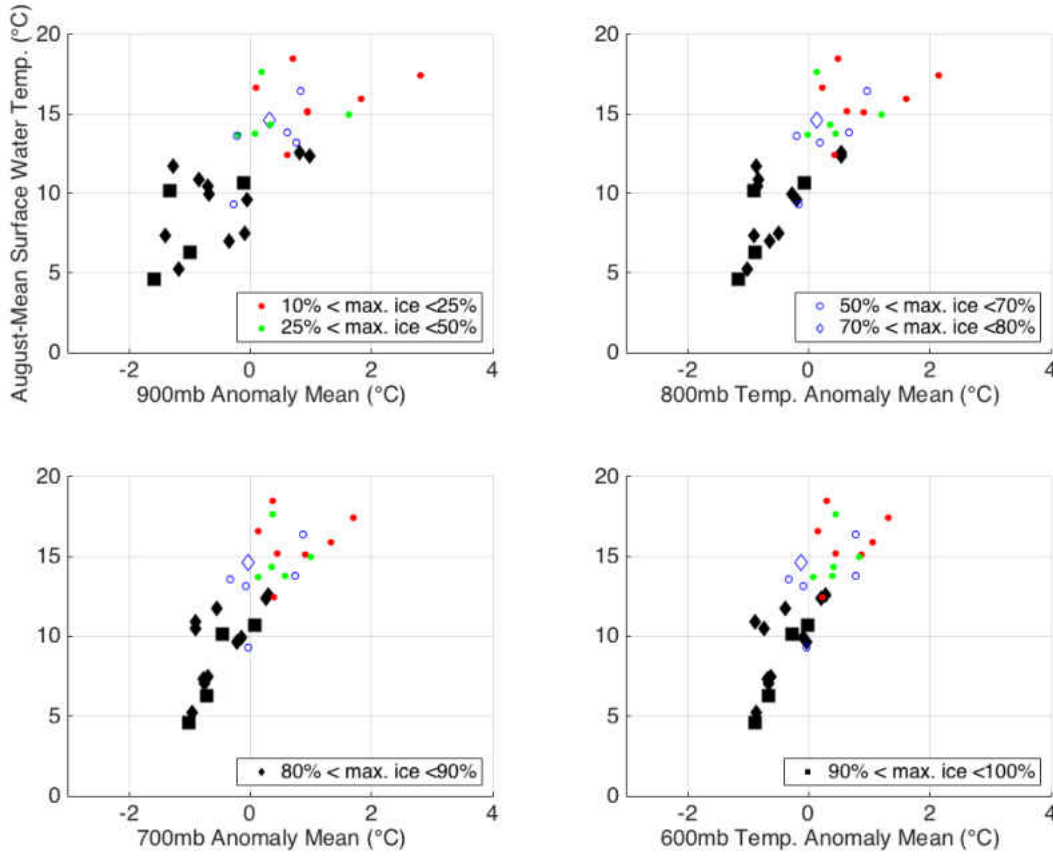one-year mean, from September of year $x - 1$ to August of year x, of air temperature
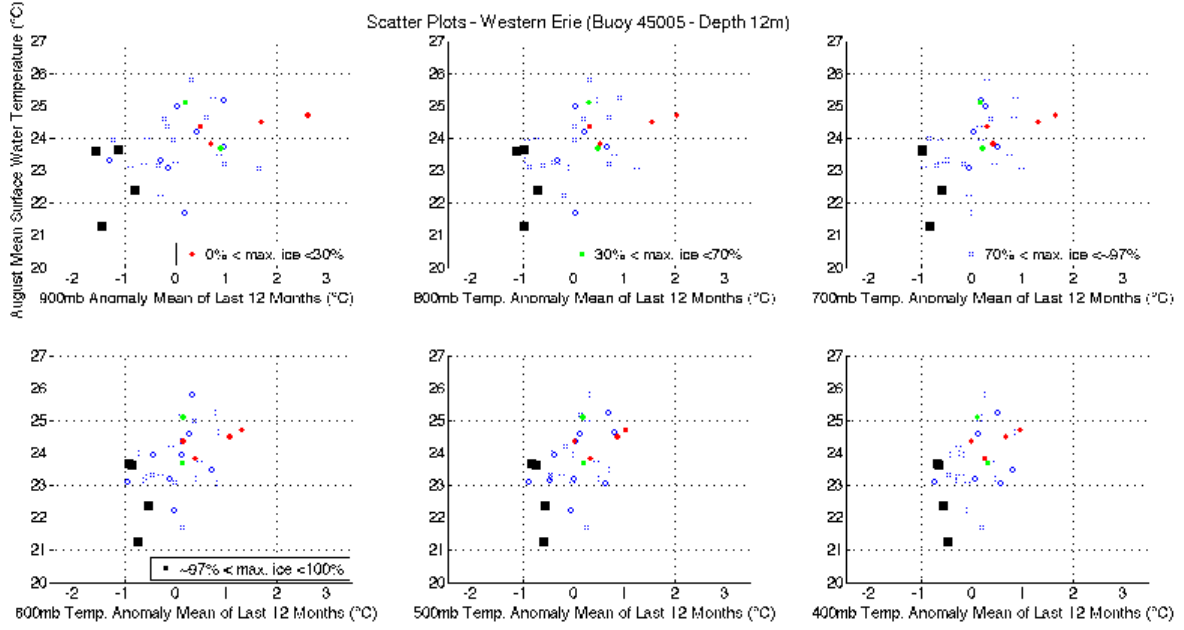
Figure 47: *The scatter plots of one-year mean, from September of year $x - 1$ to August of year x, of air temperature anomalies at various pressure levels, spatially averaged over the aforementioned box region (Figure 43), on the horizontal axis, versus August-mean surface water temperature of year x at buoy station 45005, in western Lake Erie, on the vertical axis. In these panels, black squares correspond to the cases in which ice covers more than 97% of Lake Erie during the winter of year x. Blue circles correspond to the cases in which ice covers between 70% and 97% of the lake during the winter of year x. Green circles correspond to the cases in which ice covers between 30% and 70% of the lake during the winter of year x. Red circles correspond to the cases in which ice covers less than 30% of the lake during the winter of year x. The year x runs from 1981 to 2013.*

anomalies at various pressure levels, spatially averaged over the aforementioned box region (Figure 43), on the horizontal axis, versus August-mean surface water temperature of year x at buoy station 45005, in western Lake Erie, on the vertical axis. Unlike eastern Lake Superior, we do not find any similarity to the hysteresis plots of toy lakes in §3.2.3. Black squares are always near the left end of a plot. Blue dots and green/red dots are not layered vertically in an obvious way. In each panel, we find a range of air temperature on the horizontal axis where blue, green, and red dots coexist but find no apparent structure within the range. This indicates that, over shallow lakes such as Lake Erie, finding multiple local-climate regimes is more difficult than it is over deep lakes such as Lakes Superior. A corresponding model output is in Figure 48.
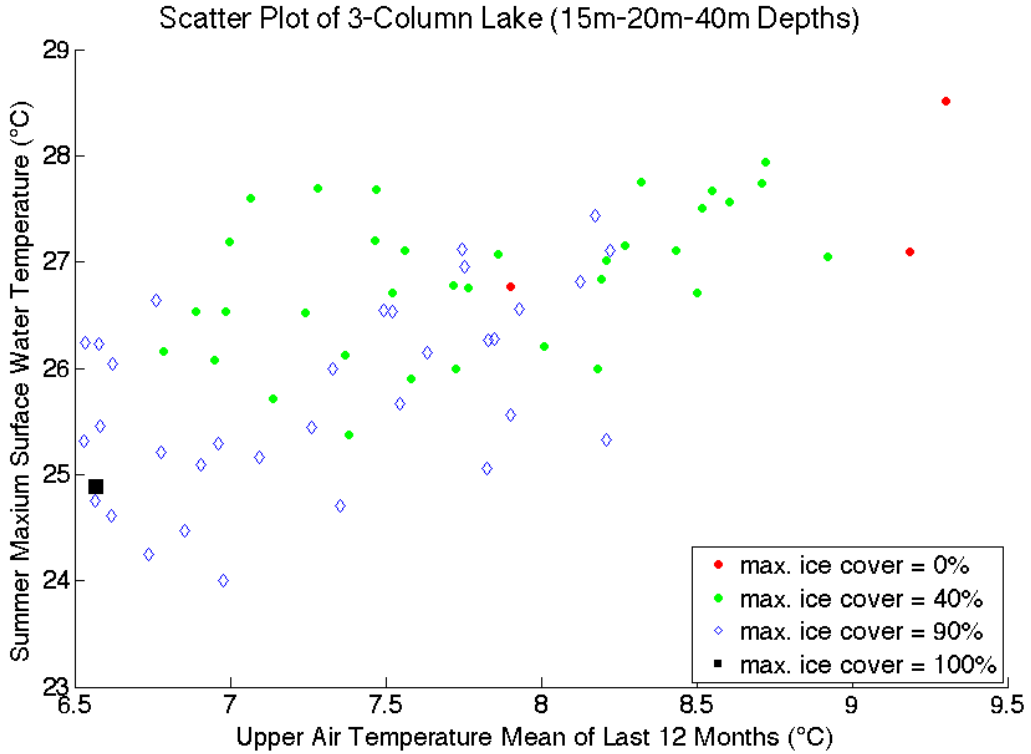
Figure 48: *The scatter plot of one-year mean, from September of year $x - 1$ to August of year x, of upper air temperature on the horizontal axis, versus summer maximum surface water temperature of year x of the deepest lake column of the Lake 4 toy lake on the vertical axis, after we run more than 50 years of time series. Filled black squares correspond to the cases in which ice covers 100% of the lake during the winter of year x. Blue diamonds correspond to the cases in which ice covers 90%, only the shallowest and intermediate lake columns, of the lake during the winter of year x. Green circles correspond to the cases in which ice covers 40%, only the shallowest lake column, of the lake during the winter of year x. Red circles correspond to the cases in which no ice covers the lake during the winter of year x.*

Figure 48 is the scatter plot of one-year mean, from September of year $x-1$ to August of year x, of upper air temperature on the horizontal axis, versus summer maximum surface water temperature of year x of the deepest lake column of the Lake 4 toy lake on the vertical axis, after we run more than 50 years of time series. Lake 4 is a shallow toy lake, introduced in §3.1.2, whose water depth is comparable to Lake Erie. The atmospheric forcing contains both the periodic component and the stochastic component, and the amounts of noise added to upper air temperature and downward shortwave radiation are the same as in §3.2.4 and earlier in this section. We note that this toy lake is completely ice-free during some winters and completely ice-covered during some other winter, given the same degree of inter-annual variability of atmospheric forcing applied to Lake 2 in §3.2.4 and earlier in this section. This is more or less consistent with what we see in the maximum-ice-cover time series of Lake Erie (Figure 3), which also shows such two extremes. More importantly, it is difficult to recognize any structure in the scatter plot, although green dots spread slightly higher than blue dots. Therefore, model results also suggest more difficulty in finding multiple local-climate regimes over shallow lakes than over deep lakes. We note that this does not necessarily mean the lack of multiple local-climate regimes over a shallow lake. The hysteresis plot of Figure 31 of Lake 4 demonstrates that there are ranges of the upper-atmospheric forcing in which two local-climate regimes exist, given identical forcing. Nevertheless, the gap between the two regimes is so small that the stochastic atmospheric forcing blurs any distinction between them. Practically, it is difficult to find any hints of multiple local-climate regimes over a shallow lake.

4.2 The Role of Multiple Climate Regimes in the Accelerated Warming of Lake Superior

Lake Superior's Ice Regimes Figure 49 contains the histograms of maximum ice cover of four of the Great Lakes between the years 1973 and 2014. Multi-modality appears in the histogram for Lakes Superior, in the top-left panel of Figure 49; we note
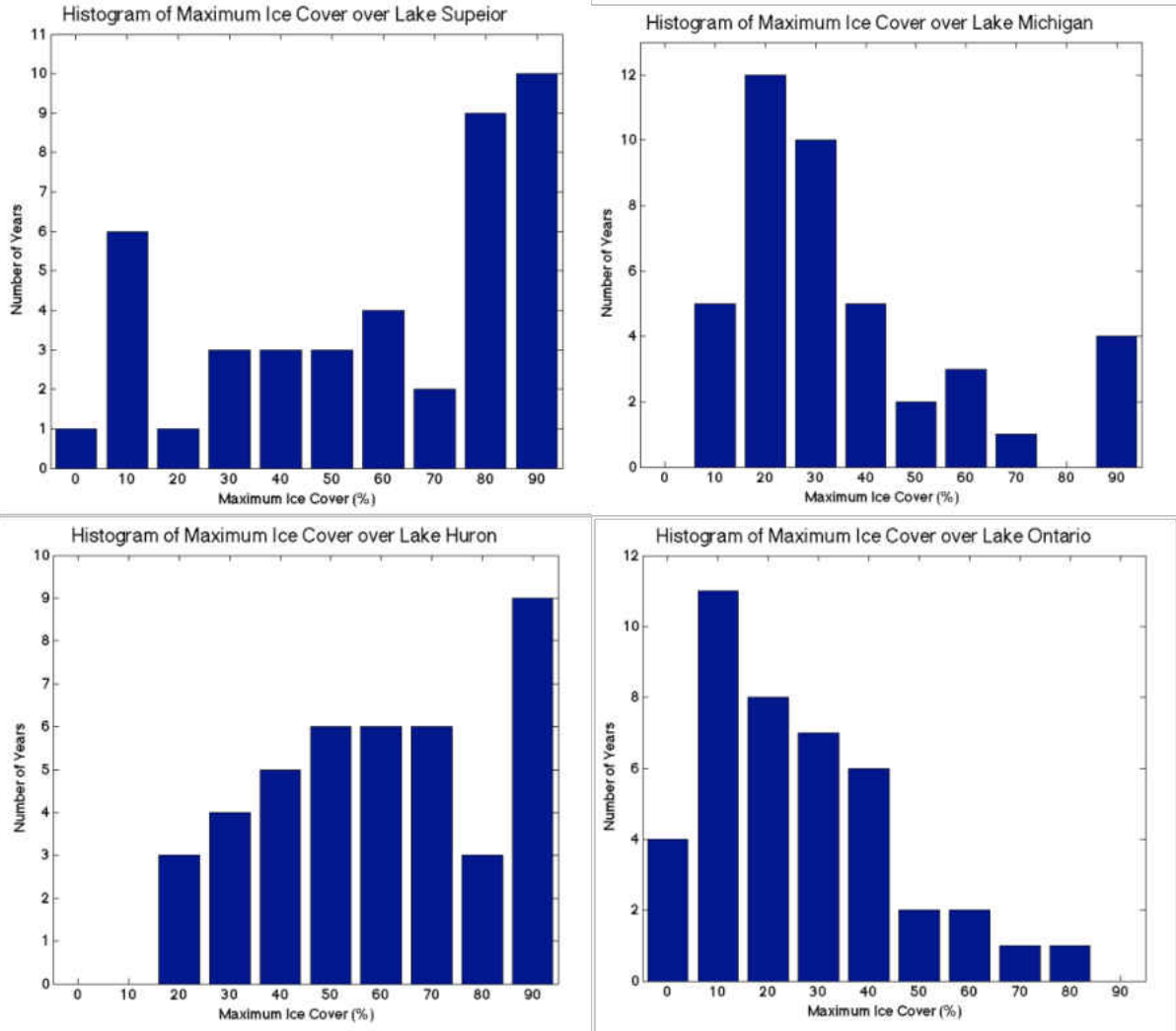
Figure 49: *The histogram of maximum ice cover of Lakes Superior (top-left), Michigan (top-right), Huron (bottom-left), and Ontario (bottom-right) for the years 1973-2014. The vertical axis is the number of winters.*

two large peaks of maximum ice cover, one in the 10%-20% slot and the other straddling between the 80%-90% and 90%-100% slots. This is interesting and worth discussing as follows.

Consider an arbitrary lake and imagine that atmospheric forcing acting on this lake contains Gaussian-distributed inter-annual variability. Suppose that the longterm mean

of maximum ice cover over the lake is, let us say, 50%, and that this value is what would appear under the longterm-mean seasonal cycle of atmospheric forcing. In addition, let us suppose two different hypotheses:

(Hypothesis 1) The Gaussian-distributed inter-annual variability of atmospheric forcing is large enough so that a third of winters are warm enough to make the lake completely ice-free and a third of winters are cold enough to make it completely ice-covered.

(Hypothesis 2) The Gaussian-distributed inter-annual variability of atmospheric forcing is small enough so that the lake experiences neither completely ice-free winters nor completely ice-covered winters.

First, let us try Hypothesis 1 and compare this thought experiment with observational data. In the histogram of maximum ice cover over the lake with Hypothesis 1, we would see two large peaks, one in the leftmost slot (that includes the 0% ice cover) and the other large peak in the rightmost slot (that includes the 100% ice cover). The left panel of Figure 50 is an illustration of such a situation.

The left-most peak corresponds to the aforementioned third of winters during which no ice appears. The right-most peak corresponds to another third of winters during which ice completely covers the lake. Also, we would see one small broad Gaussian peak in the middle slot (that includes the 50% ice cover) because the inter-annual variability of atmospheric forcing is Gaussian-distributed. In the histogram of maximum ice cover over Lake Superior, this is not quite what we observe. The sharp peak on the left side of the plot does not fall in the leftmost slot but one next to it, in the more-than-10%-and-less-than-20% category. The other large peak on the right side does not fit perfectly in the rightmost slot but straddles between the 80%-90% and 90%-100% slots. Moreover, maximum ice cover ranges from a few percent to nearly 100%, but neither 0% nor completely 100%. Finally, it is not certain whether the small broad peak somewhere near or at the 60%-70% slot is due to the Gaussian peak of the inter-annual variability
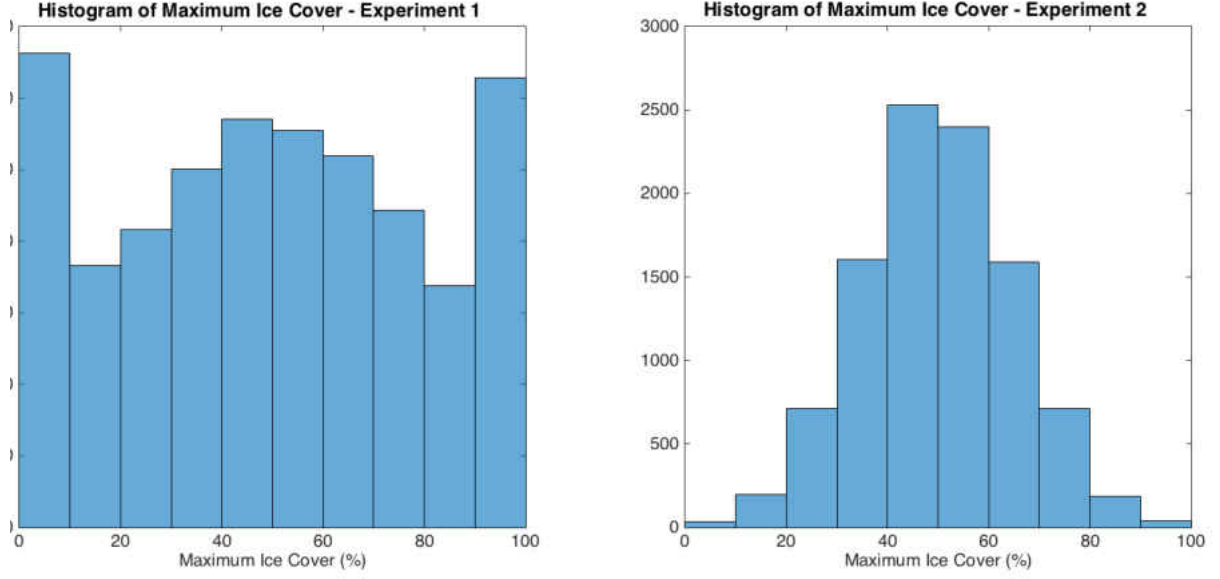
Figure 50: *Illustrations of the histograms of maximum ice cover of two thought experiments described in the main text. (Left panel) The Gaussian-distributed inter-annual variability of atmospheric forcing is large enough so that a third of winters are warm enough to make the lake completely ice-free and a third of winters are cold enough to make it completely ice-covered. (Right panel) The Gaussian-distributed inter-annual variability of atmospheric forcing is small enough so that the lake experiences neither completely ice-free winters nor completely ice-covered winters.*

of atmospheric forcing causing the small broad peak near or at this slot.

So, let us try Hypothesis 2 next. In Hypothesis 2, the inter-annual variability of atmospheric forcing is small enough so that the lake experiences neither completely ice-free winters nor completely ice-covered winters. Therefore, in the histogram of maximum ice cover over the lake with Hypothesis 2, we would only see a Gaussian peak in the middle slot (that includes the 50% ice cover) and no other peaks. The right panel of Figure 50 is an illustration of such a situation. Again, this is not what we observe in the histogram of maximum ice cover over Lake Superior. It is true that Lake Superior has undergone neither 0% nor completely 100% maximum ice cover for the years used for the histogram. Yet two large peaks show up in the maximum-ice-cover histogram in addition to a small broad peak in between.

These observations, (1) Lake Superior has undergone neither 0% nor completely 100% maximum ice cover for the years used for the histogram, and (2) yet two large peaks show up in the histogram, are at odd with the above two simple hypotheses of a maximum-ice-

cover histogram reflecting the Normally distributed inter-annual variability. This is why we seek another reason for the appearance of two large peaks in the maximum-ice-cover histogram of Lake Superior. Our hypothesis is the existence of multiple local-climate regimes over Lake Superior. We hypothesize that the reason for the two large peaks in the maximum-ice-cover histogram is that, given an identical seasonal cycle of atmospheric forcing, there is more than one equilibrium state for seasonal temperature cycles of the lake, and these multiple equilibrium states give rise to multiple peaks in the maximum-ice-cover histogram.

Manifestation of Ice Regimes on Air Temperature Data What is the role of multiple climate regimes in the accelerated surface warming of Lake Superior?

Let us take a look at air temperature data right above buoy station 45004 in eastern Lake Superior, where we found manifestations of multiple local-climate regime in §4.1.1.

Figure 51 contains the scatter plots of one-year mean, September of year $x-1$ through August of year x, of air temperature anomalies at various pressure levels right above buoy station 45004, in eastern Lake Superior, on the horizontal axis, versus August-mean surface water temperature of year x at the buoy station on the vertical axis. Let us examine the top panels. At the 900mb and 800mb pressure levels, we notice that many dots concentrate in the area between $-1.3°C$ and $-0.3°C$ of the horizontal axis. There is another area, between $0.3°C$ and $2.3°C$ of the horizontal axis, where we find relatively many dots. Curiously, at around the longterm mean, $0°C$ of the horizontal axis, we find fewer dots. This looks unusual because, in a scatter plot, we would expect more dots to appear near the longterm mean, at the center in each figure, and less dots further away. This is most likely due to manifestations of ice regimes we see above in the maximum-ice-cover histogram of Lake Superior (Figure 49). The maximum ice-cover histogram of Lake Superior contains two distinct peaks, one in the 10%-20% slot and the other in between the 80%-90% and 90%-100% slots. The black dots in Figure 51 that concentrate in the area between $-1.3°C$ and $-0.3°C$ of the horizontal axis fall in the 80%-90% or 90%-100% slot in the maximum ice-cover histogram of Lake Superior. The red dots in Figure 51 that spread in the area between $0.3°C$ and $2.3°C$ of the horizontal axis fall
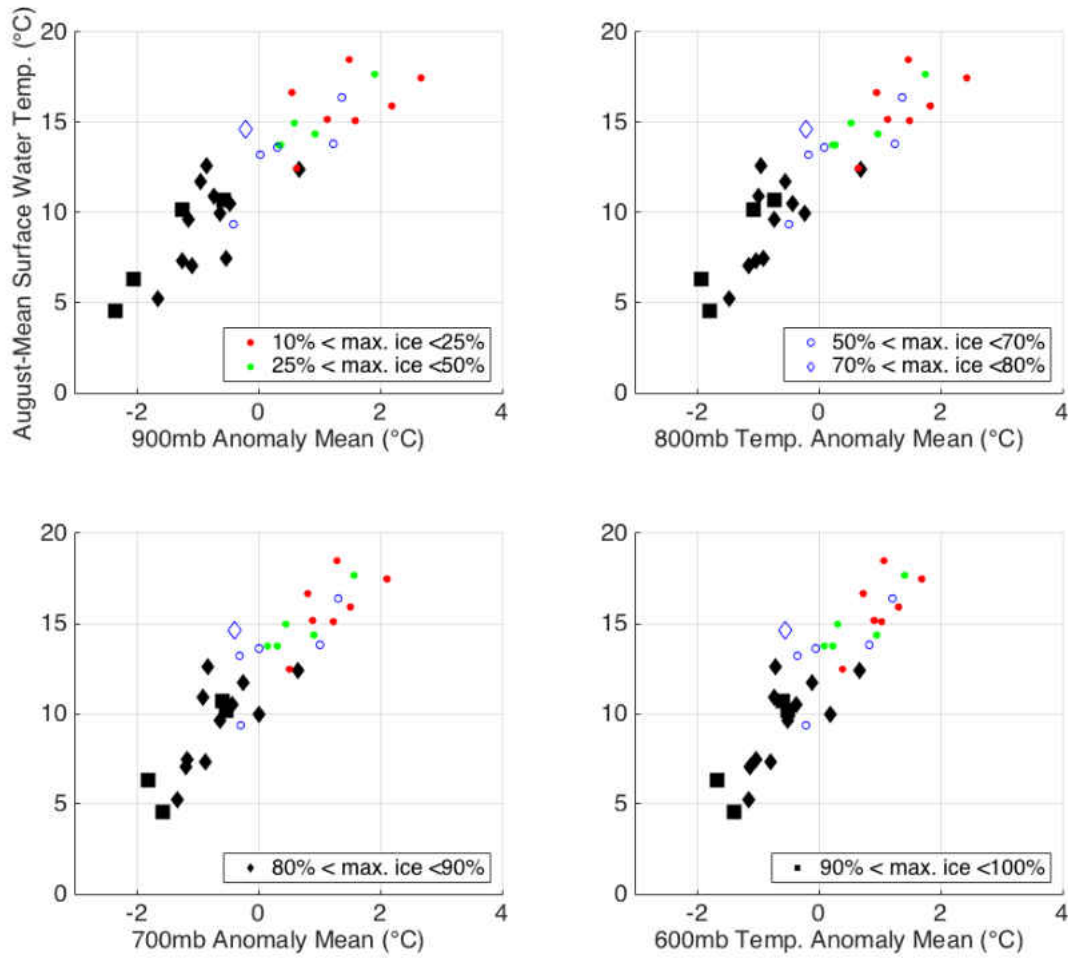
Figure 51: *The scatter plots of one-year mean, September of year $x-1$ through August of year x, of air temperature anomalies at various pressure levels right above buoy station 45004, in eastern Lake Superior, on the horizontal axis, versus August-mean surface water temperature of year x at the buoy station on the vertical axis. The figure contains four panels, whose horizontal axes are air temperature anomalies at the 900mb level, 800mb level, 700mb level, and the 600mb level. In these panels, black squares and black diamonds correspond to the cases in which ice covers more than 90% and between 80% and 90% of Lake Superior, respectively, during the winter of year x. Blue diamonds and blue circles correspond to the cases in which ice covers between 70% and 80% and between 50% and 70% of the lake, respectively, during the winter of year x. Green circles and red circles correspond to the cases in which ice covers between 25% and 50% and between 10% and 25% of the lake, respectively, during the winter of year x. The year x runs from 1981 to 2013.*

in the 0%-10% or 10%-20% slot in the maximum-ice-cover histogram of Lake Superior. This multimodal nature of the ice-cover histogram of Lake Superior manifests itself in the data of lower-altitude air temperature above eastern Lake Superior.

101

Warming Trend Amplified by Multiple Climate Regimes If the colder and warmer regimes of Lake Superior are equally likely to occur, the lake would not exhibit a warming trend. The lake would simply transition back and forth between the regimes without a preferred direction of transitions. In reality, as the maximum-ice-cover time series of Lake Superior shows, there has been a preferred direction of transitions. On the one hand, between the years 1973 and 1997, there were only four winters out of 25 during which the maximum ice cover over Lake Superior was less than 60%. There was a preference toward colder regimes during the period. On the other hand, between the years 1998 and 2014, there were only four winters out of 17 during which the maximum ice cover over Lake Superior was more than 60%. There was a preference toward warmer regimes during the period. We hypothesize that this change in preference of regime transitions is due to large-scale warming over North America.

If the temperature gap between local-climate regimes is small, then a regime transition from a colder local-climate regime to a warmer local-climate regime would result in a weak warming trend. In §4.1.2, we saw an example of this in Lake Erie. Only when the gap between local-climate regimes is large, the existence of multiple climate regimes helps amplify the local warming trend in the presence of global warming. Among the Great Lakes, the eastern part of Lake Superior is the region that exhibits clearest indications of multiple local-climate regimes, and this region exhibits the strongest warming trend (Figures 4 and 6).

4.3 Possible Roles of Wind and Cloud Feedback in the Vicinity of the Great Lakes Region

4.3.1 Dynamics of Wind and Cloud Feedback

So far, we have focused on the consequences of the ice-albedo feedback and other ice-related feedback effects without considering any changes that might happen to low-level clouds or surface winds. Desai *et al.* (2009) report a recent increase in surface wind speed

over Lake Superior during summers. We would expect the increase because lake-surface warming would make surface air more unstable. On the one hand, stronger surface winds would mix surface water deeper, slightly cooling surface water temperature. On the other hand, increased lake surface temperature also implies more buoyant surface water, more strongly resisting to sink. Competition between these two effects arises, one trying to make the surface mixed layer deeper and the other trying to make it shallower, which in turn affects surface water temperature. Computer simulation in Desai *et al.* (2009) indicates that, in the end, the surface mixed layer becomes slightly shallower when surface water temperature increases.

What is also interesting is the response of clouds and fogs to changes in lake surface temperature. Let us explore, in this section, how low-level clouds and fogs possibly respond to changes in lake surface temperature by examining data from the NARR reanalysis. When the surface of a lake is warmer than the longterm mean, it could dissipate more fogs than the longterm mean and less fogs would ascend to become low-level clouds. The topic in this subsection is about the roles its consequence might play in the dynamics of the Great Lakes' local-climate regimes.

4.3.2 Role of the Cloud Feedback in the 1997-98 Regime Transition of Lake Superior

In Chapter 1, we briefly discussed the August-mean surface water temperature time series of buoy station 45001 in central Lake Superior and that the time series contains a discontinuous behavior before and after the years 1997-1998. In this subsection, we explore if the response of clouds and fogs to the lake-surface warming helped Lake Superior quickly transition from its colder local-climate regime to its warmest local-climate regime during the years 1997-1998. The large El Nino appeared in the year 1998, and warm air reached the Great Lakes during the winter. This helped the Great Lakes remain largely ice-free throughout the winter of 1998, and the lakes absorbed an abundance of incoming shortwave radiation during the season.

The NARR reanalysis for the year 1998 shows an additional source of incoming energy
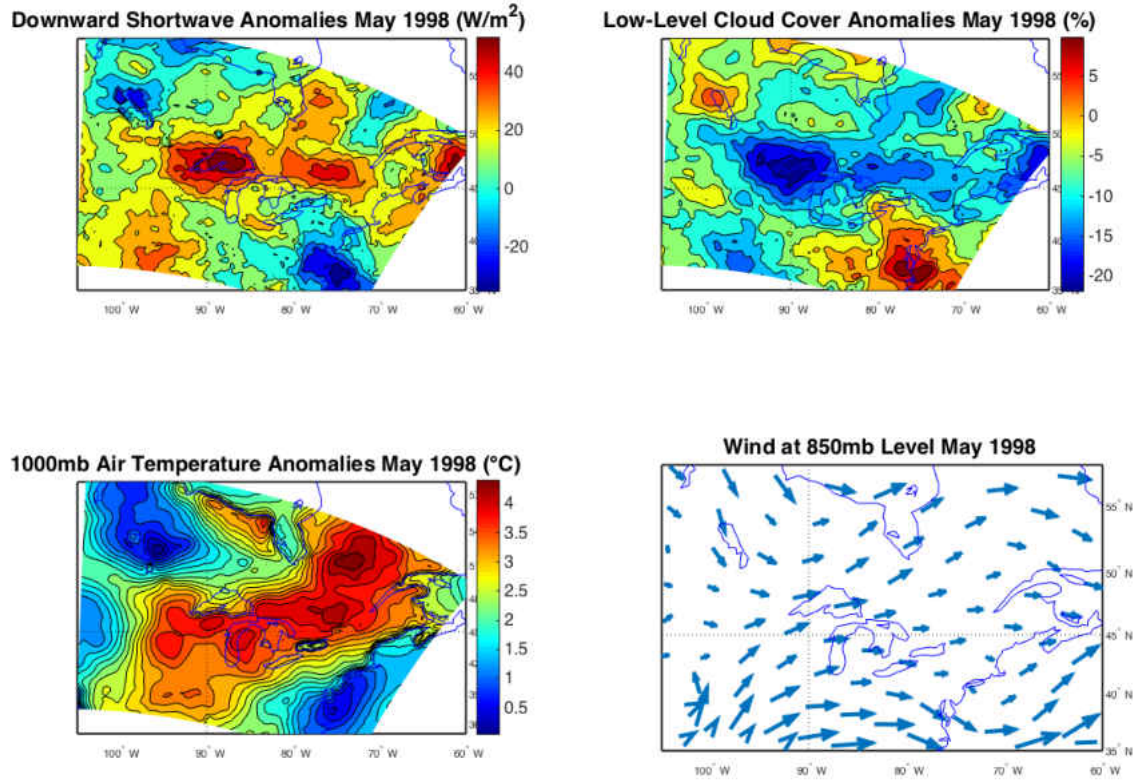
Figure 52: *Maps of the monthly-mean anomalies of (top-left) downward shortwave radiation, (top-right) low-level cloud cover, and (bottom-left) air temperature at the 1000mb level in the vicinity of the Great Lakes for May 1998. In each of these panels, the climatology for the years 1979-2013 is subtracted from the mean of May 1998. The remaining panel (bottom-right) is the longterm-mean wind field at the 850mb level averaged for the years 1979-2013. All are based on the NARR reanalysis.*

that occurred during spring for Lake Superior. Figure 52 shows monthly-mean anomalies of low-level cloud cover, downward shortwave radiation, and air temperature at the 1000mb level in the vicinity of the Great Lakes for May 1998. We notice that there was a large-scale negative anomaly in low-level cloud cover in May 1998 around the Great Lakes region. What strikes us, however, is that the amount of negative anomaly in low-level cloud cover over Lake Superior especially stands out. We expect that there was also a reduction in the amount of fogs over Lake Superior due to the lake-surface warming as well. This translates to a large positive anomaly in downward shortwave radiation over Lake Superior as seen in the top-left panel of the figure. It is approximately $50W/m^2$ of positive anomaly of downward shortwave radiation with respect to the 1979-2013 cli-

matology, and approximately additional $30W/m^2$ of downward shortwave radiation with respect to the regions surrounding Lake Superior. About a half of this positive anomaly of downward shortwave radiation was some larger-scale phenomenon, and the other half of the positive anomaly of downward shortwave radiation was given almost exclusively to the region bounded by the contours of Lake Superior. We suspect that this extra $30W/m^2$ of downward shortwave radiation given almost exclusively to Lake Superior, most likely due to the loss of low-level clouds and fogs caused by the lake-surface warming, greatly helped Lake Superior transition to its warmest local-climate regime quickly.

4.4   Other Possible Mechanisms for Lake Warming

4.4.1   Overview of Low-Level Cloud Cover Trends and Downward Shortwave Trends over North America

Low-Level Cloud Cover Trends over North America   In this section, we answer Question 4 discussed in Chapter 1: *Are different physical mechanisms at work for amplifying surface warming trends of the Great Lakes versus those of smaller lakes near Lake Superior and in California? If so, what are they?*

Figure 53 is a map of linear trends in February-mean low-level cloud cover over North America, based on the NARR reanalysis data between the years 1995 and 2012, and Figure 54 is a map of the corresponding March-mean low-level cloud cover trends. We note positive trends in February-mean low-level cloud cover over the Great Lakes region, and in March-mean low-level cloud cover over Lake Superior. The reason is a reduction in the amount of ice cover over the lakes. When ice decreases and more open water regions appear during winters, more moisture becomes available for ascent. This causes positive trends in low-level cloud cover over the Great Lakes as the amount of ice cover continues to decrease.

Downward Shortwave Radiation Trends over North America   The reduction in low-level cloud cover translates into a reduction in downward shortwave radiation.

NARR Reanalysis Low-Level Cloud Cover February Trend 1995-2012 in K/year
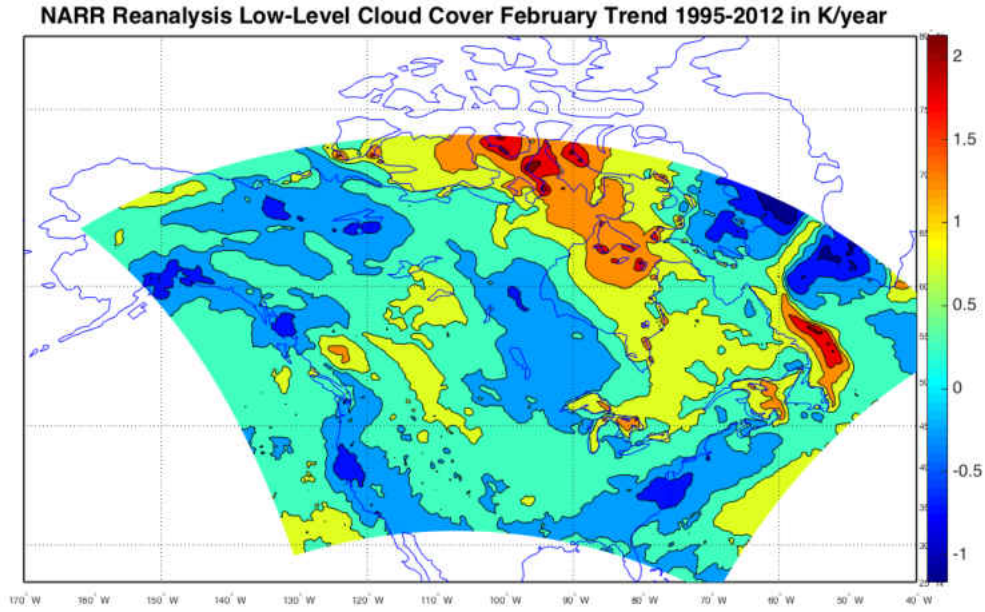
Figure 53: *A map of linear trends in February-mean low-level cloud cover over North America, based on the NARR reanalysis data between the years 1995 and 2012. The unit is in %/year.*

Figure 55 is a map of linear trends in February-mean downward shortwave radiation, based on the NARR reanalysis data between the years 1995 and 2012, and Figure 56 is a map of the corresponding March-mean downward shortwave radiation trends. In both figures, we note negative trends in downward shortwave radiation over the Great Lakes region thanks to the increase in wintertime low-level cloud cover. This makes a difference between small lakes and large lakes. Large lakes such as Lake Erie have large surface area, and the availability of moisture in the lower atmosphere depends on whether or not they are ice-covered in winter, and in turn affects the amount of low-level clouds above them. Small lakes, however, do not have a large enough surface area to affect the amount of clouds above themselves. Therefore, when there is a large-scale positive trend in downward shortwave radiation, the magnitudes of trends in annual-mean downward shortwave radiation would be different between over a large lake such as Lake Erie and a small lake such as Sparkling Lake.

106

NARR Reanalysis Low-Level Cloud Cover March Trend 1995-2012 in K/year
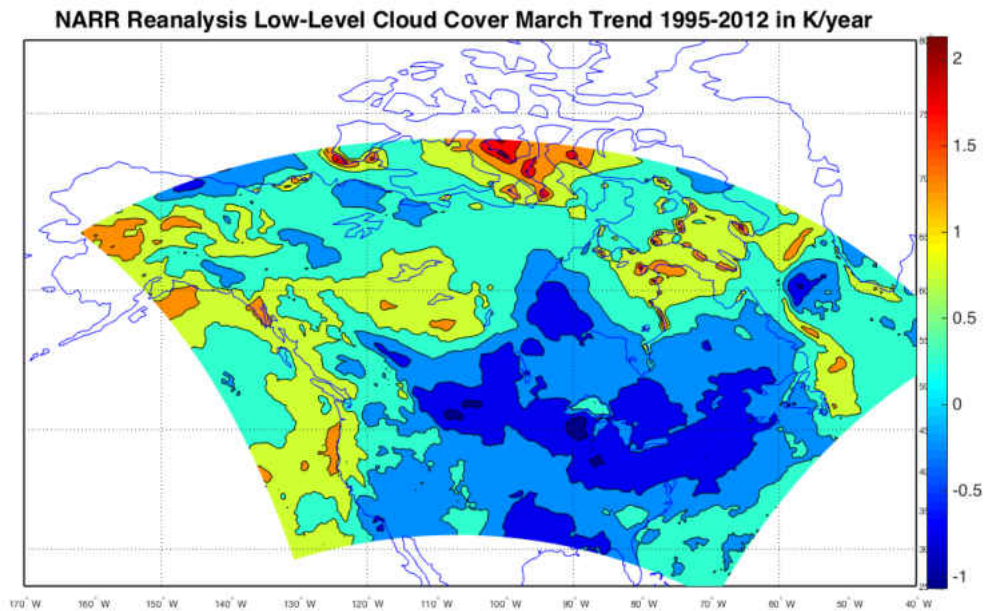
Figure 54: *A map of linear trends in March-mean low-level cloud cover over North America, based on the NARR reanalysis data between the years 1995 and 2012. The unit is in %/year.*

Downward Shortwave Radiation Trends in California and Regions South of the Great Lakes Let us take a look at a map of linear trends in annual-mean downward shortwave radiation over North America, which is Figure 57. In the figure, we note two regions where a positive trend in downward shortwave radiation is strong: a region that includes California and a region south of the Great Lakes. Naturally, these are the regions where we find relatively strong warming trends in summer surface water temperature among small lakes, including Sparkling Lake south of Lake Superior discussed in Chapter 1 (Schneider *et al.*, 2010). In addition, we note that the boundary between the red color and the orange color in the figure nicely follows the contours of Lakes Superior, Huron, and Erie, showing that, indeed, large lakes dampen the positive trends in annual-mean downward shortwave radiation by sending more moisture to the atmosphere in winter.

107

Figure 55: *A map of linear trends in February-mean downward shortwave radiation over North America, based on the NARR reanalysis data between the years 1995 and 2012. The unit is in $W/m^2 year$.*

4.4.2 Simulation of Warming Trends of Lakes with a Positive Trend in Downward Shortwave Radiation

Let us see whether our lake-atmosphere-land model reproduces a strong warming trend in summer surface water temperature of a small lake with a positive trend in downward shortwave radiation. In this experiment, the forcing is all periodic except that the amount of downward shortwave radiation has a linear trend of $1W/m^2 year$. This trend of $1W/m^2 year$ is comparable to the trends we observe in the region including California and the region south of the Great Lakes (Figure 57). The following lists all the forcing and the behaviors of the forcing, whether periodic or constant, and whether or not there is a non-zero linear trend.

NARR Downward Shortwave Radiation March Trend for 1995-2012 in W/(m²year)
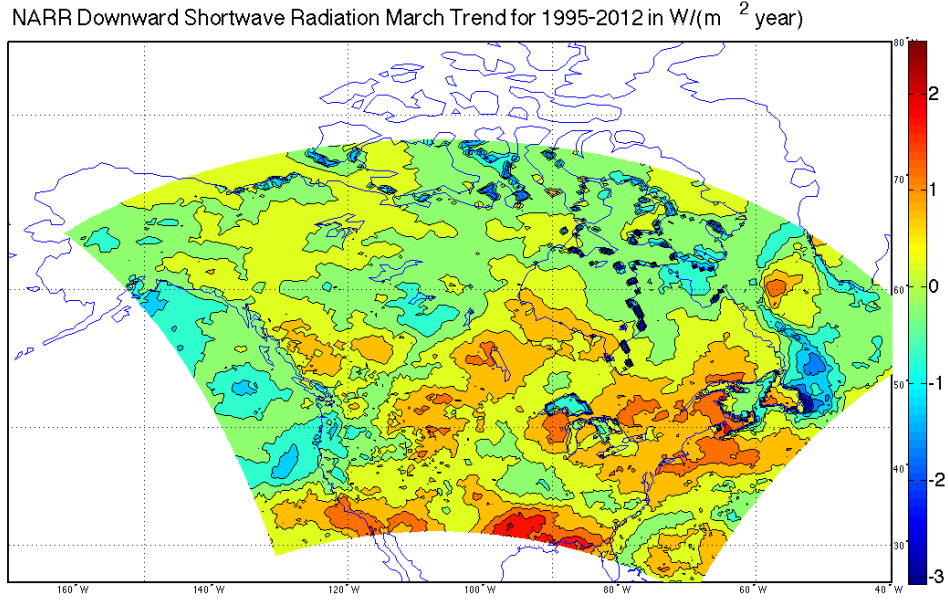
Figure 56: *A map of linear trends in March-mean downward shortwave radiation over North America, based on the NARR reanalysis data between the years 1995 and 2012. The unit is in W/m^2year.*

List of Forcing	
Temperature of the upper atmosphere	periodic
Downward shortwave radiation	periodic + linear trend of $1W/m^2year$
Surface wand speed	periodic
Surface relative humidity	constant

The periodic parts of the temperature of the upper atmosphere, downward shortwave radiation, and surface wind speed are given by Equations (3.10-3.12).

Figure 58 shows the 20-year warming trends in daily-mean surface water temperature of 15m-deep lakes, whose horizontal axis is Julian day starting from day 1 (January 1) to day 365 (December 31). One of the lakes is perennially ice-free (the solid curve) and the other is wintertime ice-covered (the dash dotted curve). The ice season of the wintertime ice-covered lake is between February and May. The warming trends are evaluated by linear regression after sampling a period of 20 years out of computed time series. Of
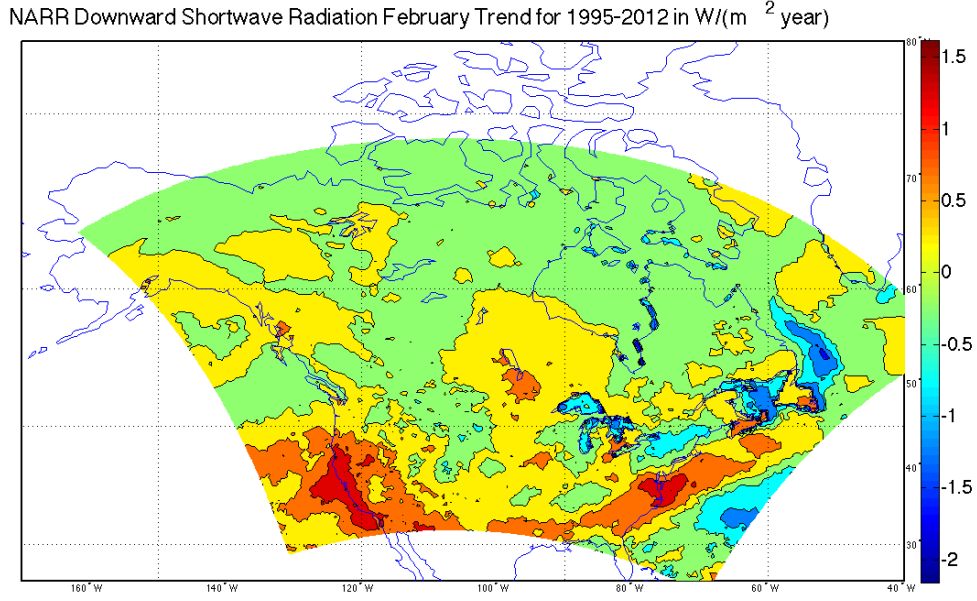
109
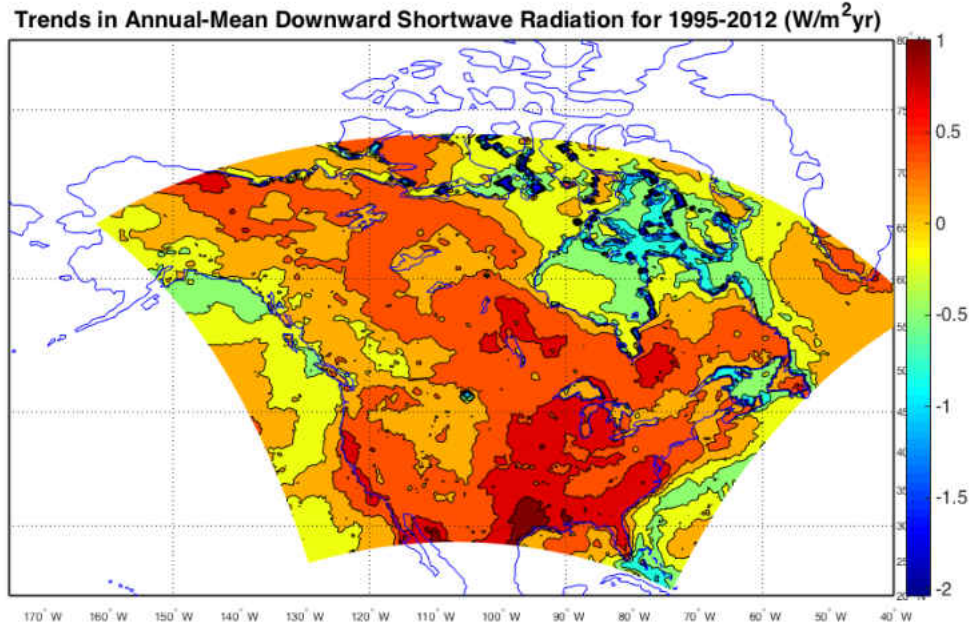
Figure 57: *A map of linear trends in annual-mean downward shortwave radiation over North America, based on the NARR reanalysis data between the years 1995 and 2012. The unit is in $W/m^2 year$.*

the sampled 20 years, the warming trend in annual-mean surface water temperature of the perennially ice-free lake is $0.14°C/year$ and that of the wintertime ice-covered lake is $0.17°C/year$. Therefore, our simple lake-atmosphere-land model demonstrates that the trend of $1W/m^2 year$, comparable to the trends we observe in the region including California and the region south of the Great Lakes, is enough to generate strong warming trends in summer surface water temperature of small lakes we observe in California and south of the Great Lakes.

Lake Erie versus Sparkling Lake In large lakes such as Lake Erie, when climate warming results in a reduction in wintertime ice cover, this reduction in ice cover translates into an increase in wintertime low-level cloud cover, which translates into a decrease in wintertime downward shortwave radiation. Even if a year-round large-scale increase
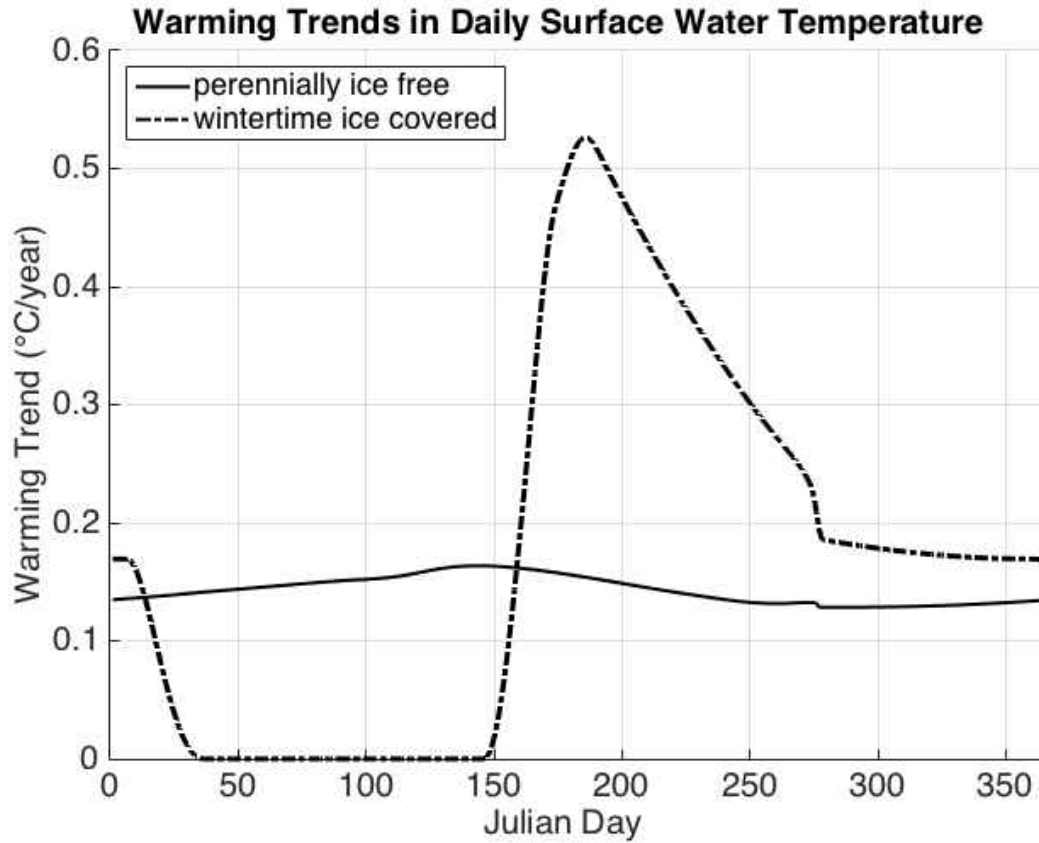
Figure 58: *Warming trends in daily-mean surface water temperature of a 15m-deep perennially ice-free lake (the solid curve) and a 15m-deep wintertime ice-covered lake (the dash dotted curve). The forcing contains the positive linear trend of $1W/m^2year$ of downward shortwave radiation. The unit of the warming trends is in $°C/year$. The warming trends are evaluated by linear regression after sampling a period of 20 years out of computed time series.*

in downward shortwave radiation exists, this wintertime decrease in downward shortwave radiation reduces the overall impact of downward shortwave radiation on the amplification of the lake's surface-water warming trend. Therefore, Lake Erie does not exhibit a surface-water warming trend as strong as Sparkling Lake, which is not large enough to affect the amount of low-level cloud above it. Similarly, Lake Superior and the other Great Lakes, being large lakes, are also like Lake Erie in that a reduction in ice cover translates into an increase in wintertime low-level cloud cover, which translates into a decrease in wintertime downward shortwave radiation (Figures 55 and 56). Lake Superior and Lake Erie exhibit different magnitudes of surface-water warming trends just like Sparkling Lake and Lake Erie do, but their reasons are different. The difference between Lake Superior and Lake Erie stems from how the ice-albedo feedback impacts differently

on deep lakes and shallow lakes.

Chapter 5

Summary and Conclusion

In this thesis, we focused our attention to one-dimensional eddy-diffusion-based lake models, namely, modified versions of Hostetler and Bartlein (1990). It is known that many existing one-dimensional models poorly simulate seasonal temperature cycles of deep lakes ($> 200m$). A number of attempts exist to improve versions of Hostetler and Bartlein (1990) by parameterizing unresolved physical processes in the form of "enhanced minimum diffusion" (e.g., Fang and Stephan, 1998; Bennington *et al.*, 2014). We suggested a modification to the parametrization of these unresolved physical processes. Seasonal temperature cycles of deep lakes simulated with this 1-D lake model are comparable to those obtained by recent 3-D lake models (e.g., White *et al.*, 2012).

After we presented improved results of simulation of deep lakes with this modified model, we used the model to explore the dynamics of the regional climate of the Great Lakes. There have been discussions of the existence of multiple ice-cover regimes of the Great Lakes in the literature (e.g., Assel *et al.*, 2003). We examined the existence of ice-cover regimes and the impact of the regimes on their summer climate. We found clearer indications of the existence of multiple regional-climate regimes over the eastern part of Lake Superior, where the lake's deepest basin was located.

For the last couple of decades, the Great Lakes have undergone rapid surface warming. The magnitudes of the summer surface-warming trends of the Great Lakes have been greater than those of surrounding land (Austin and Colman, 2007). Among the Great Lakes, Lake Superior exhibits the strongest warming trend in annual as well as summer surface water temperature.

We found that the reason Lake Superior exhibited the strongest warming trend among the Great Lakes was that the eastern part of the lake exhibited clearly distinct regional-climate regimes. As global warming changes the tendency of Lake Superior's local climate, from being more attracted to its colder local-climate regime to being more attracted to its warmer regime, the surface water temperature of the lake undergoes a more drastic change than the surface temperature of surrounding land. As this shift happens, its surface water temperature time series exhibits a discontinuous behavior, and we found such a behavior in the August-mean surface water temperature time series at buoy stations in

Lake Superior at around the years 1997-98. Moreover, we found that the surface water temperature of Lake Superior warmed faster than those of the other Great Lakes that exhibited less clear indications of the existence of regional-climate regimes.

we addressed six questions concerning the warming trends of a number of lakes at mid-latitudes. Below, we summarize our answers to these questions.

(*Question 1*) *Are the ice-albedo feedback and other ice-related feedback effects enough to give rise to the strong surface-water warming trends observed in some of the Great Lakes?*

When ice appears on the surface of a lake, ice reflects a good amount of downward shortwave radiation, resulting in less amount of radiation energy absorbed by the lake. If global warming warms the lake further, the amount of ice cover in winter will decrease, and consequently, the amount to incoming shortwave radiation will increase and the lake will acquire more heat content. This is called *the ice-albedo feedback*. In addition, the amount of sensible and latent heat fluxes at the lake surface also change with the appearance of ice. We have seen that the difference in heat content of a lake between when ice covers the surface and when it does not is enough to give rise to distinct local-climate regimes of the eastern part of Lake Superior, and we have found indications of their existence in §4.1.1 in the scatter plot of August-mean surface water temperature at buoy station 45004 versus one-year mean of air temperature anomalies at various pressure levels upwind of the Great lakes. Also in §4.1.1, we have found that simulations of our toy Lake 2 model with stochastic forcing produces a gap between the coldest and warmest regimes comparable to what we have found in the aforementioned scatter plot of the eastern part of Lake Superior. Since this part of Lake Superior is the most rapidly warming region among the Great Lakes, this is an indication that the variation in the amount of wintertime ice cover is enough to give rise to the large enough gap between the distinct local-climate regime of eastern Lake Superior. In §3.3, we presented some global warming experiments on various toy lakes, with the added warming trend of $0.04°C/year$ and the

inter-annual variability of STD of $2°C$ in the upper atmospheric forcing, and we found that the toys Lakes 1 and 2, comparable in depth to some of the deeper of the Great Lakes, give rise to warming trends in annual-mean surface water temperature comparable to those of the deeper of the Great Lakes. These are indications that the ice effects can account for a good portion of the surface-water warming trends of the Great Lakes.

(*Question 2*) *Why are water depth and surface-water warming trends over regions of the Great Lakes correlated?*

Shallower lakes go through longer duration of summer stratification than deeper lakes. For a certain duration of time before spring overturn, water temperature becomes nearly homogeneous from the top to the bottom and the vertically near-homogeneous profile of water encourages vertical mixing of much of the lake column. Deeper lake columns have more water to mix. For this reason, surface water temperature of a deeper lake does not increase much during the period, and the vertical density profile of a deeper lake stays near-homogeneous longer than that of a shallower lake. The end of spring overturn and the appearance of the summertime surface mixed layer occur later for a deeper lake than a shallower lake; for example, spring overturn occurs even during August at buoy station 45004 in easter Lake Superior in some years (e.g., Austin and Colman, 2007). For this reason, shallower lakes go through longer duration of summer stratification, i.e., longer duration of a summertime mixed layer, than deeper lakes.

The duration of the summertime surface mixed layer affects how effectively and to what extent the lake responds to atmospheric forcing of a summer. The rate of change in temperature of the surface mixed layer is approximated by the following equation, which is a modification of Equation (2.1) for a uniform-temperature mixed layer.

$$C_w h \frac{\partial T}{\partial t} = \Delta \Phi \qquad (5.1)$$

where h is the depth of the surface mixed layer, C_w is the volume heat capacity of water, and $\Delta \Phi$ is the energy the mixed layer receives from the outside source. We note that the

shallower the surface mixed layer is, the faster and more efficient the change in surface water temperature is, given the same $\Delta\Phi$. The typical depth of a summertime surface layer of the Great Lakes is somewhere between $10m$ and $20m$. By contrast, the depth of a wintertime surface layer can be much deeper; it can be deeper than $100m$ below the regions of large water depth (for example, see Assel, 1986).

A shallow lake point such as buoy station 45005 in western Lake Erie starts to stratify on average sometime in May, while a deep lake point such as buoy station 45004 in eastern Lake Superior starts to stratify on average sometime in July (Austin and Colman, 2007). This is a difference of almost two months; shallow lakes have more time to efficiently respond to the atmosphere. This is the reason that the difference in summer maximum heat content between two local-climate regimes is small in shallow lakes. Consequently, this is also the reason that the range of upper-atmospheric temperature in which two regimes exist is small in shallow lakes. Therefore, we obtained the two important results in the case of bi-modal regimes in wintertime-ice-covered lakes in §3.2.1,

(1) The difference in summer maximum heat content between the two regimes is larger for deeper lakes.

(2) The range of upper-atmospheric temperature in which the two regimes exist is larger for deeper lakes.

What these two results would lead to is that shallower lakes more easily transition between regimes than deeper lakes do because of the less distinction between the regimes, because of their "shorter memory." The more frequently the lake transitions between the warmer and colder climate regimes, the smaller its warming trend becomes. In addition, since the difference in heat content between the two regimes is larger for deeper lakes, deeper lakes often experience a larger temperature jump when they transition from the colder to the warmer regime than shallower lakes do. In the presence of global warming, these properties of wintertime-ice-covered lakes give rise to the correlation between water

depth and surface-water temperature.

In the case of Lakes Michigan and Ontario, the surface lake points of largest water depths of these lakes have been mostly ice-free even during the colder winters for the last forty years. Therefore, these surface lake points of largest water depths did not receive extra downward shortwave radiation due to a reduction in ice cover in the later years of this period. However, as we discussed in §3.3, with atmospheric stochasticity, we expect that the deepest lake column responds to atmospheric noise more like a deep lake does, retaining anomalous heat or loss of heat better, and a shallower lake column responds to atmospheric noise more like a shallow lake does, losing anomalous heat or loss of heat faster. Our hypothesis is that, even though surface lake points of largest water depths do not directly receive ice-albedo-feedback-type extra shortwave radiation, these surface lake points still exhibit the strongest warming trends with help of extra heat or loss of heat being transported by atmospheric transport and lake circulation from neighboring shallower ice-decreasing regions. Figure 28 demonstrates that a regime transition of a shallower lake column affects the surface water temperatures of the deepest columns considerably. What we suspect is that lake circulation plays an equally important role in transporting heat. Once the deepest lake points receive heat or loss of heat from the neighboring regions, they retain the heat or the loss of heat longer than their shallower neighbors do. With the combination of the lower-atmospheric heat transport and the heat transport by lake circulation, we suspect that the surface lake points of largest water depths of Lakes Michigan and Ontario exhibit stronger surface warming trends than their shallower neighbors. We would need a full 3D lake model to verify this hypothesis, and here we are content to only state this speculation.

(*Question 3*) *What is the origin of the qualitative difference between the surface water temperature time series of deep lakes and those of shallow lakes?*

In §1.2, we have found that the surface water temperature time series of buoy station 45001, in central Lake Superior, has an apparently discontinuous behavior before and after the years 1997-1998. Its August-mean surface water temperature averaged between 1979 and 1997 is $11.0°C$, and that averaged between 1998 and 2013 is $14.1°C$. Between 1979 and 1997, its linear trend is $-0.10°C/year$, and between 1998 and 2013, its linear trend is $-0.12°C/year$. Here, one notices a small negative trend prior to the years 1997-1998, followed by a large jump in the time series at around the years 1997-1998, then followed by another small negative trend after the years 1997-1998. We have also found that the August-mean surface water temperature time series of Lake Erie and Sparking Lake nearby Lake Superior, however, lack such a sudden change. Lake Superior is a deep lake, while Lake Erie and Sparkling Lake are shallow lakes.

This difference arises because wintertime-ice-covered shallower lakes more easily transition between regimes than wintertime-ice-covered deeper lakes do because of the less distinction between the regimes, as in the answer to *Question 2*. This does not mean that Lake Superior, the deep lake, was always in its colder local-climate regime prior to the years 1997-98 and always in its warmer local-climate regime afterward. Instead, regime transitions between colder and warmer regimes of shallow lakes such as Lake Erie and Sparkling Lake have been more frequent in number and less noticeable in appearance than those of Lake Superior.

(***Question 4***) ***Are different physical mechanisms at work for amplifying surface warming trends of the Great Lakes versus those of smaller lakes near Lake Superior and in California? If so, what are they?***

The NARR reanalysis data indicates that positive trends in downward shortwave radiation almost as large as $1W/m^2 year$ appear in California and regions south of the Great Lakes (Figure 57). Results of simulation of a 15m-deep lake in our lake-atmosphere-land couple model suggest that the $1W/m^2 year$ trend in downward shortwave radiation is enough to give rise to a warming trend in annual-mean surface water temperature larger than $0.1°C/year$ both of wintertime-ice-covered lakes and perennially ice-free lakes

(Figure 58). Therefore, the strong surface-water warming trends observed in a number of small lakes in California and regions south of the Great Lakes are likely to be caused by the downward shortwave radiation trends.

The NARR reanalysis data also indicates positive trends in low-level cloud cover over the Great Lakes in winter (Figures 55-56). The reason is that the decrease in the amount of ice cover over that Great Lakes has resulted in more availability of moisture from the lakes to the atmosphere. This has resulted in reducing the magnitude of trends in annual-mean downward shortwave radiation over the Great Lakes (Figure 57). Instead, our lake-atmosphere-land coupled model demonstrates that, without a trend in downward shortwave radiation, the $0.04°C/year$ trend in the upper atmosphere is enough to generate many observed features in the atmospheric and surface-water data of the Great Lakes.

(**Question 5**) **Why are the summer surface water temperature of the Great Lakes and their winter maximum ice cover correlated?**

Our lake-atmosphere-land coupled model qualitatively reproduces many features in the atmospheric and surface-water data of the Great Lakes with toy lakes of comparable water depths. In addition, global-warming experiments with the $0.04°C/year$ trend and inter-annual variability of $2°C$ in the upper atmosphere give rise to comparable magnitudes of surface-water warming trends of these toy lakes. These are indications that the ice-albedo feedback and other ice-related feedback effects combined are enough to generate the essential features of the warming trends of the Great Lakes. The correlation between the summer surface water temperature and the winter maximum ice cover of the Great Lakes are its natural consequence.

Our essential finding is the indications of the existence of multiple local-climate regimes over the eastern part of Lake Superior. Multiple climate regimes arise due to an abrupt change in lake surface albedo and the amount of sensible and latent heat fluxes with the appearance of ice. On the one hand, when ice appears over the surface of a lake, the surface albedo of a lake significantly increases, reducing the amount of incom-

120

ing shortwave radiation impinging upon the lake. This reduction in incoming shortwave radiation further encourages the formation of ice on the lake surface. On the other hand, when ice does not appear on the surface of a lake, a good amount of incoming shortwave radiation continues to impinge upon the lake. This abundance in incoming energy continues to discourage the formation of ice on the lake surface. Whether ice starts to appear at the surface on the day of the coldest water temperature in winter is the point of bifurcation, giving rise to two stable equilibrium states of the lake in experiments with periodic forcing without inter-annual variability. Depending on whether ice covers the lake during winters, the heat content of the lake changes as well; the two different stable seasonal cycles of the lake have different summer lake temperatures (Figure 21). Although the real atmosphere contains stochastic inter-annual variability, the gap between the colder and warmer regimes of Lake Superior is large enough to exhibit multi-modality in its maximum-ice-cover histogram (Figure 11) as well as discontinuous behaviors in the time series of August-mean surface water temperature at the lake's buoy stations (Figure 8).

(*Question 6*) *Is there more than one local-climate regime over Lake Superior? Is there more than one local-climate regime over the Great Lakes?*

In the scatter plots of Figure 44, in §4.1.1, with August-mean surface water temperature at buoy station 45004 in easter Lake Superior on the vertical axis and one-year mean of air temperature anomalies at various pressure levels upwind of the Great Lakes, we found parallelogram structures, indicating a bifurcation of climate regimes over the easter part of Lake Superior at the bottoms of the parallelograms. In all panels of Figure 44, we find a range of air temperature anomalies, roughly between $-0.5°C$ and $0.5°C$, where black, blue, green, and red dots all coexist but are layered vertically. This range is where multiple local-climate regimes exist. In this range of multiple climate regimes, the vertical spread in August-mean surface water temperature at buoy station 45004 in eastern Lake Superior is between $5°C$ and $10°C$, which is comparable to the vertical spread in a model result of the Lake 2 toy model in Figure 59, with upper air temperature on the horizontal

axis. The width of the range of upper air temperature where multiple climate regimes exist in this model result in Figure 59 is also approximately $1°C$, again comparable to that of the eastern part of Lake Superior. These results strongly indicate the existence of multiple local-climate regimes over the eastern part of Lake Superior, where its deepest basin is located.

In the rest of the Great Lakes region, indications of the existence of multiple local-climate regimes are less clear at best. Especially, the shallow Lake Erie does not indicate the existence of multiple local-climate regimes at all. However, there are indications that regime transitions in the local-climate of Lake Superior affect the climate of its neighboring regions as well as its downwind regions considerably, and much of the Great Lakes is located either downwind or near Lake Superior. We examine the influence of Lake Superior on downwind regions in Appendix B. Exactly how much regime transitions in the local-climate of Lake Superior can influence the rest of the Great Lakes region remains to be studied.

Outstanding Questions and Future Work We have summarized answers to the six questions. However, for the answers to become more definitive, we would need to the following.

(1) We need to establish the existence of multiple regional-climate regimes of more realistic lakes, which mimic the bathymetry of the Great Lakes, simulated by a regional climate model.

In this thesis, we simulated only lakes of uniform depth and those of three lake columns. The question is, *What if we increase the number of lake columns?* For example, in the RegCM4 regional climate model mentioned in §2.2.1, a lake is divided into numerous lake columns, and each lake column is treated by a one-dimensional lake model (Bennington *et al,*, 2014). We need to examine such lakes of more realistic bathymetry, and see if a realistic toy Lake Superior exhibits multiple climate regimes as well.

(2) We need to examine analytically the properties of the $n \to \infty$ limit of n-column lakes under a simpler lake-atmosphere model.

Since we simulated only lakes of uniform depth and those of three lake columns, the value of n was either 1 or 3. Our lake-atmosphere-land coupled model is much simpler than regional climate models, but it is not simple enough to obtain properties of the solutions of the $n \to \infty$ limit of n-column lakes. When $n = 1$, we saw the existence of at most two climate regimes under identical atmospheric forcing. When $n = 3$, we sometimes saw the existence of three climate regimes under identical atmospheric forcing. If we construct a simpler lake-atmosphere model and we take $n \to \infty$, what will happen to the range of possibilities of the number of multiple climate regimes and their properties? What we are most interested in is whether multiple climate regimes disappear in the $n \to \infty$ limit under some conditions, and if they do, in what conditions. What we are also interested in is whether the number of climate regimes remain finite or approaches infinity in some conditions, and if it does, in what conditions.

The reason that these future problems are important is based on these two observations.

(A) In the scatter plots of Figure 44 in §4.1.1, with August-mean surface water temperature at buoy station 45004 in easter Lake Superior on the vertical axis and one-year mean of air temperature anomalies at various pressure levels upwind of the Great Lakes, we saw parallelogram structures, indicating a bifurcation of climate regimes over the easter part of Lake Superior at the bottoms of the parallelograms.

(B) In the scatter plots of Figure 51 in Appendix A, with August-mean surface water temperature at buoy station 45004 in easter Lake Superior on the vertical axis and one-year mean of air temperature anomalies at various pressure levels *right above* the buoy station, at higher pressure levels (lower altitudes), the atmosphere was greatly influenced

by the lake, but even at lower pressure levels (higher altitudes), we still saw slightly different relationships between surface water temperature and air temperature anomalies from those in Figure 44. Namely, the vertical spread between the warmer and colder regimes is not as wide as that in Figure 44.

Both of these figures *qualitatively* indicate the existence of multiple climate regimes over the eastern part of Lake Superior, but how the regimes manifest themselves in the aforementioned scatter plots is not identical. Examination of uniform-depth lakes or three-column lakes has limitations in this regard because their bathymetry is too simple to predict the properties of the multiple local-climate regimes of Lake Superior *quantitatively.*

Another line of research would be to quantify separate contributions of the ice-related feedback effects of winter as well as various atmospheric feedback on lake-surface warming of spring/summer, to the warming trends of the Great Lakes. When ice appears on the surface of a lake, its surface albedo and the amounts of sensible and latent heat fluxes change. In addition, there are cloud feedback and surface-wind feedback on lake-surface warming in spring and summer. How much they contribute to the amplification or reduction of the warming trends of the Great Lakes remains to be studied.

Yet another line of research would be to explore how various external events might influence a lake's inclination of regime transitions. For example, recently, water transparency of some of the Great Lakes has increased due to the recent invasion of mussels into the area (for example, see Kerfoot *et al.*, 2012). On the one hand, the more water becomes transparent, the larger the depth of its surface mixed layer becomes, resulting in a slight decrease in summertime surface water temperature. On the other hand, the larger the depth of its surface mixed layer becomes, the more its heat content is protected from the interaction at the surface between the lake and the atmosphere, making the lake behave slightly more like a deeper lake. This make ice slightly more difficult to appear in winter and makes the lake slightly easier to transition from a colder climate regime to a warmer climate regime.

Bibliography

[1] Alexander, M. A., C. Penland (1996), Variability in a mixed layer ocean model driven by stochastic atmospheric forcing. *J. Climate*, 9, 2424-2442.

[2] Assel, R., K. Cronk, and D. Norton (2003), Recent trends in Laurentian Great Lakes ice cover. *Climatic Change*, 57(1-2):185-204.

[3] Assel, R. (1986), Fall and Winter Thermal Structure of Lake Superior. *J. of Great Lakes Res.*, 12(4), 251-262.

[4] Austin, J. A., and S. M. Colman (2007), Lake Superior summer water temperatures are increasing more rapidly than regional air temperatures: a positive ice-albedo feedback. *Geophys. Res. Lett.*, 34, L06604.

[5] Bai. X., J. Wang, D. J. Schwab, Y. Yang, L. Luo, G. A. Leshkevich, and S. Liu (2013), Modeling 1993-2008 climatology of seasonal general circulation and thermal structure in the Great Lakes using FVCOM. *Ocean Modeling*, 65, 40-63.

[6] Bennington, V., M. Notaro, K. D. Holman (2014), Improving Climate Sensitivity of Deep Lakes within a Regional Climate Model and Its Impact on Simulated Climate. *J. Climate*, 27, 2886-2911.

[7] Byrne, M. P., and P. S. O'Gorman (2012), Land-ocean warming contrast over a wide range of climates: convective quasi-equilibrium theory and idealized simulations. *J. Climate*, 26, 4000-4016.

[8] Dake , J. M. K., and D. R. F. Papadopoulos (1986), Mathematical prediction of thermal stratification of Lake Ostrovo (Vegoritis), Greece, *Water Resour. Res.*, 22, 1590-1596.

[9] Desai, A. R., J. A. Austin, V. Bennington, and G. A. McKinley (2009), Stronger winds over a large lake in response to weakening air-to-lake temperature gradient. Nature Geoscience 2, 855-858 (2009)

[10] Fang, X., and H. G. Stefan (1998), Temperature variability in lake sediments, *Water Resour. Res.*, 34, 717?729, doi:10.1029/97WR03517.

[11] Frankignoul, C., and K. Hasselmann (1977), Stochastic climate models, Part II Application to sea-surface temperature anomalies and thermocline variability. *Tellus*, 29,289-305

[12] Hakanson, L., (1995) Models to Predict Secchi Depth in Small Glacial Lakes. *Aquat. Sci.*, 57, 31-53.

[13] Hanrahan, Janel L., S. V. Kravtsov, and P. J. Roebber (2010), Connecting past and present climate variability to the water levels of Lake Michigan and Huron. *Geophys. Res. Lett.*, 37, L01701.

[14] Heggen, R. J., Thermal dependent properties of water, *J. Hydraul. Eng.*, 109, 298-302, 1983.

[15] Henderson-Sellers, B., Calculating the surface energy balance for lake and reservoir modeling: A review, *Rev. Geophys.*, 24, 625-649, 1986.

[16] Henderson-Sellers, A. and A. J. Pitman (1992), Land-surface schemes for future climate models: Specification, aggregation, and Heterogeneity. *J. Geophys. Res.*, 97(D), 2687-2696.

[17] Hostetler, S., and P. J. Bartlein (1990), Simulation of lake evaporation with application to modeling lake-level variations at Harney-Malheur Lake, Oregon. *Water Resource Res.*, 26, 2603-2612.

[18] Joshi, M. M., and J. M. Gregory (2008), Dependence of the land-sea contrast in surface climate response on the nature of the forcing. *Geophs. Res. Lett.*, 35, L24802.

[19] Joshi, M. M., J. M. Gregory, M. J. Webb, D. M. H. Sexton, and T. C. John (2008), Mechanism for the land/sea warming contrast exhibited by simulations of climate change. *Clim. Dyn.*, 30: 455-465.

[20] Kerfoot, W. C., F. Yousef, S. A. Green, J. W. Budd, D. J. Schwab, H. A. Vanderploeg (2010), Approaching storm: Disappearing winter bloom in Lake Michigan. *J. of Great Lakes Res.*, 36(sp3), 30-41.

[21] Lau, N.-C., M. J. Nath (1996), The role of the "atmospheric bridge" in linking tropical pacific ENSO events to extratropical SST anomalies. *J. Climate*, 9, 2036?2057.

[22] Manabe, S., R. J. Stouffer, M. J. Spelman, and K. Bryan (1991), Transit responses of a coupled ocean- atmosphere model to gradual changes of atmospheric CO! part I: Annual mean response. *J. Clim.*, 4, 785-818.

[23] Martynov, A., L. Sushama, and R. Laprise, (2010), Simulation of temperate freezing lakes by one- dimensional lake models: performance assessment for interactive coupling with regional climate models. *Boreal Environment Research*, 15, 143-164.

[24] Merryfield, W., M. M. Holland, and A. H. Monahan (2008), Multiple Equilibria and Abrupt Transitions in Arctic Summer Sea Ice Extent, in *Arctic Sea Ice Decline: Observations, Projections, Mechanisms, and Implications, Geophys. Monger. Ser.*, vol. 180, edited by E. T. DeWeaver, C. M. Bitz, and L.-B. Tremblay, pp151-174, AGU, Washington, D. C.

[25] Patterson, J. C., and P. F. Hamblin (1988), Thermal simulation of a lake with winter ice cover. *Limnol. Oceanogr.*, 33, 323-338.

[26] Prinsenberg, S., and I. K. Peterson (2002), Variations in air-ice drag coefficient due to ice surface roughness, *International Journal of Offshore and Polar Engineering*, Vol.12, No.2, June 2002 (ISSN 1053-5381).

[27] Schneider, P., and S. J. Hook (2010), Space observations of inland water bodies show rapid surface warming since 1985, *Geophys. Res. Lett.*, 37, L22405.

[28] Schwab, D. J., D. J. Leshkevich, and G. C. Muhr (1992), Satellite measurements of surface water temperature in the Great Lakes: Great Lakes Coast Watch. *J. of Great Lakes Res.*, 18(2), 247-258.

[29] Semtner, A. J. (1976), A Model for the Thermodynamic Growth of Sea Ice in Numerical Investigations of Climate. *J. Phys. Oceanogr.*, 6, 379-389.

[30] Subin, Z. M., W. J. Riley, and D. Mironov (2012), An Improved Lake Model for Climate Simulations: Model Structure, Evaluation, and Sensitivity Analyses in CESM1. *J. Adv. Mod. Earth Sys.* 4, M02001. doi:10.1029/2011MS000072

[31] Sutton, R. T., B. Dong, and J. M. Gregory (2007), Land/sea warming ratio in response to climate change: IPCC AR4 model results and comparison with observations. *Geophys. Rev. Lett.*, 34, L02701.

[32] Wang, J., X. ai, H. Hu, A. Clites, M.Colton, and B. Lofgren (2012), Temporal and Spatial Variability of Great Lakes Ice Cover, 1973-2010. *J. Climate*, 25, 1318-1329.

[33] White, B., J. Austin, and K. Matsumoto (2012), A three-dimensional model of Lake Superior with ice and biogeochemistry, *J. Great Lakes Res.*, 38(1), 61-71.

Appendix A: Multi-Modality in Atmospheric Data – The Great Lakes' Influence on the Atmosphere above the Lakes

In §4.1, we have looked at air temperature at various pressure levels upwind of the Great Lakes. In this appendix, let us take a look at air temperature right above the Great Lakes.

Model Results: Mixing the Upper and Lower Atmospheres   In our lake-atmosphere-land coupled model, the temperature of the upper atmosphere is used as the boundary condition. The upper atmosphere is not affected by whatever happens below, and the lower atmosphere is affected both by the upper atmosphere and the surface. This asymmetric direction of influence gives rise to the difference in appearance of two scatter plots, one whose horizontal axis is one-year mean of *upper* air temperature, and the other whose horizontal axis is one-year mean of *lower* air temperature. With model results shown in Figure 41 in §4.1, we have an expectation of how scatter plots would change if air temperature on the horizontal axis changes from a near-surface level to a high-altitude level, as follows. With one-year mean of air temperature at a near-surface level on the horizontal axis, the spread in the scatter plot would look almost linear. With one-year mean of air temperature at a high altitude on the horizontal axis, the scatter plot would show the existence of multiple regimes, similar to what we see in the right panel of Figure 41.

What would a scatter plot look like if air temperature plotted on the horizontal axis is somewhere between these near-surface and high-altitude levels? We have two different sets of air temperatures from model outputs: that of the upper atmosphere and that of
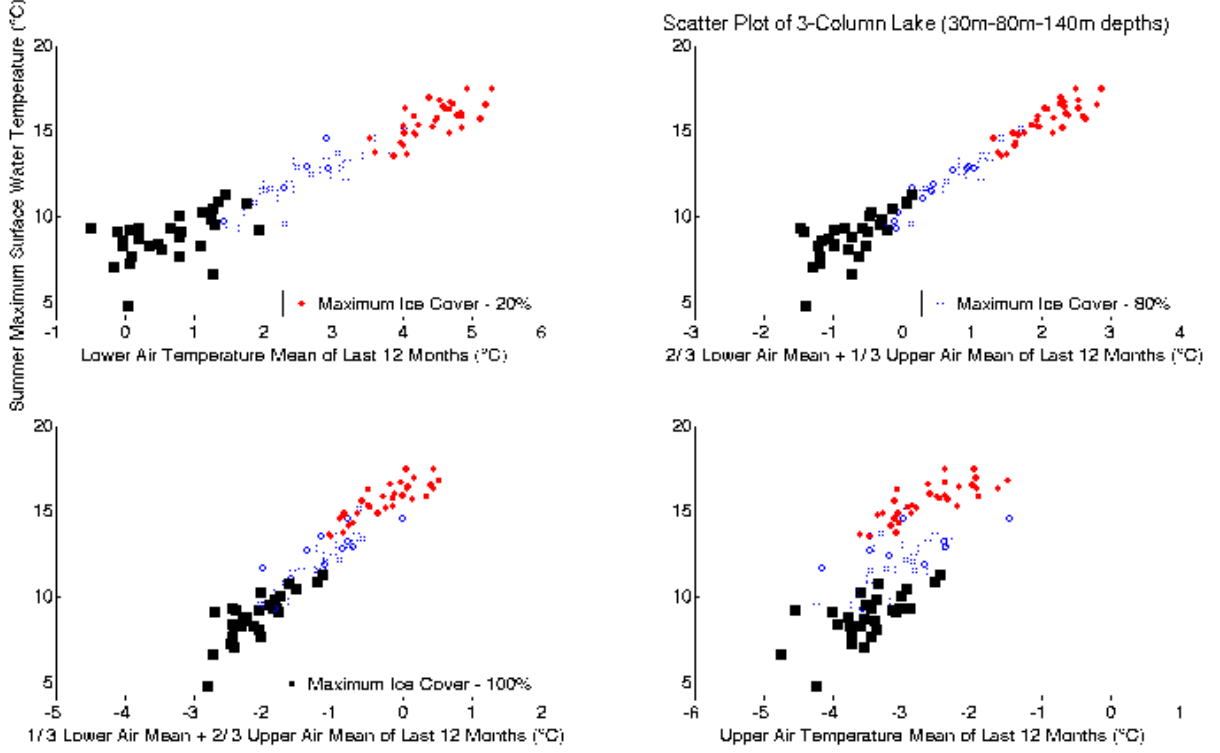
Figure 59: *The scatter plot of one-year mean of upper, lower, or a mixture of air temperature versus summer maximum surface water temperature of the deepest column of Lake 2. (Top-left) The scatter plot of one-year mean, from September of year $x-1$ to August of year x, of lower air temperature on the horizontal axis, versus summer maximum surface water temperature of the deepest column of the Lake 2 toy model of year x on the vertical axis, after we run more than 50 years of time series. Filled black squares correspond to the cases in which ice covers 100% of the lake during the winter of year x. Blue circles correspond to the cases in which ice covers 80%, only the shallowest and intermediate lake columns, of the lake during the winter of year x. Red circles correspond to the cases in which ice covers 20%, only the shallowest lake column, of the lake during the winter of year x. (Top-right) Similar to the plot on the top-left corner, but with the mix of 2/3 times one-year mean of lower air temperature and 1/3 times one-year mean of upper air temperature on the horizontal axis. (Bottom-left) Similar to the plot on the top-left corner, but with the mix of 1/3 times one-year mean of lower air temperature and 2/3 times one-year mean of upper air temperature on the horizontal axis. (Bottom-right) Similar to the plot on the top-left corner, but with one-year mean of upper air temperature on the horizontal axis.*

the lower atmosphere. So, let us mix the two sets in certain proportions. For example, we can add 1/3 times lower air temperature and 2/3 times upper air temperature together, and see what happens. Figure 59 shows some experimental results from model outputs. The top-right panel of Figure 59 is the scatter plot with the mix of 2/3 times lower air temperature and 1/3 times upper air temperature on the horizontal axis. The bottom-

left panel is the scatter plot with the mix of 1/3 times lower air temperature and 2/3 times upper air temperature on the horizontal axis. An interesting observation is that, in the top-right panel, when 2/3 times lower air temperature and 1/3 times upper air temperature are mixed together, the dots are more squeezed into a thinner line than those in the top-left panel with lower air temperature on the horizontal axis. Another observation is that the spread of dots is restrained even when a higher proportion of upper air temperature is mixed with lower air temperature. In Figure 59(bottom-left), 1/3 times lower air temperature and 2/3 times upper air temperature are mixed together on the horizontal axis, yet the dots are still aligned in a very narrow line, being still difficult to see any signature of multiple climate regimes. It is only in the bottom-right panel, with upper air temperature on the horizontal axis, the dots finally spread out vertically and we finally see some signatures of multiple climate regimes.

A Deep–Lake Example: Manifestations of Ice Regimes of Lake Superior With these experimental results in mind, let us take a look at scatter plots based on the NARR reanalysis air temperature data. Figure 60 is the same figure we saw in §4.2, which contains the scatter plots of one-year mean, September of year $x - 1$ through August of year x, of air temperature anomalies at higher pressure levels right above buoy station 45004, in eastern Lake Superior, on the horizontal axis, versus August-mean surface water temperature of year x at the buoy station on the vertical axis. Figure 61 contains the corresponding panels for lower pressure levels. We immediately recognize that the distribution of dots looks linear in the panels corresponding to higher pressure levels (lower altitudes), consistent with model results. This must be at least partly due to the lake effect; lake warming (or lake cooling) amplifies air warming (or air cooling) adding more heat (or less heat) to the atmosphere.

As we look at the panels from the top-left to the bottom-right of Figure 60, air temperature on the horizontal axis changes from the 900mb level to the 600mb level and we notice that the spread of the dots is restrained until at quite a high altitude, and the dots in the bottom panels, with air temperature at an intermediate level on the horizontal axis, spread thinner and tighter than those in the top-left panel, with air temperature at
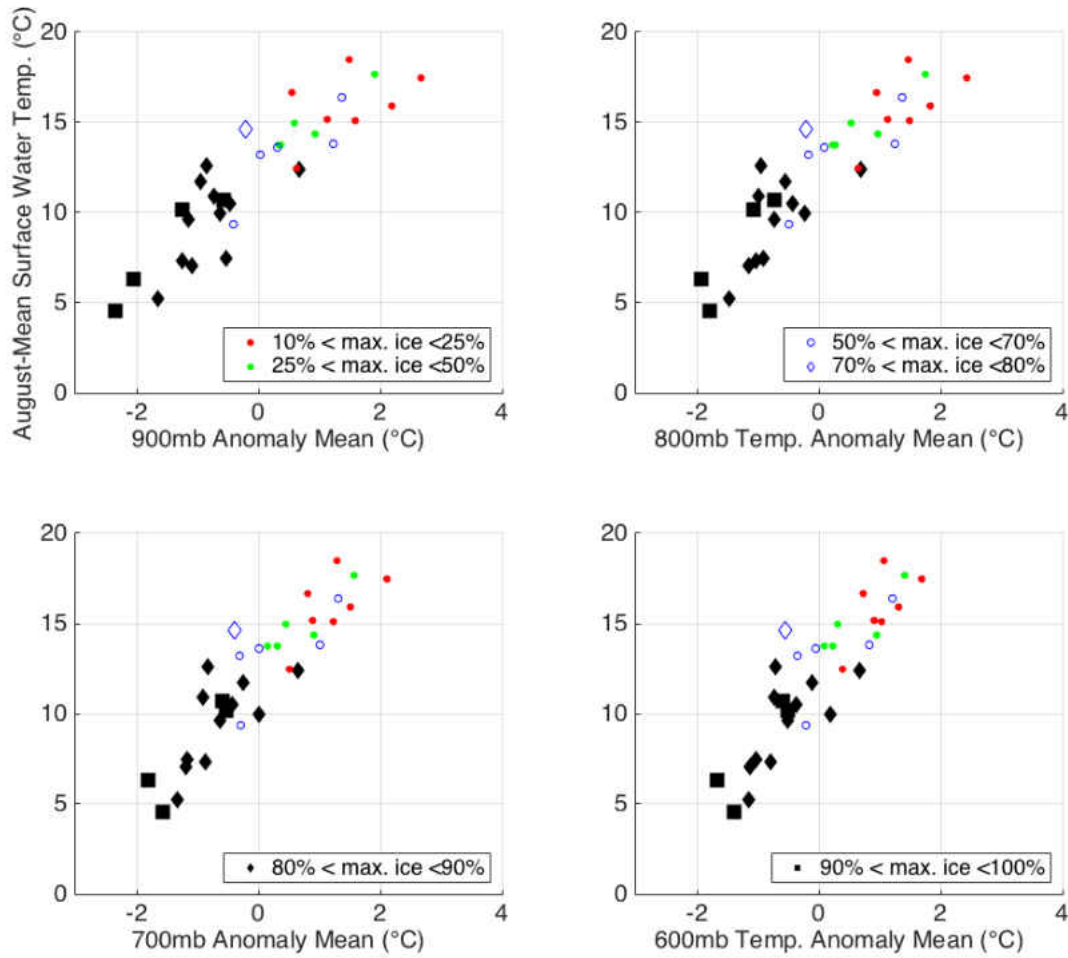
Figure 60: *The scatter plots of one-year mean, September of year $x-1$ through August of year x, of air temperature anomalies at various pressure levels right above buoy station 45004, in eastern Lake Superior, on the horizontal axis, versus August-mean surface water temperature of year x at the buoy station on the vertical axis. The figure contains four panels, whose horizontal axes are air temperature anomalies at the 900mb level, 800mb level, 700mb level, and the 600mb level. In these panels, black squares and black diamonds correspond to the cases in which ice covers more than 90% and between 80% and 90% of Lake Superior, respectively, during the winter of year x. Blue diamonds and blue circles correspond to the cases in which ice covers between 70% and 80% and between 50% and 70% of the lake, respectively, during the winter of year x. Green circles and red circles correspond to the cases in which ice covers between 25% and 50% and between 10% and 25% of the lake, respectively, during the winter of year x. The year x runs from 1981 to 2013.*

the 900mb level. This is qualitatively what we expect with the aforementioned models

results (Figure 59). Indications of multiple local-climate regimes start to appear in the

scatter plot with air temperature anomalies at the 700mb level on the horizontal axis,

where black, blue, and green dots coexist between -0.5 °C and 0.5 °C of the horizontal
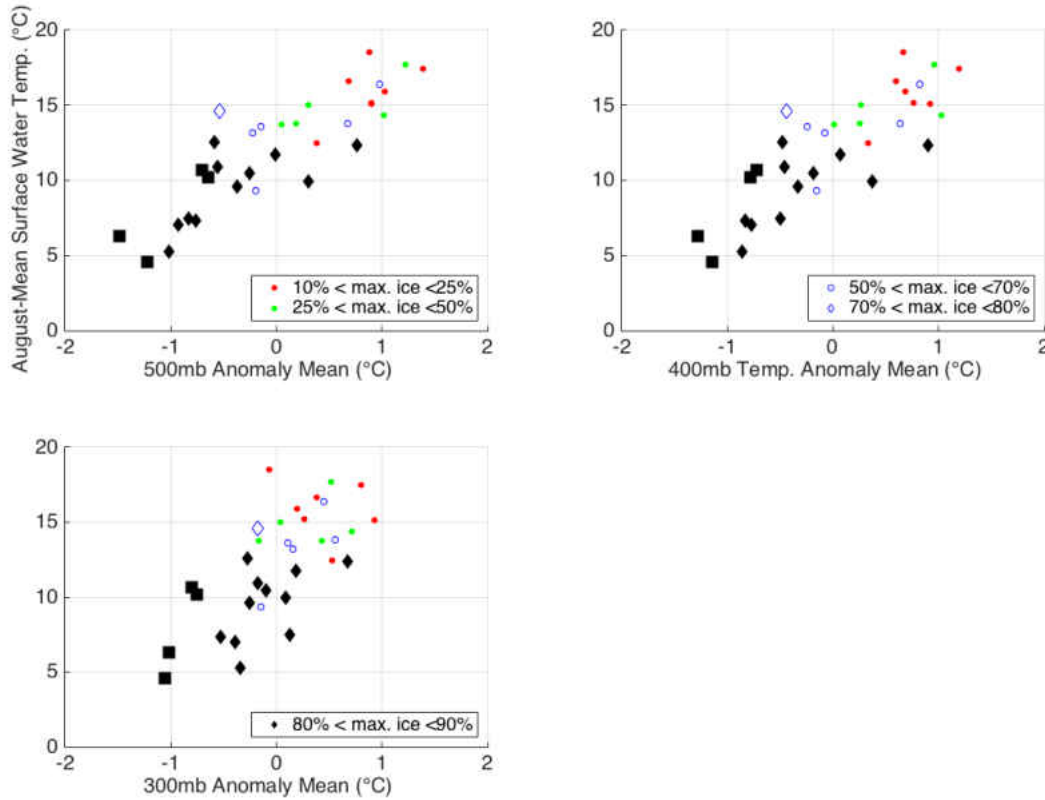
Figure 61: *The scatter plots of one-year mean, September of year $x-1$ through August of year x, of air temperature anomalies at various pressure levels right above buoy station 45004, in eastern Lake Superior, on the horizontal axis, versus August-mean surface water temperature of year x at the buoy station on the vertical axis. The figure contains three panels, whose horizontal axes are air temperature anomalies at the 500mb level, 400mb level, and the 300mb level. In these panels, black squares and black diamonds correspond to the cases in which ice covers more than 90% and between 80% and 90% of Lake Superior, respectively, during the winter of year x. Blue diamonds and blue circles correspond to the cases in which ice covers between 70% and 80% and between 50% and 70% of the lake, respectively, during the winter of year x. Green circles and red circles correspond to the cases in which ice covers between 25% and 50% and between 10% and 25% of the lake, respectively, during the winter of year x. The year x runs from 1981 to 2013.*

axis with black dots occupying the lower half. In the bottom panels of Figure 60 as well as the panels of Figure 61, the existence of multiple local-climate regimes are once again apparent between -0.5 °C and 0.5 °C on the horizontal axis with black dots occupying the lower half of the spread.

A Shallow–Lake Example: Climate Regimes of Lake Erie Once again, by contrast, Lake Erie looks quite different. Figure 62 contains the scatter plots of one-year
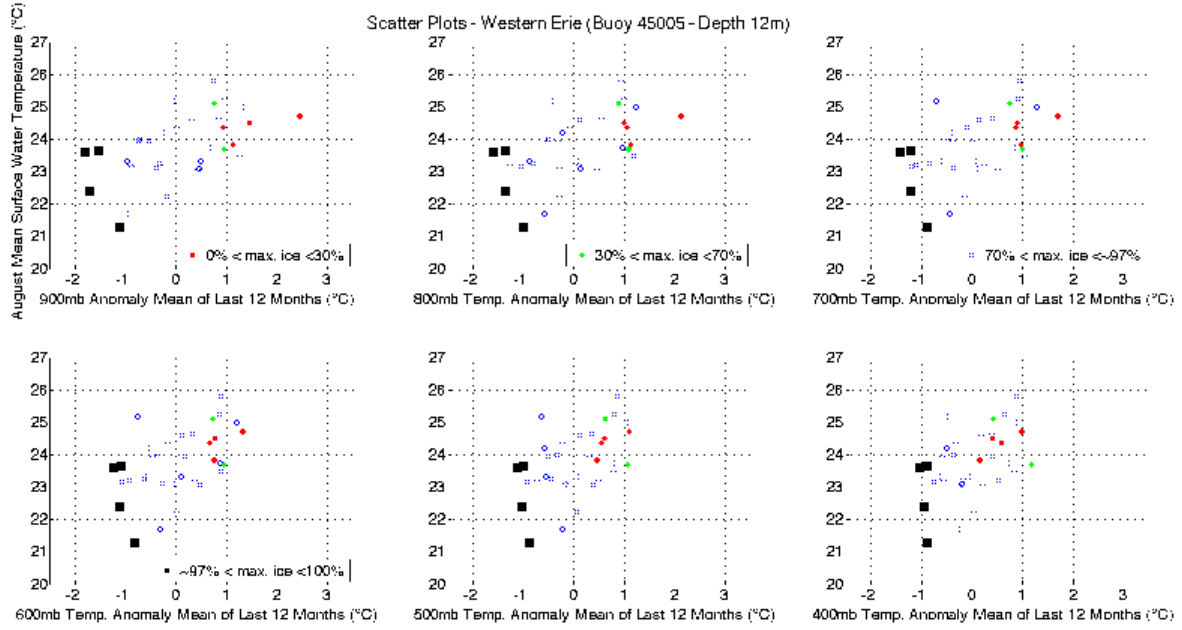
Figure 62: *The scatter plots of one-year mean, from September of year $x-1$ to August of year x, of air temperature anomalies at various pressure levels right above buoy station 45005, in western Lake Erie, on the horizontal axis, versus August-mean surface water temperature of year x at the buoy station on the vertical axis. In these panels, black squares correspond to the cases in which ice covers more than 97% of Lake Erie during the winter of year x. Blue circles correspond to the cases in which ice covers between 70% and 97% of the lake during the winter of year x. Green circles correspond to the cases in which ice covers between 30% and 70% of the lake during the winter of year x. Red circles correspond to the cases in which ice covers less than 30% of the lake during the winter of year x. The year x runs from 1981 to 2013.*

mean, from September of year $x-1$ to August of year x, of air temperature anomalies at various pressure levels right above buoy station 45005, in western Lake Erie, on the horizontal axis, versus August-mean surface water temperature of year x at the buoy station on the vertical axis. Unlike eastern Lake Superior, we do not find clear indications of multiple local-climate regimes over western Lake Erie. Black squares, which correspond to the winters in which ice covers more than 97% of Lake Erie, are always near the left end of a plot. Blue dots and green/red dots are not layered vertically in an obvious way. In each panel, we find a range of air temperature on the horizontal axis where blue, green, and red dots coexist but find no apparent structure within the range. This indicates that, over shallow lakes such as Lake Erie, finding multiple local-climate regimes is more difficult than it is over deep lakes such as Lakes Superior.

Manifestations of Multiple Climate Regimes of Lake Superior in July and August The atmosphere above the regions of largest water depths of Lake Superior is stable in July and August. The reason is that surface water temperatures over these region in July and August are often much colder than air temperatures above them. During these months, we do not expect surface air to ascend much, and we expect to see manifestations of multiple climate regimes in the July-August air temperature data right above the eastern part of Lake Superior.
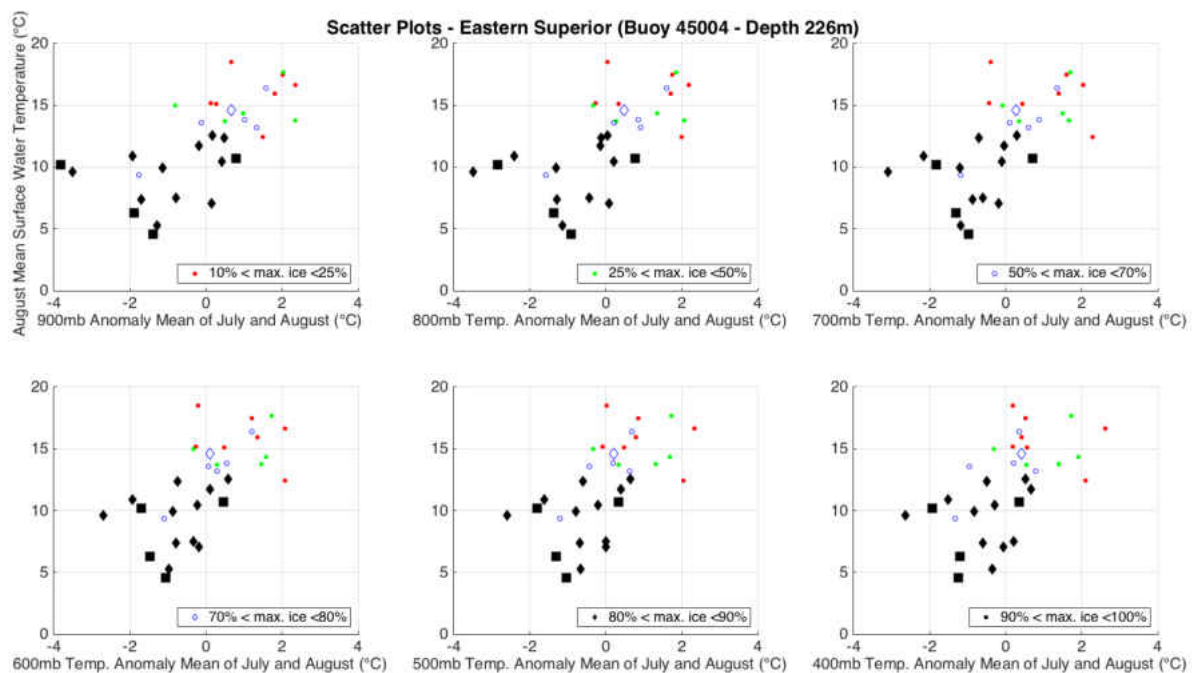
Figure 63: *Scatter plots of two-month mean, July and August of year x, of air temperature anomaly at a certain pressure level right above buoy station 45004, in eastern Lake Superior, on the horizontal axis, versus August-mean surface water temperature of year x at the buoy station on the vertical axis. The figure contains six panels, whose horizontal axes are air temperature anomalies at the 900mb level, 800mb level, 700mb level, all the way to the 400mb level. In these panels, black squares and black diamonds correspond to the cases in which ice covers more than 90% and between 80% and 90% of Lake Superior, respectively, during the winter of year x. Blue diamonds and blue circles correspond to the cases in which ice covers between 70% and 80% and between 50% and 70% of the lake, respectively, during the winter of year x. Green circles and red circles correspond to the cases in which ice covers between 25% and 50% and between 10% and 25% of the lake, respectively, during the winter of year x. The year x runs from 1981 to 2013.*

Figure 63 contains the scatter plots of two-month-mean, July and August, of air temperature anomalies at various pressure levels right above buoy station 45004, in eastern

Lake Superior, on the horizontal axis, versus August-mean surface water temperature at the buoy station on the vertical axis. At the 800mb level and above, we see that two apparent local-climate regimes coexist between $-0.5°C$ and $1°C$ on the horizontal axis, and the vertical spreads within this range are as much as $10°C$. This roughly $1.5°C$ range of coexistence is similar to model results. For example, in the right panel of Figure 41, the warmest and coldest regimes coexist between $-3.5°C$ and $-2.5°C$ on the horizontal axis, which is roughly $1°C$. The vertical spread of dots within this range is roughly $8°C$. Therefore, when the atmosphere above Lake Superior is stable, such as in July and August, we find resemblance between observed data of Lake Superior and model results of the toy Lake 2. Moreover, the black dots and red/green dots of Figure 63 are clearly vertically separated, although horizontally they overlap. This is a good indication of the existence of multiple climate regimes of eastern Lake Superior.

Uncertainty in Atmospheric Data: the Atmosphere right above the Great Lakes In this appendix, we have been discussing the atmosphere above the Great Lakes, but there is a caveat. The NARR air temperature data over the region of the Great Lakes, especially above the deeper lakes points of Lake Superior, are often not accurate, especially in June, July, and August. Figure 64 compares air temperature 4m above the lake surface at buoy station 45004, in eastern Lake Superior, based on the NDBC buoy data, with air temperature 2m above the lake surface near the buoy station based on the NARR reanalysis, for the years 1995-1996.

The green curve is the air temperature based on the NARR reanalysis and the red curve is the air temperature based on the buoy data. We note a large discrepancy between the two air-temperature curves in June, July, and August, when surface water temperature is still cold. The most likely reason for these errors in NARR is the overestimate of surface water temperatures at deeper lake points of the Great Lakes, especially Lake Superior. However, we note that, before Julian day 150 and after Julian day 250 in the figure, the two air-temperature curves are much closer to each other. This demonstrates how difficult it is in general to estimate surface water temperatures at deeper lake points of the Great Lakes during summer months, consequently giving rise to those errors in the
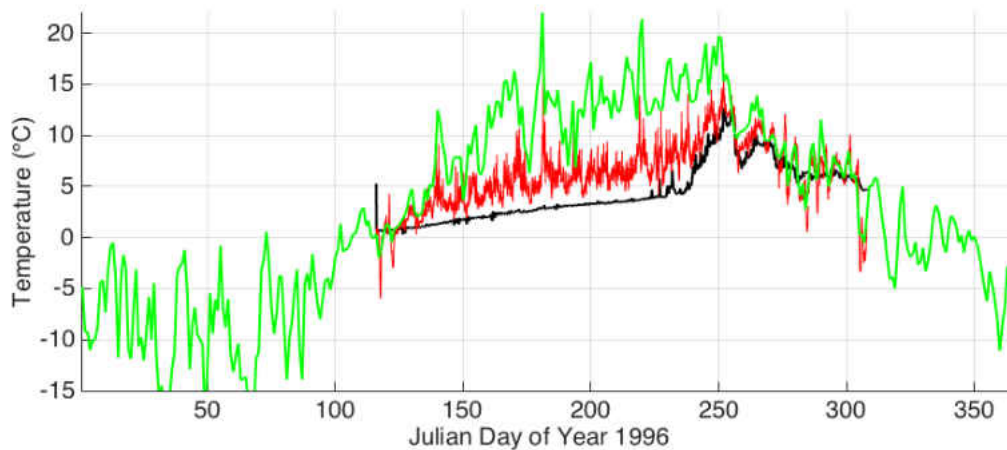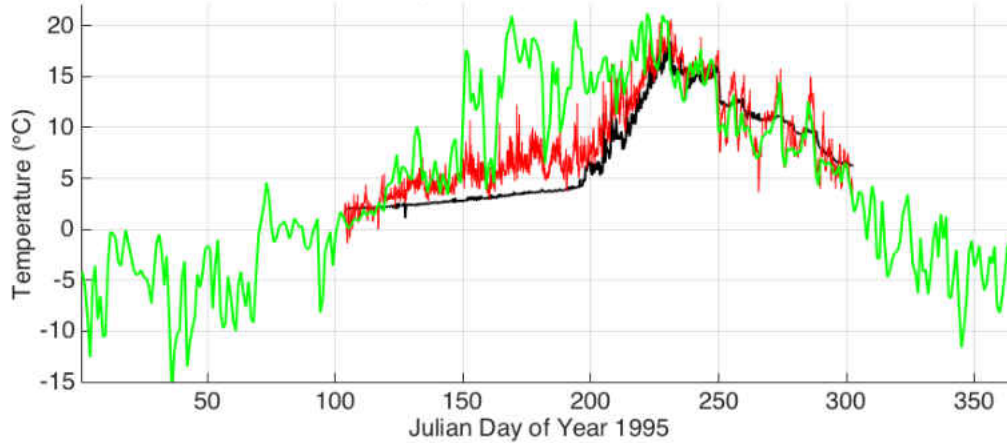
Figure 64: *Surface air and water temperatures at buoy station 45004. (Red) The time series of air temperature 4m above the lake surface at buoy station 45004, in eastern Lake Superior for the years 1995-1996, based on the buoy data. (Green) The time series of air temperature 2m above the lake surface near the buoy station based on the NARR reanalysis, for the years 1995-1996. (Black) The time series of water temperature 1m below the surface, based on the buoy data, for the years 1995-1996.*

air-temperature reanalysis. Given that the data of air temperature 2m above the lake surface contains this much inaccuracy, we expect that the NARR air temperature data at lower and intermediate altitudes also contain errors, especially in these three months. Therefore, with all the NARR air temperature data at hand, we are still not very certain about how high the Great Lakes, especially the eastern part of Lake Superior, affect the atmosphere above them. Despite these uncertainties, to a limited degree we can still obtain qualitative understanding of the lake-atmosphere interaction above the Great Lakes, as seen in this appendix, by comparing model results with the NARR reanalysis data, but our discussions are only meant to be qualitative when we use the air temperature data right above the Great Lakes.

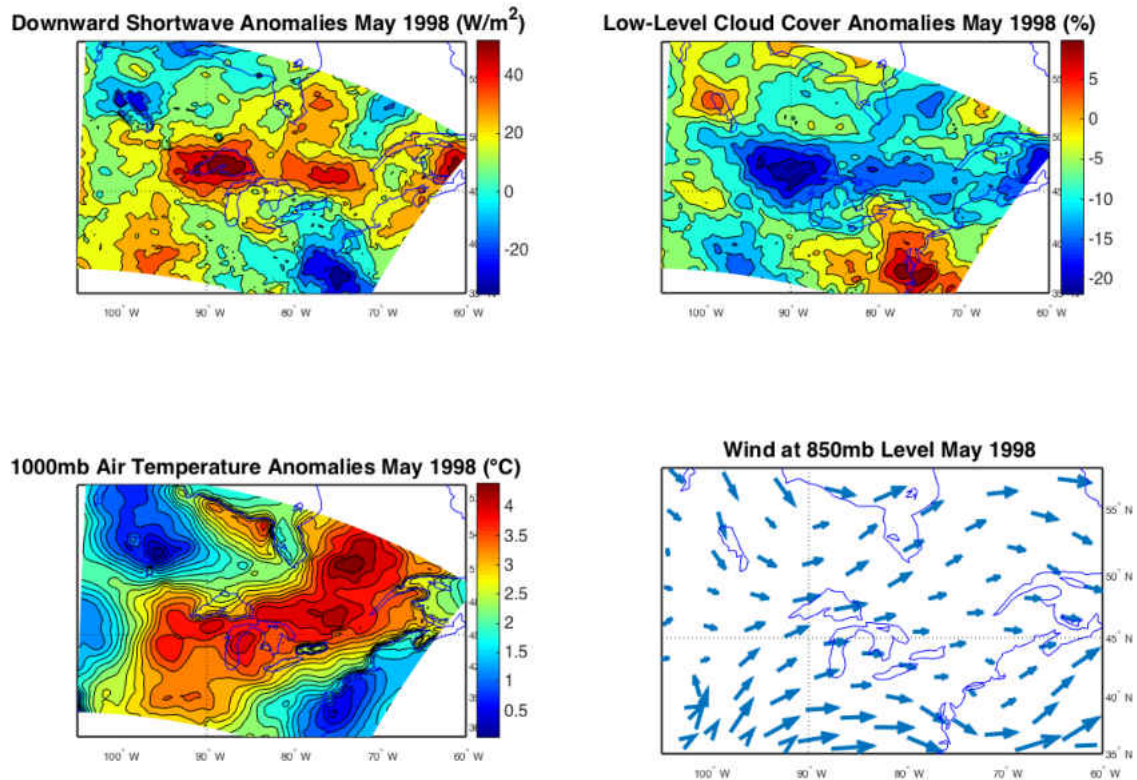# Appendix B: The Great Lakes' Influence on Downwind Regions

Figure 65: *Maps of the monthly-mean anomalies of (top-left) downward shortwave radiation, (top-right) low-level cloud cover, and (bottom-left) air temperature at the 1000mb level in the vicinity of the Great Lakes for May 1998. In each of these panels, the climatology for the years 1979-2013 is subtracted from the mean of May 1998. The remaining panel (bottom-right) is the longterm-mean wind field at the 850mb level averaged for the years 1979-2013. All are based on the NARR reanalysis.*

In §4.3.1, we saw negative anomalies in low-level cloud cover in downwind regions of Lake Superior in May 1998 (Figure 65). As if following the flow of winds from the east to the west, the regions of negative anomalies in low-level cloud cover looked like a long strip that starts from a region that contains Lake Superior and extends to the east. These strips of land of negative trends in low-level cloud cover might be an example of

Lake Superior affecting its downwind regions. For example, let us take a look at the air temperature plot in Figure 65, about the Great Lakes region for May 1998. The bottom-left panel of this figure is a map of air temperature anomalies at the 1000mb pressure level. Compared with the top-right panel in the figure, a map of anomalies in low-level cloud cover, the regions of positive air temperature anomalies and the regions of negative anomalies in low-level cloud cover approximately match. The flow of the longterm-mean May winds over the Great Lakes (bottom-right panel) is consistent with the distribution of the regions of these anomalies, supporting our speculations that winds carried negative low-level cloud cover anomalies to Lake Superior's downwind regions.

Lake Superior's Influence on Downwind Regions in June May 1998 is one of the most conspicuous examples, but when we examine trends of the June climate around the Great Lakes region, we find a general trend similar to these examples as follows.

Figure 66 contains maps of warming trends in June-mean air temperature at 2m above the surface, the 1000mb level, 900mb level, and 800mb level over the regions containing the Great Lakes, Hudson Bay, and a part of Greenland. In the top panels, we see a long strip of land that shows strong warming trends in air temperature that spreads from the Great Lakes eastward.

For comparison, Figure 67 contains the June-mean wind fields (left) at the 925mb level and (right) at the 850mb level averaged for the years 1979-2013, based on the NARR reanalysis data. Again, a possibility is that lake-surface warming of the Great Lakes has dissipated more fogs, less low-level clouds have appeared over the lakes consequently, and with the climatological wind flowing eastward, the less cloudy air over the Great Lakes is carried to their downwind regions, increasing air temperature there due to increased shortwave radiation. We also note that the region of the strongest warming trends within a vicinity of the Great Lakes is exactly at the location of Lake Superior at the 1000mb pressure level, yet as we examine the trends at the 900mb level, and then the 800mb level, the region of the strongest warming trends there gradually moves eastward, consistent with the flow of the climatological wind at each level.
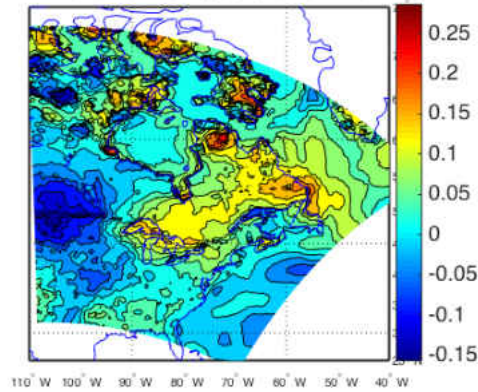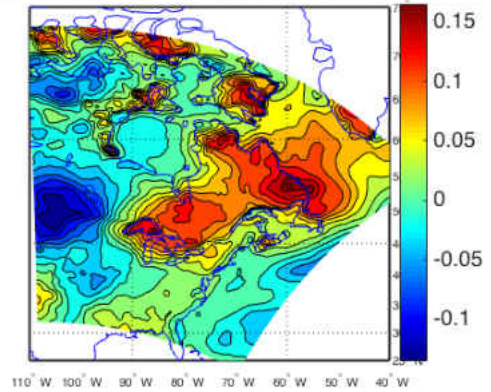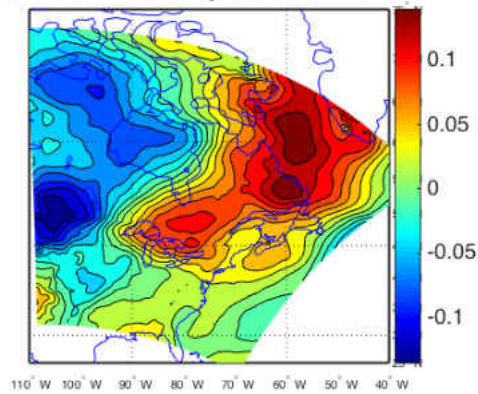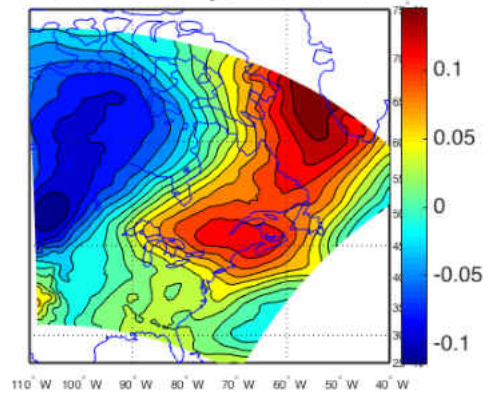
Figure 66: *Maps of warming trends in June-mean air temperature at 2m above the surface, the 1000mb level, 900mb level, and 800mb level over the regions containing the Great Lakes, Hudson Bay, and a part of Greenland. The units are in °C/year.*

The Great Lakes and Hudson Bay's Influence on the Atmospheric Circulation

When a change in surface air temperature of this spatial scale occurs, it also changes a large-scale horizontal temperature gradient as well, possibly affecting the pattern of atmospheric circulation. Figures 68-70 contain maps of warming trends in annual-mean air temperature at the 1000mb level, 900mb level, and 800mb level over North America. In these figures, we see that the Great Lakes, especially Lake Superior, affect the temperatures of downwind regions. One way to affect is to change the amount of low-level cloud cover there by westerly winds from Lake Superior in late spring/early summer, as suggested in this subsection. Another way would be that warm air over Lake Superior ascends high enough to be carried to these downwind regions in autumn and winter, when
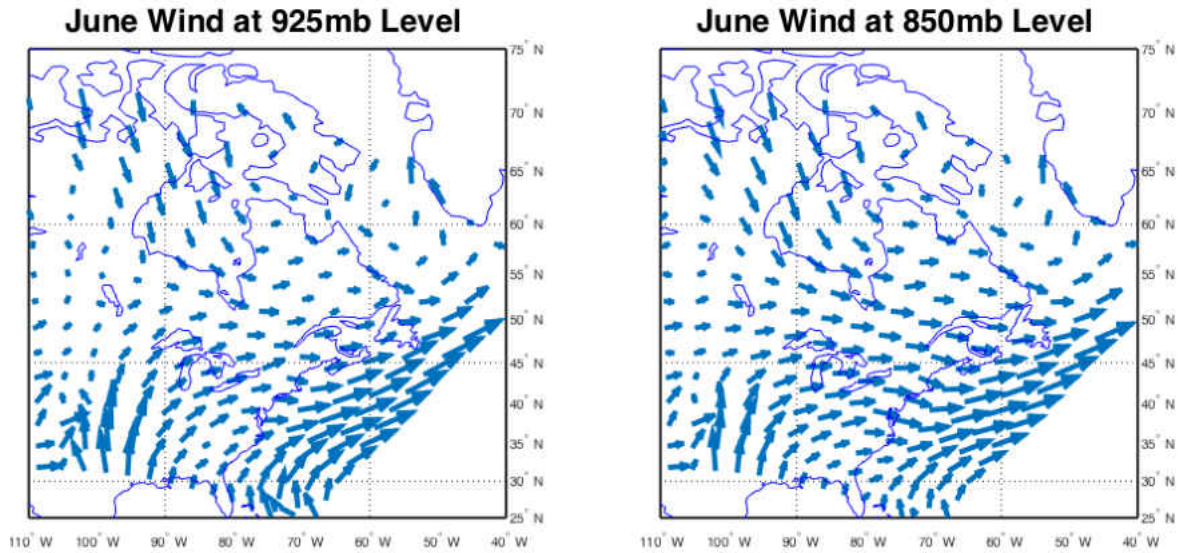
Figure 67: *The June-mean wind fields (left) at the 925mb level and (right) at the 850mb level averaged for the years 1979-2013 over the eastern part of North America, based on the NARR reanalysis data.*

the atmosphere becomes unstable due to lake-surface warming. We saw indications in §4.2 and Appendix 1 that Lake Superior affected the atmosphere at least as high as the 800mb pressure level. The Figures 68-70 suggest that these amplified warming trends give rise to thermal-wind anomalies over the Great Lakes region that flow from the east, change the direction over Lake Superior, and then flow to the north (Figure 71). These thermal-wind anomalies would act as a positive feedback to the existing warming trends there.

Another reason that thermal-wind anomalies would act as a positive feedback to the existing warming trends of the Great Lakes is the existence of even stronger warming trends over the eastern part of Hudson Bay, regions southwest of Greenland, and numerous other regions in the Arctic ocean, as we see in Figures 68-70. It turns out that, the regions of strong warming trends in Figure 68, a map of warming trends in annual-mean
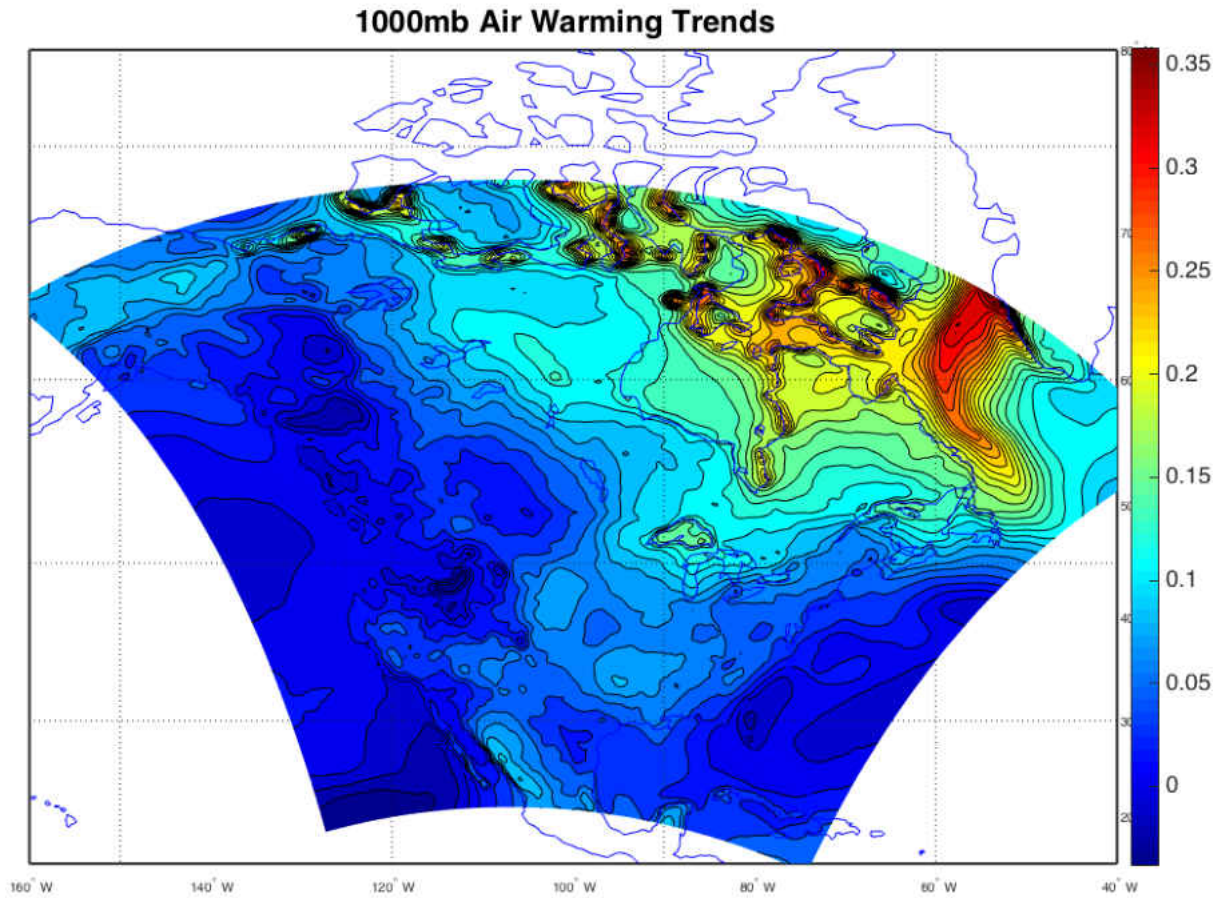
Figure 68: *A map of warming trends in annual-mean air temperature at the 1000mb pressure level over North America for the years 1988-2007, based on the NARR reanalysis and computed by linear regression. The unit is in $^\circ C/year$.*

air temperature at the 1000mb level over North America, matches the locations of strong negative trends in sea-ice cover, which in turn matches the locations of sea-ice "shorelines," the lines along which sea-ice-covered regions meet open-water regions. This is an indication that, not only the amount of sea ice is decreasing, but also, the atmosphere above regions where the amount of sea ice is decreasing is warming rapidly.

Figure 71 implies that, when the Great Lakes' ice, the sea-ice over Hudson Bay and over regions southwest of Greenland all decrease together, the atmospheric circulation above the Great Lakes would change so that the lakes receive warmer air from the Atlantic ocean more often, and when they all increase together, the atmospheric circulation above
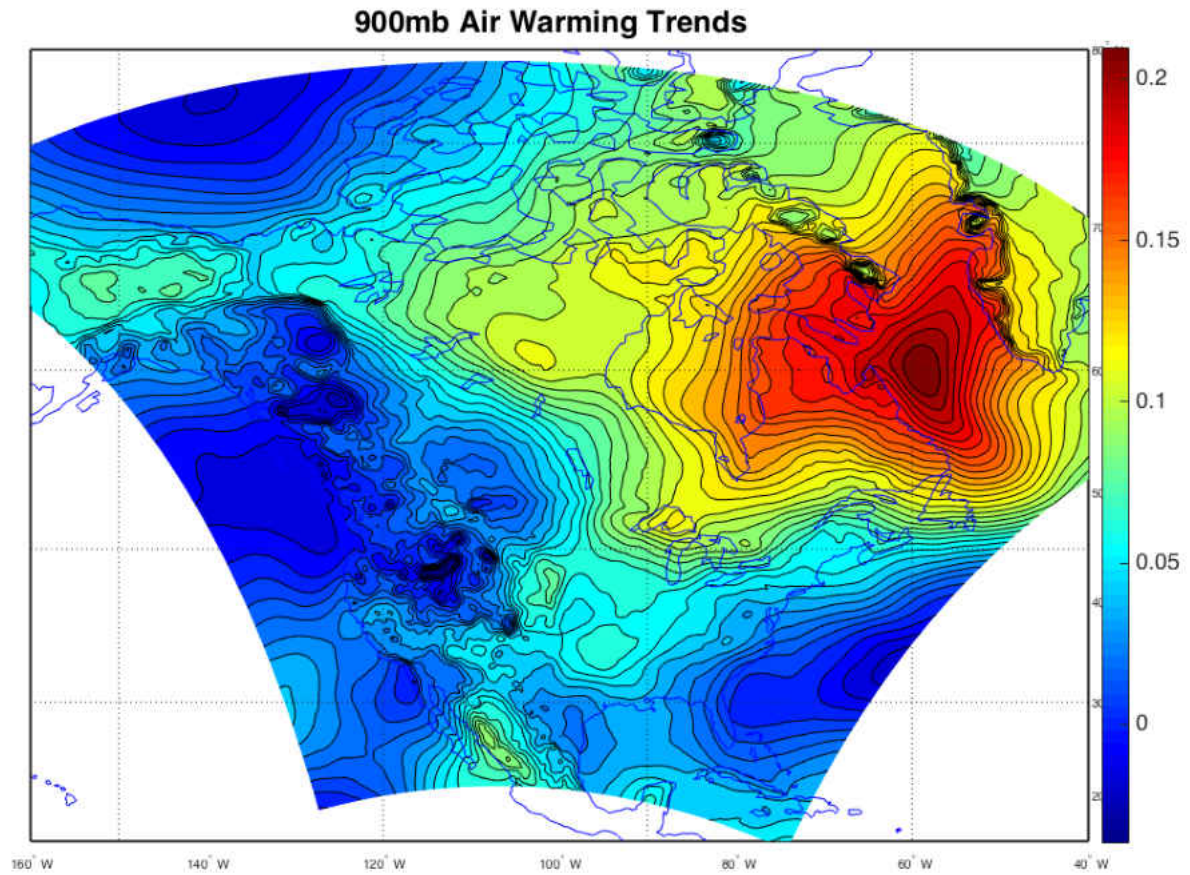
143

Figure 69: *A map of warming trends in annual-mean air temperature at the 900mb pressure level over North America for the years 1988-2007, based on the NARR reanalysis and computed by linear regression. The unit is in °C/year.*

the Great Lakes would change so that the lakes receive colder air from the north more
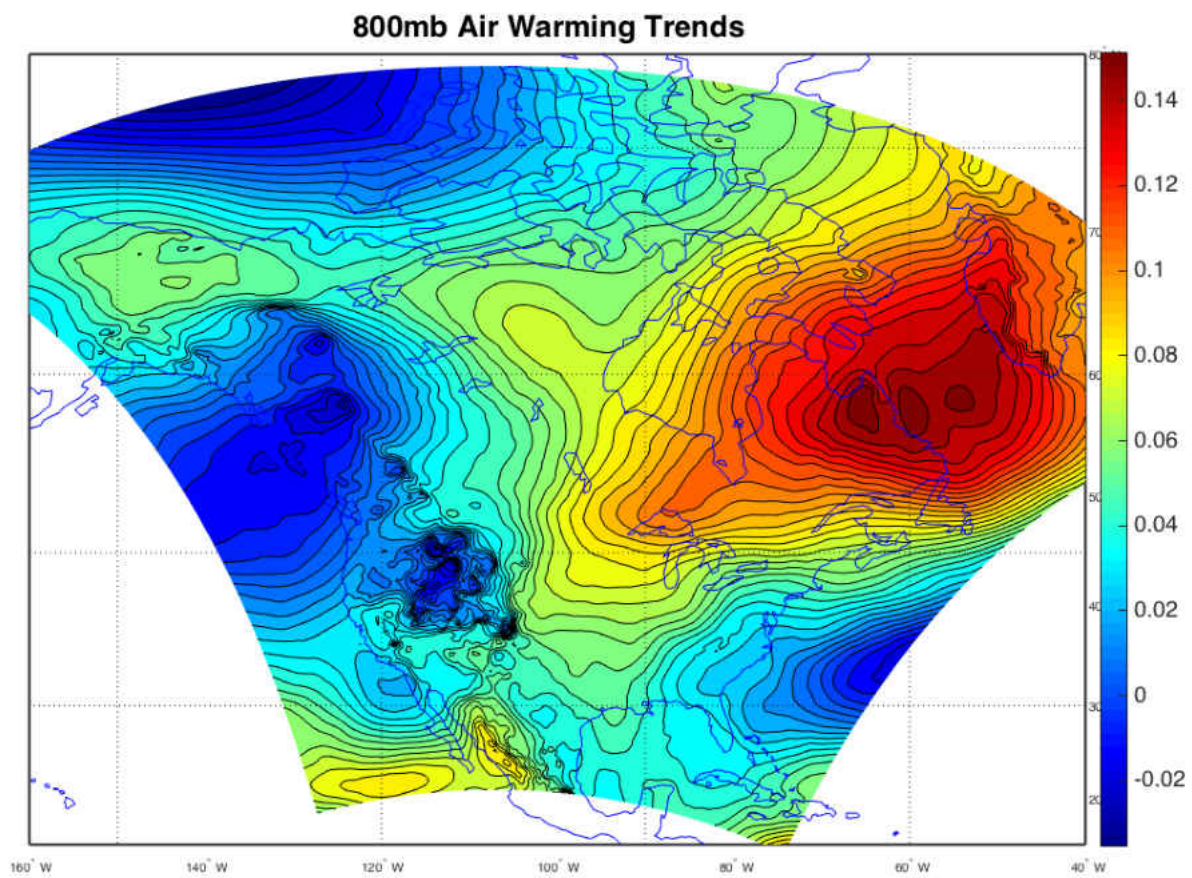
often.

Figure 70: *A map of warming trends in annual-mean air temperature at the 800mb pressure level over North America for the years 1988-2007, based on the NARR reanalysis and computed by linear regression. The unit is in °C/year.*
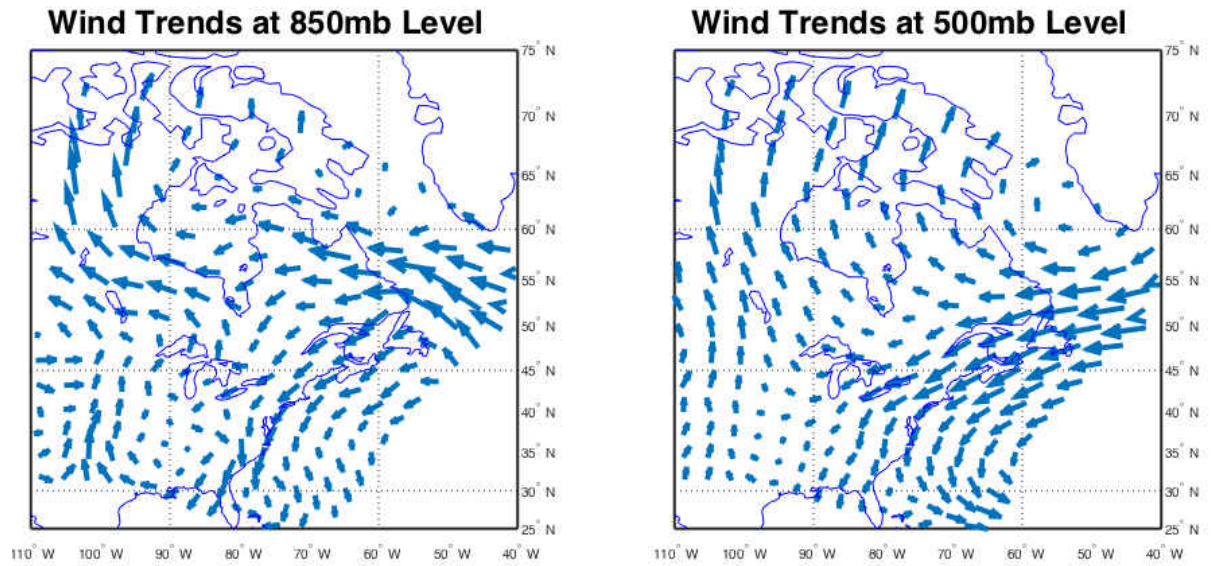
Figure 71: *The trends in annual-mean wind fields (left) at the 850mb level and (right) at the 500mb level over the eastern part of North America for the years 1988-2007, based on the NARR reanalysis data and computed by linear regression. The magnitudes of the largest trends south of Greenland in the left panel is roughly $0.12ms^{-1}year^{-1}$. The magnitudes of the largest trends south of Greenland in the right panel is roughly $0.20ms^{-1}year^{-1}$.*

CURRICULUM VITAE

Noriyuki Sugiyama

Place of birth: Maebashi, Gunma Prefecture, Japan

Education

B.S., University of Michigan, April 2003

Majors: Mathematics, General Physics, and Astronomy/Astrophysics

M.S., University of Wisconsin-Milwaukee, December 2008

Major: Physics

Dissertation Title: THE GREAT LAKES' REGIONAL CLIMATE REGIMES